BETA DOSE DISTRIBUTION FOR RANDOMLY PACKED MICROSPHERES

A Thesis

by

ALEXANDER URASHKIN

Submitted to the Office of Graduate Studies of
Texas A&M University
in partial fulfillment of the requirements for the degree of

MASTER OF SCIENCE

December 2006

Major Subject: Health Physics

BETA DOSE DISTRIBUTION FOR RANDOMLY PACKED MICROSPHERES

A Thesis

by

ALEXANDER URASHKIN

Submitted to the Office of Graduate Studies of
Texas A&M University
in partial fulfillment of the requirements for the degree of

MASTER OF SCIENCE

Approved by:

Chair of Committee, Warren D. Reece
Committee members, John R. Ford
Leslie A. Braby
Michael A. Walker
Head of Department, William E. Burchill

December 2006

Major Subject: Health Physics

ABSTRACT

Beta Dose Distribution for Randomly Packed Microspheres. (December 2006)

Alexander Urashkin, B.S.; M.S., Obninsk State Technical University, Russia

Chair of Advisory Committee: Dr. Warren D. Reece

Brachytherapy refers to the therapeutic use of encapsulated radionuclides within or close to a tumor. Today brachytherapy is used as an alternative to surgery or beam therapy to treat different kinds of cancers such as breast, lung, prostate, ovarian and pancreatic, primary and metastatic hepatic tumors and rheumatoid arthritis. Microspheres are one therapy utilized in brachytherapy procedures. Despite the development of advanced equipment and methods, there is still a limited knowledge of radiation dose distribution when utilizing this technique.

This study focuses on random packing of microspheres and seeks to determine dose distributions for specific cases. The Monte Carlo Neutral Particle code (MCNP) developed by Los Alamos National Laboratory is used to simulate beta particle transport. Pr-142 is the beta source utilized for all calculations. The cylinder radii are 0.1, 0.15 and 0.3 cm and sphere radii are 0.03, 0.05 and 0.07 cm. The results are verified by examining limiting cases: uniformly distributed source and line of microspheres.

Based on the data collected, the correlations between the average dose, its related variance, and distance from the cylinder were determined. An approach for estimating the surface average dose was developed and suggestions regarding an approach to assess surface variance estimation were presented.

ACKNOWLEDGEMENTS

I would like to thank my academic advisor Dr. W.D. Reece for his guidance, support and patience throughout my studying at Texas A&M University and pursuing master's degree. Also, I thank Dr. J.R. Ford, Dr. L.A. Braby and Dr. M.A. Walker for their time, reviews and comments on this thesis, as well as for serving on my thesis committee.

I would like to express my deepest appreciation to all of my professors from the Nuclear Engineering Department for their contribution to my knowledge and professional development in the field. The department staff deserve my thanks for helping with my study.

I would like to thank my family and friends for their support when I needed it most.

TABLE OF CONTENTS

TABLE OF CONTENTS (CONTINUED)

LIST OF FIGURES

LIST OF FIGURES (CONTINUED)

LIST OF FIGURES (CONTINUED)

LIST OF FIGURES (CONTINUED)

LIST OF TABLES

CHAPTER I

INTRODUCTION

Cancer treatment using radiation began shortly before the turn of the last century, soon after the discovery of x-rays by Roentgen, radioactivity by Becquerel, and radium by Marie and Pierre Curie. The first radiation cure of cancer, a basal cell epithelioma, was reported in the literature in 1899. Since then radiation therapy has evolved far beyond the early uses of radium sources.

In the early days of external therapy, surgeons or dermatologists who administered radiation treatment had little understanding or knowledge of radiation transport or biological effects of radiation. No method of calculating radiation dose existed. The equipment used to deliver the radiation was primitive, unreliable, and low energy so that few cancer cases could be treated.

The radiation treatment of this era generally was a massive exposure to a large area of the body with the hope that the tumor would be destroyed with a single treatment. Many post-radiation complications occurred due to destruction of normal tissues. The literature of this decade has many examples of radiation-induced tissue necrosis, infection, and death.

In the late 1920's x-ray therapy was introduced and fractionated daily doses of radiation rather than a single massive dose became the preferred treatment. During this era, treatment schedules were defined and implemented, and the relationship between

---

This thesis follows the style of the Health Physics Journal.

radiation dose and biological effects was studied. In this era of kilo-voltage x-rays, radiotherapy was seen mostly as a palliative treatment with little or no curative effect. With the introduction of vacuum x-ray tubes, capable of energies as high as 200 kV, cures of superficial cancers were soon reported. It also became clear that machines capable of producing higher energies had to be developed to treat cancers located deeper in the body effectively.

Soon after WWII, radioactive cobalt, and a man-made substitute for radium was developed. This time period, designated as the mega-voltage era, witnessed the widespread use of radioactive cobalt along with the development of high-energy devices such as linear accelerators and betatrons. These machines produced deeply penetrating x-rays making it possible to treat tumors located deep in the body. Severe skin reactions, an expected side effect of radiation therapy before this time, lessened in frequency and severity since the maximum radiation effect now occurred below the skin surface rather than on the skin surface.

Starting in the 1960's advances in radiobiology, computer controls, and controlled clinical trials, all contributed to the growth of radiation therapy. Machines could deliver adequate doses of radiation to tumors located anywhere in the body.

In contrast to teletherapy there is internal radiation therapy or brachytherapy. The word "brachytherapy" is derived from the Greek word "brachios" meaning near and refers to the therapeutic use of encapsulated radionuclides within or close to a tumor. In 1901, Pierre Curie suggested to Danlos at St. Louis Hospital in Paris that a small radium tube be inserted into a tumor, thus heralding the birth of brachytherapy. In 1903,

Alexander Graham Bell made a similar independent suggestion in a letter to the Editor of Archives Roentgen Ray. These early experiences demonstrated that inserting radioactive materials into tumors caused cancers to shrink.

In the early twentieth century, major brachytherapy work was done at the Curie Institute in Paris and at Memorial Hospital in New York. Dr. Robert Abbe, the chief surgeon at St. Lukes Hospital of New York, placed tubes into tumor beds after resection. In 1905 the afterloading technique which utilized removable radium sources was introduced. Dr. William Myers at Ohio State University developed several radioisotopes, including gold-198, cobalt-60, iodine-125, and phosphorus-32 for clinical brachytherapy. These were implanted surgically by Drs. Arthur James (surgeon) and Ulrich Henschke (radiation oncologist).

Towards the middle of last century the advent of ortho-voltage teletherapy for deeper tumors and the problems associated with radiation exposure from high-energy radionuclides led to a decline in the use of brachytherapy. However, over the past three decades, several advances have renewed interest in brachytherapy. New man-made radioisotopes and remote afterloading techniques have reduced radiation exposure hazards. Newer imaging techniques (CT scan, magnetic resonance imaging, transrectal ultrasound) and sophisticated computerized treatment planning have helped achieve increased positional accuracy and superior, optimized dose distribution. Finally, although initially used only for treatment of cancer, brachytherapy has also been found to be useful in non-malignant diseases. Brachytherapy can be the optimum way of

delivering conformal radiotherapy tailored to the shape of the tumor and thereby better sparing surrounding normal tissues (American Brachytherapy Society web site 2006).

The problem of dose specification in brachytherapy is made difficult by the inability to limit dose to the target volume, the steep dose gradients within the treatment volume, and intense hot spots in the implanted region. Although transport codes can give complete dose distributions in any plane, this does not simplify the problem of specifying the dose by a single value, the target dose. On the other hand, when brachytherapy is used for boost therapy, the overall uncertainty in dose prescriptions matters less (American Brachytherapy Society web site 2006).

Today dose specification is based on clinical experience with careful analysis of the irradiation technique and dosimetry. Existing systems provide guidelines for dose specification but none of the systems guarantees precise determination of target dose.

Microspheres are one type of microparticle utilized in brachytherapy procedures. In general radioactive microspheres have a wide range of diagnostic, therapeutic, and research applications such as diagnostic imaging, radiation synovectomy, intracavitary and intratumor therapy, blood flow measurements, and drug delivery and targeting.

Radioactive microspheres are a new treatment originally implemented for patients with rheumatoid arthritis, ovarian and pancreatic cancer, and primary and metastatic hepatic tumors. They are effective in treating arthritis, delivering the desired dose to the membrane for treatment or ablation of synovium to reduce joint effusion. In ovarian cancer, the microspheres are introduced into the abdominal cavity to deliver radiation to cancer cells. Microspheres are also effective in controlling growth in benign

cystic brain lesions, craniopharyngioma, and possibly pancreatic and hepatic tumors (American Brachytherapy Society web site 2006).

One example of microsphere treatment is the Therasphere™ treatment technique for liver cancer. Theraspheres™ incorporate yttrium-90 into the embolic spheres to deliver radiation directly to the tumor. The yttrium-90 coated microspheres are injected through a catheter extending from the femoral artery in the groin to the liver artery supplying the tumor, and are carried to the smallest blood vessels where, because of their size, they become entrapped. This technique provides high local doses while mostly sparing peripheral normal tissue.

Although surgical removal of liver tumors offers the best chance for cure, it is not feasible for more than three-fourths of patients with primary liver cancer or for 90 percent of patients with secondary liver cancer. For now radioembolization is a palliative, not curative, treatment but patients benefit by life-extension and quality-of-life improvement (American Brachytherapy Society web site 2006).

Another application of radioactive microspheres being investigated is the treatment of arteriovenous malformations (AVM's). An AVM is a localized tangle of arteries and veins within the brain. Arteries carry oxygen-rich blood away from the heart to the body's cells and veins return oxygen-depleted blood to the lungs and heart. The presence of an AVM disrupts this process. The microsphere approach is a substitute for surgical procedures that are too difficult or dangerous. The injected radioactive microspheres permanently embolize the blood vessels and provide relatively low doses of beta radiation that induce hyperplasia of the vascular endothelium, leading to the

blockage of the blood stream. The nidus will be isolated and the AVM symptoms cured (Mayfield clinic web site 2006).

Microsphere injection has shown promise as an alternative to surgery and to beam therapy. Unfortunately the lack of knowledge about dose specification limits application of this technique. The research in this area of radiation therapy is vital for future applications.

Two well-studied limiting cases in microsphere therapy are a perfect line of microspheres and a uniformly distributed source in a specific volume. Dose calculation methods for these limiting cases are considered in the next chapter of this thesis. This study focuses on the case of randomly distributed microspheres and is bounded by the cases mentioned above. A uniformly distributed source is approached when the radius of spheres is decreased and number of spheres in the artery is increased. A perfect line of microspheres is approached when the radius of microspheres becomes equal to the radius of the artery.

The most complicated and rarely studied case is the one lying between these two limiting ones. The difficulty of multiple microsphere calculation lies in the random nature of sphere distribution in the volumes. Lucile Dauffy considered in her thesis (Dauffy 1998) an idealized case of line of sphere distribution within a human artery. She evaluated dose rate distribution around a line of spheres utilizing geometrical and calculational approaches based on the Berger beta dose point kernel (DPK). This case is used in this study as a limiting case for verification of results. Sung-Woo Lee in his dissertation (Lee 2004) improved the understanding of dose specification in microsphere

applications. His study focused on microsphere technique for AVM treatment using Pr-142 beta sources and considered random close packing of microspheres in human arteries. Lee examined several typical cases of microsphere and artery sizes, and determined dose rates at different distances around the arteries using MCNP and DPK methods. Although the model he used in calculations was simplified, it provided initial data for dose specification technique and for future studies.

This study focuses on random packing of microspheres (but not close packing as was done in Lee's work). The dose distributions for specific sphere cases are calculated and techniques are given for estimation of average dose and its related variance. For consistency with Lee's data the Pr-142 beta source and the same set of artery and microsphere sizes are considered. The Monte Carlo Neutral Particle code (MCNP) developed by Los Alamos National Laboratory is used to simulate beta particle transport (X-5 Monte Carlo Team 2003). The distribution is determined at three different distances and based on 56 tallies at each distance. The results obtained are verified by comparing to data from limiting cases: a uniformly distributed source and a line of microspheres. The correlation curves between an average dose, related variance and distance from the cylinder are determined. The technique for estimating the surface average dose and related variance is developed.

CHAPTER II

THEORY

Beta particle dosimetry

Beta particles are electrons ejected from a nucleus. An unstable nucleus may attain a stable state by changing a neutron into a proton and ejecting a negative beta particle (electron), or by changing a proton into a neutron and ejecting a positive beta particle (positron). In either case, some or all of the excess nuclear energy is carried away by the ejected beta particle and neutrino. If the beta particle and neutrino do not carry away all the excess nuclear energy, the emission of the beta particle will be followed by one or more gamma rays. The decay energy is shared between the electron and neutrino. Thus, beta particles do not have one energy like a gamma photon. Its energy is in range from zero to maximum decay energy, and average energy is about one third of its maximum decay energy (Attix 1986).

Beta particles lose energy by a variety of processes when they pass through matter. These processes include resonance absorption, collisions with nuclei and electrons, excitation of atoms, radiation production, and electrodisintegration of nuclei. For the beta electrons in this study, collisions which produce ionization and excitation of atoms, and radiation production (bremsstrahlung) are the predominant methods of energy loss.

The energy of the electron is attenuated by a multitude of inelastic collisions until it reaches thermal levels. The energy loss per unit path length by an electron of mass m and velocity v can be described by eqn (2.1) (Bethe and Ashkin 1953). The Born approximation that the velocity of the primary electron exceeds that of the atomic orbital electron is used in this equation.

$$-\left(\frac{dT}{dx}\right)_{coll} = \frac{2\pi e^4 ZN}{m_o v^2}\left[\ln\frac{m_0 v^2 T}{2I^2(1-\beta^2)} - \left(2\sqrt{1-\beta^2} - 1 + \beta^2\right)\ln 2 + \right.$$

$$\left. + (1-\beta^2) + \frac{1}{8}\left(1-\sqrt{1-\beta^2}\right)^2\right], \qquad (2.1)$$

where dT is kinetic energy loss per increment of path length, dx in centimeters, N is number of atoms per cubic centimeter, Z is the nuclear charge, T is the relativistic kinetic energy of the electron, and I is the average excitation potential of the atom.

The production of x-rays (bremsstrahlung) by the deceleration of electrons is an unlikely process at low energies (below 1 MeV); at higher energies it becomes an increasingly important process of energy loss. When an electron is deflected in a nuclear field, energy must be radiated. Momentum is generally conserved by a nearby nucleus. The radiation energy lost by an electron per unit path length is approximately proportional to its energy and to the square of the nuclear charge. The energy loss by electrons due to negative acceleration in the field of nuclei and atomic electrons can be described by eqn (2.2) (Bethe and Ashkin 1953; Heitler 1954).

$$-\left(\frac{dT}{dx}\right)_{rad} = NE\frac{Z(Z+1)}{137}\left(\frac{e^2}{m_0c^2}\right)^2\left(4\ln\frac{2E}{m_0c^2}-\frac{4}{3}\right), \quad (2.2)$$

where dT is kinetic energy loss per increment of path length, dx in centimeters, N is number of atoms per cubic centimeter, E is electron energy, Z is the nuclear charge, where e is electronic charge and m_0 is the electron mass.

The electrons moving in a medium are deflected by their interaction with the electric field of the nuclei and orbital electrons. Because of their light mass, electrons are easily deflected and experience frequent elastic scattering. The fundamental equation for collisional loss was developed by Rutherford. The cross-section may be written as:

$$\sigma_{ruth}(E,T) = \frac{2\pi z^2 Z^2 e^4}{(4\pi\varepsilon_0)^2 Mv^2 T^2}, \quad (2.3)$$

where E is electron energy, T is target recoil energy e is electronic charge, z is the electron charge, Z is the nuclear charge, ε_o is electric constant, M is target atomic mass and ν is electron velocity (Rutherford 1911).

Calculation of absorbed radiation dose from beta emitting radionuclides is very complex, depending on a number of variables, and there is a much higher degree of uncertainty in beta dosimetry than in that of gamma dosimetry. The most important factor is the energy of beta radiation.

Another factor in beta dosimetry calculations is the density of the medium that the electrons traverse. The rate of electron kinetic energy loss, and hence the amount of absorbed radiation energy, is proportional to the density of the media.

Distribution of radioactive sources in tissue is also critical, because the penetration range of beta particles in soft tissue is only a few millimeters. But precise particle distribution in the patient is difficult to determine. For intraarticular and intracavitary therapy it is usually assumed that radioactive source distribution is uniform inside a thin film on the affected tissue. This is why the ability of imaging radioactive source distribution in the body is important. In addition, imaging also aids dosimetry calculations in nontarget tissues in case the particles leak from the target site.

This complexity of absorbed dose estimation is the main reason why only a few absorbed dose estimates for different radionuclides are available. Most procedures apply what has been effective in the past or use early estimates of medical internal radiation dose (MIRD) formulation, which is used primarily for gamma emitters. This method is based on average beta energy, and dose average over an entire site, rather than actual dose distribution in the target volume.

Electron transport in MCNP

The transport of electrons and other charged particles is fundamentally different from that of neutrons and photons. The interaction of neutral particles is characterized by relatively infrequent isolated collisions, with simple free flight between collisions. By

contrast, the transport of electrons is dominated by the long-range Coulomb force, resulting in large numbers of small interactions. As an example, a neutron in aluminum slowing down from 0.5 MeV to 0.0625 MeV will have about 30 collisions, while a photon in the same circumstances will experience fewer than ten. An electron accomplishing the same energy loss will undergo about 10^5 individual interactions. This great increase in computational complexity makes a single-collision Monte Carlo approach to electron transport unfeasible for most situations of practical interest.

Considerable theoretical work has been done to develop a variety of analytic and semi-analytic multiple-scattering theories for the transport of charged particles. These theories attempt to use the fundamental cross section and the statistical nature of the transport process to predict probability distributions for significant quantities, such as energy loss and angular deflection. The most important of these theories for the algorithms in MCNP are the theory for angular deflections (Goudsmit and Saunderson 1940), the theory of energy-loss fluctuations (Landau 1944), and the enhancements of the Landau theory (Blunck and Leisegang 1950). These theories rely on a variety of approximations that restrict their applicability, so that they cannot solve the entire transport problem. In particular, it is assumed that the energy loss is small compared to the kinetic energy of the electron.

In order to follow an electron through a significant energy loss, it is necessary to break the electron's path into many steps. These steps are chosen to be long enough to encompass many collisions (so that multiple-scattering theories are valid) but short enough that the mean energy loss in any one step is small (so that the approximations

necessary for the multiple-scattering theories are satisfied). The energy loss and angular deflection of the electron during each of the steps can then be sampled from probability distributions based on the appropriate multiple-scattering theories. This accumulation of the effects of many individual collisions into single steps that are sampled probabilistically constitutes the "condensed history" Monte Carlo method.

The most influential reference for the condensed history method is the paper presented in 1963 (Berger 1963). Based on the techniques described in that work the ETRAN series of electron/photon transport codes were developed (Berger 1963; Seltzer 1988). These codes have been maintained and enhanced for many years at the National Bureau of Standards (now the National Institute of Standards and Technology).

The following paragraphs on the electron transport present the data obtained from the MCNP manual developed at the Los Alamos National Laboratory (X-5 Monte Carlo Team 2003).

Electron steps and substeps

The condensed random walk for electrons can be considered in terms of a sequence of sets of values:

$$(0,E_0,t_0,u_0,r_0),\ (s_1,E_1,t_1,u_1,r_1),\ (s_2,E_2,t_2,u_2,r_2),\ \ldots$$

where s_n, E_n, t_n, u_n, and r_n are the total path length, energy, time, direction, and position of the electron at the end of n steps. On the average, the energy and path length are related by:

$$E_n - E_{n-1} = -\int_{S_{n-1}}^{S_n} \frac{dE}{ds} ds, \tag{2.4}$$

where dE/ds is the total stopping power in energy per unit length. This quantity depends on energy and on the material in which the electron is moving. ETRAN-based codes customarily choose the sequence of path lengths $\{s_n\}$ such that:

$$\frac{E_n}{E_{n-1}} = k \tag{2.5}$$

The most commonly used value is $k = 2^{-1/8}$, which results in an average energy loss per step of 8.3%.

Electron steps with (energy-dependent) path lengths $s = s_n - s_{n-1}$ determined by eqns (2.4-2.5) are called major steps or energy steps. The condensed random walk for electrons is structured in terms of these energy steps. For example, all precalculated and tabulated data for electrons are stored on an energy grid whose consecutive energy values obey the ratio in eqn (2.5). In addition, the Landau and Blunck-Leisegang theories for energy straggling are applied once per energy step. For a single step, the

angular scattering could also be calculated with satisfactory accuracy, since the Goudsmit-Saunderson theory is valid for arbitrary angular deflections. However, the representation of the electron's trajectory as the result of many small steps will be more accurate if the angular deflections are also required to be small. Therefore, the ETRAN codes and MCNP further break the electron steps into smaller substeps. A major step of path length s is divided into m substeps, each of path length s/m. Angular deflections and the production of secondary particles are sampled at the level of these substeps. The integer m depends only on material (average atomic number Z). Appropriate values for m have been determined empirically, and range from m=2 for Z<6 to m=15 for Z>91.

Condensed random walk

In the initiation phase of a transport calculation involving electrons, all relevant data are either precalculated or read from the electron data file and processed. These data include the electron energy grid, stopping powers, electron ranges, energy step ranges, substep lengths, and probability distributions for angular deflections and the production of secondary particles. Although the energy grid and electron steps are selected according to eqns (2.4-2.5), energy straggling, the analog production of bremsstrahlung, and the intervention of geometric boundaries and the problem time cutoff will cause the electron's energy to depart from a simple sequence s_n satisfying eqn (2.5). Therefore, the necessary parameters for sampling the random walk will be interpolated from the points on the energy grid.

At the beginning of each major step, the collisional energy loss rate is sampled. In the absence of energy straggling, this will be a simple average value based on the nonradiative stopping power described in the next section. In general, however, fluctuations in the energy loss rate will occur. The number of substeps m per energy step will have been preset, either from the empirically determined default values, or by the user, based on geometric considerations.

Except for the energy loss and straggling calculation, the detailed simulation of the electron history takes place in the sampling of the substeps. The Goudsmit-Saunderson theory is used to sample the distribution of angular deflections, so that the direction of the electron can change at the end of each substep. Based on the current energy loss rate and the substep length, the projected energy for the electron at the end of the substep is calculated. Finally, appropriate probability distributions are sampled for the production of secondary particles. These include electron-induced fluorescent X-rays, "knock-on" electrons (from electron-impact ionization), and bremsstrahlung photons.

Note that the length of the substep ultimately derives from the total stopping power used in eqn (2.4), but the projected energy loss for the substep is based on the nonradiative stopping power. The reason for this difference is that the sampling of bremsstrahlung photons is treated as an essentially analog process. When a bremsstrahlung photon is generated during a substep, the photon energy is subtracted from the projected electron energy at the end of the substep. Thus the radiative energy loss is explicitly taken into account, in contrast to the collisional (nonradiative) energy

loss, which is treated probabilistically and is not correlated with the energetics of the substep. Two biasing techniques are available to modify the sampling of bremsstrahlung photons for subsequent transport. However, these biasing methods do not alter the linkage between the analog bremsstrahlung energy and the energetics of the substep.

MCNP uses identical physics for the transport of electrons and positrons, but distinguishes between them for tallying purposes, and for terminal processing. Electron and positron tracks are subject to the usual collection of terminal conditions, including escape (entering a region of zero importance), loss to time cutoff, loss to a variety of variance-reduction processes, and loss to energy cutoff.

Stopping power

a. Collisional Stopping Power

Berger gives the restricted electron collisional stopping power, i.e., the energy loss per unit path length to collisions resulting in fractional energy transfers ε less than an arbitrary maximum value ε_m, in the form:

$$-\left(\frac{dE}{ds}\right)_{\varepsilon_m} = NZC\left\{\ln\frac{E^2(\tau+2)}{2I^2} + f^-(\tau,\varepsilon_m) - \delta\right\}, \qquad (2.6)$$

where

$$f^{-}(\tau,\varepsilon_m) = -1-\beta^2+\left(\frac{\tau}{\tau+1}\right)^2\frac{\varepsilon_m^2}{2}+\frac{2\tau+1}{(\tau+1)^2}\ln(1-\varepsilon_m)+\ln[4\varepsilon_m(1-\varepsilon_m)]+\frac{1}{1-\varepsilon_m} \quad (2.7)$$

Here ε and ε_m represent energy transfers as fractions of the electron kinetic energy E; I is the mean ionization potential in the same units as E; β is v/c; τ is the electron kinetic energy in units of the electron rest mass; δ is the density effect correction (related to the polarization of the medium); Z is the average atomic number of the medium; N is the atom density of the medium in cm^{-3}; and the coefficient C is given by:

$$C = \frac{2\pi e^4}{mv^2}, \quad (2.8)$$

where m, e, and v are the rest mass, charge, and speed of the electron, respectively.

The ETRAN codes and MCNP do not make use of restricted stopping powers, but rather treat all collisional events in an uncorrelated, probabilistic way. Thus, only the total energy loss to collisions is needed, and eqns (2.6-2.7) can be evaluated for the special value $\varepsilon_m = 1/2$. The reason for the 1/2 is the indistinguishability of the two outgoing electrons. The electron with the larger energy is, by definition, the primary. Therefore, only the range $\varepsilon < 1/2$ is of interest. With $\varepsilon_m = 1/2$, eqn (2.7) becomes:

$$f^{-}(\tau,\varepsilon_m) = -\beta^2 + (1-\ln 2) + \left(\frac{1}{8}+\ln 2\right)\left(\frac{\tau}{\tau+1}\right)^2 \tag{2.9}$$

On the right side of eqn (2.6), we can express both E and I in units of the electron rest mass. Then E can be replaced by τ on the right side of the equation. We also introduce supplementary constants:

$$\begin{aligned} C2 &= \ln(2I^2) \\ C3 &= 1-\ln 2 \\ C4 &= \frac{1}{8}+\ln 2 \end{aligned} \tag{2.10}$$

so that eqn (2.6) becomes:

$$-\left(\frac{dE}{ds}\right) = NZ\frac{2\pi e^4}{mv^2}\left\{\ln[\tau^2(\tau+2)] - C2 + C3 - \beta^2 + C4\left(\frac{\tau}{\tau+1}\right)^2 - \delta\right\} \tag{2.11}$$

This is the collisional energy loss rate in MeV/cm in a particular medium. In MCNP, we are actually interested in the energy loss rate in units of MeV barns (so that different cells containing the same material need not have the same density). Therefore,

we divide eqn (2.11) by N and multiply by the conversion factor 10^{24} barns/cm^2. We also use the definition of the fine structure constant:

$$\alpha = \frac{2\pi e^2}{hc}, \tag{2.12}$$

where h is Planck's constant, to eliminate the electronic charge e from eqn (2.11). The result is as follows:

$$-\left(\frac{dE}{ds}\right) = \frac{10^{24}\,\alpha^2 h^2 c^2}{2\pi mc^2} Z\left\{\ln[\tau^2(\tau+2)] - C2 + C3 - \beta^2 + C4\left(\frac{\tau}{\tau+1}\right)^2 - \delta\right\}\frac{1}{\beta^2} \tag{2.13}$$

This is the form actually used in MCNP to preset the collisional stopping powers at the energy boundaries of the major energy steps.

The mean ionization potential and density effect correction depend upon the state of the material, either gas or solid. In the fit utilized, the physical state of the material also modifies the density effect calculation (Sternheimer and Peierls 1982). The calculation of the density effect uses the conduction state of the material to determine the contribution of the outermost conduction electron to the ionization potential (Sternheimer, Berger and Seltzer 1982). The occupation numbers and atomic binding energies used in the calculation are from the paper presented in 1975 (Carlson 1975).

b. Radiative Stopping Power

The radiative stopping power is:

$$-\frac{dE}{ds}\Big|_{rad} = 10^{24}\, Z(Z+\bar{\eta})(\alpha\, r_e^2)(T+mc^2)\,\Phi_{rad}^{(n)}\,, \qquad (2.14)$$

where $\Phi_{rad}^{(n)}$ is the scaled electron-nucleus radiative energy-loss cross-section based upon evaluations by Berger and Seltzer; $\bar{\eta}$ is a parameter to account for the effect of electron-electron bremsstrahlung; α is the fine structure constant; mc^2 is the mass energy of an electron; and r_e is the classical electron radius. The dimensions of the radiative stopping power are the same as the collisional stopping power.

Energy straggling

Because an energy step represents the cumulative effect of many individual random collisions, fluctuations in the energy loss-rate will occur. Thus the energy loss will not be a simple average Δ; rather there will be a probability distribution $f(s,\Delta)d\Delta$ from which the energy loss Δ for the step of length s can be sampled. Landau studied this situation under the simplifying assumptions that the mean energy loss for a step is small compared with the electron's energy, that the energy parameter ξ defined below is large compared with the mean excitation energy of the medium, that the energy loss can

be adequately computed from the Rutherford cross section, and that the formal upper limit of energy loss can be extended to infinity. With these simplifications, Landau found that the energy loss distribution can be expressed as:

$$f(s,\Delta)\,d\Delta = \varphi(\lambda)\,d\lambda \tag{2.15}$$

in terms of $\varphi(\lambda)$, a universal function of a single scaled variable:

$$\lambda = \frac{\Delta}{\xi} - \ln\left[\frac{2\xi m v^2}{(1-\beta^2)I^2}\right] + \delta + \beta^2 - 1 + \gamma \tag{2.16}$$

Here m and v are the mass and speed of the electron, δ is the density effect correction, β is v/c, I is the mean excitation energy of the medium, and γ is Euler's constant ($\gamma = 0.5772157\ldots$). The parameter ξ is defined by:

$$\xi = \frac{2\pi e^4 NZ}{m v^2} s, \tag{2.17}$$

where e is the charge of the electron, N and Z is the number density of atomic electrons, and the universal function is:

$$\varphi(\lambda) = \frac{1}{2\pi i}\int_{x-i\infty}^{x+i\infty} e^{\mu \ln\mu + \lambda\mu}\, d\mu\,, \tag{2.18}$$

where x is a positive real number specifying the line of integration.

For purposes of sampling, $\varphi(\lambda)$ is negligible for $\lambda < -4$, so that this range is ignored. Originally $\varphi(\lambda)$ tabulated in the range $-4 \le \lambda \le 100$, and derived for the range $\lambda > 100$ the asymptotic form:

$$\varphi(\lambda) \approx \frac{1}{w^2 + \pi^2} \tag{2.19}$$

in terms of the auxiliary variable w, where

$$\lambda = w + \ln w + \gamma - \frac{3}{2} \tag{2.20}$$

Angular deflections

The ETRAN codes and MCNP rely on the Goudsmit-Saunderson theory for the probability distribution of angular deflections. The angular deflection of the electron is sampled once per substep according to the distribution:

$$F(s,\mu) = \sum_{l=0}^{\infty}\left(l+\frac{1}{2}\right)\exp(-sG_l)\,P_l(\mu), \tag{2.21}$$

where s is the length of the substep, $\mu = \cos\theta$ is the angular deflection from the direction at the beginning of the substep, $P_l(\mu)$ is the l^{th} Legendre polynomial, and G_l is:

$$G_l = 2\pi N\int_{-1}^{+1}\frac{d\sigma}{d\Omega}[1-P_l(\mu)]\,d\mu, \tag{2.22}$$

where $d\sigma/d\Omega$ is the microscopic cross section, and the atom density N of the medium.

For electrons with energies below 0.256 MeV, the microscopic cross section is taken from numerical tabulations (Riley et al. 1975). For higher-energy electrons, the microscopic cross section is approximated as a combination of the Mott and Rutherford cross sections, with a screening correction. Seltzer presents this "factored cross-section" in the form:

$$\frac{d\sigma}{d\Omega} = \frac{Z^2e^2}{p^2v^2(1-\mu+2\eta)^2}\left[\frac{(d\sigma/d\Omega)_{\text{Mott}}}{(d\sigma/d\Omega)_{\text{Rutherford}}}\right], \tag{2.23}$$

where e, p, and ν are the charge, momentum, and speed of the electron, respectively. The screening correction η was originally given as:

$$\eta = \frac{1}{4}\left(\frac{\alpha mc}{0.885\,p}\right) Z^{2/3}\left[1.13 + 3.76(\alpha Z/\beta)^2\right], \qquad (2.24)$$

where α is the fine structure constant, m is the rest mass of the electron, and $\beta = v/c$. MCNP now follows the recommendation of Seltzer, and the implementation in the Integrated TIGER Series, by using the slightly modified form:

$$\eta = \frac{1}{4}\left(\frac{\alpha mc}{0.885\,p}\right) Z^{2/3}\left[1.13 + 3.76(\alpha Z/\beta)^2 \sqrt{\frac{\tau}{\tau+1}}\right], \qquad (2.25)$$

where τ is the electron energy in units of electron rest mass. The multiplicative factor in the final term is an empirical correction which improves the agreement at low energies between the factored cross section and the more accurate partial-wave cross sections of Riley (Riley, MacCallum and Biggs 1975).

Bremsstrahlung

MCNP addresses the sampling of bremsstrahlung photons at each electron substep. The tables of production probabilities are used to determine whether a bremsstrahlung photon will be created. For data from the el03 library (X-5 Monte Carlo Team 2003), the bremsstrahlung production is sampled according to a Poisson

distribution along the step so that none, one or more photons could be produced; the el03 library allows for either none or one bremsstrahlung photon in a substep. If a photon is produced, the new photon energy is sampled from the energy distribution tables. By default, the angular deflection of the photon from the direction of the electron is also sampled from the tabular data. The direction of the electron is unaffected by the generation of the photon because the angular deflection of the electron is controlled by the multiple scattering theory. However, the energy of the electron at the end of the substep is reduced by the energy of the sampled photon because the treatment of electron energy loss, with or without straggling, is based only on nonradiative processes.

K-shell electron impact ionization and auger transitions

Data tables on the el03 library use the same K-shell impact ionization calculation as data tables on the el library, except for how the emission of relaxation photons is treated; the el03 evaluation model has been modified to be consistent with the photo-ionization relaxation model. In the el03 evaluation, a K-shell impact ionization event generated a photon with the average K-shell energy.

Auger transition are handled the same for data tables from the el03 and el libraries. If an atom has undergone an ionizing transition and can undergo a relaxation, if it does not emit a photon it will emit an Auger electron. The difference between el03 and el is the energy with which an Auger electron is emitted, given by $E_A = E_{\bar{K}}$ or $E_A = E_{\bar{K}} - 2E_{\bar{L}}$ for el or el03, respectively. The el value is that of the highest energy

Auger electron while the el03 value is the energy of the most probable Auger electron. It should be noted that both models are somewhat crude.

Knock-on electrons

The cross section for scattering of an electron by an electron is:

$$\frac{d\sigma}{d\varepsilon} = \frac{C}{E}\left\{\frac{1}{\varepsilon^2} + \frac{1}{(1-\varepsilon)^2} + \left(\frac{\tau}{\tau+1}\right)^2 - \frac{2\tau+1}{(\tau+1)^2}\frac{1}{\varepsilon(1-\varepsilon)}\right\}, \tag{2.26}$$

where ε, τ, E, and C have the same meanings as in eqns (2.6-2.8)

When calculating stopping powers, one is interested in all possible energy transfers. However, for the sampling of transportable secondary particles, one wants the probability of energy transfers greater than some ε_c representing an energy cutoff, below which secondary particles will not be followed. This probability can be written:

$$\sigma(\varepsilon_c) = \int_{\varepsilon_c}^{1/2} \frac{d\sigma}{d\varepsilon} d\varepsilon \tag{2.27}$$

The reason for the upper limit of 1/2 is the same as in the discussion of eqn (2.9). Explicit integration of eqn (2.26) leads to:

$$\sigma(\varepsilon_c) = \frac{C}{E}\left\{\frac{1}{\varepsilon_c} - \frac{1}{1-\varepsilon_c} + \left(\frac{\tau}{\tau+1}\right)^2\left(\frac{1}{2} - \varepsilon_c\right) - \frac{2\tau+1}{(\tau+1)^2}\ln\frac{1-\varepsilon_c}{\varepsilon_c}\right\} \qquad (2.28)$$

Then the normalized probability distribution for the generation of secondary electrons with $\varepsilon > \varepsilon_c$ is given by:

$$g(\varepsilon, \varepsilon_c)\,d\varepsilon = \frac{1}{\sigma(\varepsilon_c)}\frac{d\sigma}{d\varepsilon}d\varepsilon \qquad (2.29)$$

At each electron substep, MCNP uses $\sigma(\varepsilon_c)$ to determine randomly whether knock-on electrons will be generated. If so, the distribution of eqn (2.29) is used to sample the energy of each secondary electron. Once energy has been sampled, the angle between the primary direction and the direction of the newly generated secondary particle is determined by momentum conservation. This angular deflection is used for the subsequent transport of the secondary electron. However, neither the energy nor the direction of the primary electron is altered by the sampling of the secondary particle. On the average, both the energy loss and the angular deflection of the primary electron have been taken into account by the multiple scattering theories.

Pulse height tally

The pulse height tally provides the energy distribution of pulses created in a cell that models a physical detector. It also can provide the energy deposition in a cell. Although the entries on the F8 card are cells, this is not a track length cell tally. F8 tallies are made at source points and at surface crossings.

The pulse height tally is analogous to a physical detector. The F8 energy bins correspond to the total energy deposited in a detector in the specified channels by each physical particle (history). All the other MCNP tallies record the energy of a scoring track in the energy bin.

In the analogous MCNP pulse height tally, the source cell is credited with the energy times the weight of the source particle. When a particle crosses a surface, the energy times the weight of the particle is subtracted from the account of the cell that it is leaving and is added to the account of the cell that it is entering. The energy is the kinetic energy of the particle plus $2m_0c^2$ = 1.022016 MeV if the particle is a positron. At the end of the history, the account in each tally cell is divided by the source weight. The resulting energy determines which energy bin the score is put in. The value of the score is the source weight for an F8 tally and the source weight times the energy in the account for a F8 tally. The value of the score is zero if no track entered the cell during the history (X-5 Monte Carlo Team 2003).

Radioactive microsphere applications

Radioactive microspheres are a new treatment technique becoming widely used in cases where surgery or beam therapy can not be implemented. Today it is employed for patients with different kinds of cancers such as breast, lung, prostate, ovarian and pancreatic; primary and metastatic hepatic tumors and also for treatment of rheumatoid arthritis.

Intracavitary therapy of malignant effusions with microspheres has three aims: cover the cavity surface and irradiate adherent malignant cells; destroy tumor cells in the fluid; and alter the cavity surface in such a way that is less favorable for implantation and growth of further malignant cells. There are two major approaches utilized in intratumor therapy: direct and indirect tumor therapy.

Direct tumor therapy deals with introduction of radioactive microspheres directly into tumors and offers the possibility of localized high radiation exposure. However, there are two major difficulties:

1. Microspheres reaching small vessels in a tumor may be carried away, because most particles used are smaller than mean capillary diameter. Particles released from a tumor are likely to deposit in liver, and increase the radiation dose to this organ.

2. As a tumor undergoes radiation-induced changes, these changes may cause additional particle leakage from the site.

Indirect tumor therapy employs two major routes: intravenous and intraarterial.

The intravenous route is clinically the easiest, but there are still considerable developmental problems to be overcome in delivering microparticles specifically to the tumor (i.e. without delivery to other sites).

The intraarterial route which utilizes delivery of theraspheres to a tumor via an artery that supplies the tumor appears very attractive, because hepatic tumors (both primary and metastatic) usually have high arteriolar density. Particle deposition is proportional to blood flow and hence the arterial route could result in at least 3-fold higher tumor irradiation compared with normal liver. However, initial studies with Y-90 resin based microspheres have met with the difficulties of accurately measuring the absorbed dose, monitoring regional perfusion that lead to GI toxicity, excessive leakage of radionuclide from particles and myelosuppression due to Y-90 deposition in bone.

More recent preparations of Y-90 microspheres have significantly reduced leakage for both glass and resin based microspheres. Also modern angiographic technique can be used to identify tumor vascular architecture. Thus, combination of different imaging techniques should enable more accurate monitoring of absorbed dose, and safely delivery to determine tumor and hepatic volumes.

An ideal radionuclide possesses the following characteristics:

1. Pure beta emitter
2. Accompanying gamma emission is acceptable if photon energy is less than 300keV and abundance is less than 10%
3. Readily available from a generator
4. Inexpensive, and produced in reactor rather than a cyclotron

5. Short physical and biological half lives
6. Well established chemistry and readily available compounds suitable for attachment to microparticles
7. Suitable compounds for forming stable composite with, or link to, microparticles to avoid leakage
8. Simple labeling procedure, low production cost, and not involving high radiation exposure to personnel

Table 2.1 illustrates radionuclides available today for microspheres applications (Archady 2001).

Table 2.1 Radioactive microspheres for therapeutic applications

Application	Type of radioactive microsphere used
Radioembolization of liver and spleen tumors	^{90}Y-glass microspheres
	^{186}Re/^{188}Re-glass microspheres
	^{188}Re-Aminex microspheres
Radiosynoviorthesis of arthritic joints	^{35}S-colloid
	^{90}Y-resin microspheres
	^{186}Re-sulfur-colloid
	^{188}Re-macro-aggregated albumin
Local radiotherapy	^{90}Y-labeled poly microspheres
	^{165}Dy-acetylacetone poly microspheres
	^{166}Ho-acetylacetone poly microspheres
	^{186}Re/^{188}Re-labeled poly microspheres
Peritoneal ovarian tumor metastases treatment, cystic brain tumor	^{32}P-chromate
Local restenosis prevention in coronary arteries	^{141}Ce microspheres

Microspheres specification

The microspheres are tiny spheres made of glass, ceramic, polymers and minerals and are manufactured in both solid and hollow forms. Hollow microspheres do not have the crush resistance exhibited by solid spheres and cannot be used in systems requiring high-shear mixture or high-pressure molding.

A type of microsphere used in the pharmaceutical industry is called therasphere. Therasphere is a therapeutic device that has been approved for use in patients as a Humanitarian Use Device (HUD) by the FDA office of orphan products and granted a humanitarian device exemption (HDE 980006) for treatment of rare cancers. It was originally developed in 1986 and patented in 1988, consisting of glass microspheres, mean diameter ranging from 20 to 30 microns that are chemically bonded to a radioactive pure beta emitter (e.g. yttrium-90 in case of liver cancer). Spherical particles are described as microspheres if they are larger than about $1\,\mu m$, and nanospheres (or colloidal particles) if smaller than about $1\,\mu m$.

There are two widely used approaches for producing microspheres: precipitation and polycondensation, and solvent removal and cross-linking. Fig. 2.1 presents basic steps of these methods (Archady 2001).

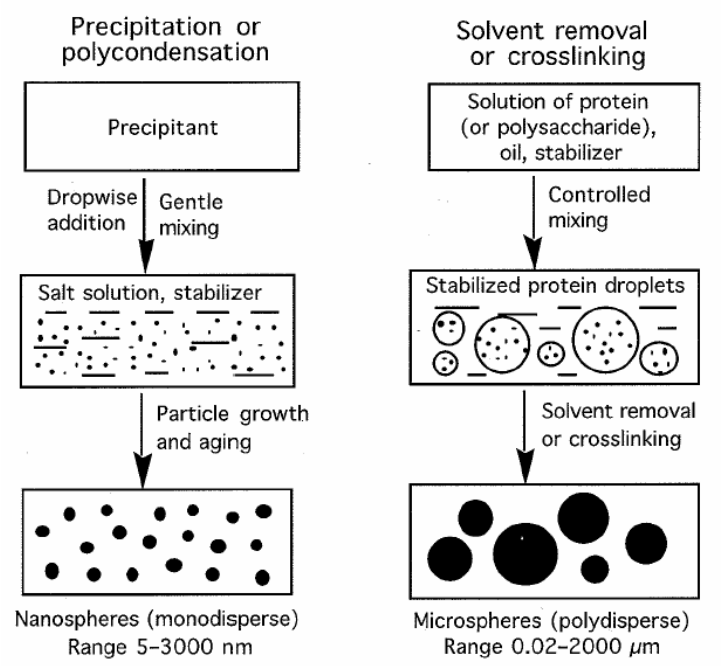

Fig. 2.1 Basic methods of producing small monodisperse colloidal particles (nanospheres) and large polydisperse (but relatively uniform) microspheres

Incorporation of radioactive material into microspheres can be accomplished by two basic routes: during particle formation (route 1), and radiolabeling of preformed microparticles (route 2). Both methods are in principle applicable to most microsphere types. In practice, however, inorganic particles are usually produced by the first route and organic by the second. In route 1, the radionuclide is usually coprecipitated with the same (or chemically similar) nonradioactive compound to form the particles, and hence the radionuclide is randomly distributed throughout the particle matrix. In route 2, the radionuclide may be incorporated into particles by covalent attachment, chelation or ion exchange. Here, the particles are often radiolabeled mainly on their surfaces, unless they swell fully in the reaction medium and become permeable to the radionuclide.

Table 2.2 illustrates beta emitting radionuclides widely used for radiotherapy (Archady 2001).

Table 2.2 Characteristics of beta emitting microparticulate radiopharmaceuticals for radionuclide therapy

Microparticles	Particle size (um)	Radionuclide production	Nuclide $T_{1/2}$ (d)	E_{max} (MeV), γ energy (%)	Tissue range (mm)	
					Max	Min
^{198}Au-gold colloid	0.001-0.07	$^{197}Au(n,\gamma)^{198}Au$	2.7	0.962, γ 0.412(96)	3.6	1.2
^{169}Er-citrate colloid	0.01-0.03	$^{168}Er(n,\gamma)^{169}Er$	9.5	0.34	1.0	0.3
^{186}Re-sulfur colloid	0.005-0.01	$^{185}Re(n,\gamma)^{186}Re$	3.7	1.07, γ 0.137(9)	3.6	1.2
^{90}Y-silicate colloid	0.1	$^{89}Y(n,\gamma)^{90}Y$	2.7	2.28	11.0	3.6
^{32}P-phosphate, chromic	0.5-1	$^{32}S(n,p)^{32}P$	14.3	1.71	7.9	2.6
^{90}Y-resin microsphere	29-35		14.3			
^{153}Sm-hydroxyapatite (microspheres)	5-40	$^{152}Sm(n,\gamma)^{153}Sm$	1.9	0.8, γ 0.103(28)	2.5	
^{165}Dy-ferric hydroxide (macroaggregates)	93%, 0.5-5 2%, <0.4	$^{164}Dy(n,\gamma)^{165}Dy$	0.1	1.29 γ 0.095(4)	5.7	1.8
165Dy-Dy hydroxide (macroaggregates)	2-5		0.1			
^{166}Ho-hydroxyapatite (microspheres)	27 and 50	$^{165}Ho(n,\gamma)^{166}Ho$ ^{166}Dy/^{166}Ho(^{166}Dy 3.4d)	1.1	1.85 γ 0.081(6)	8.5	
^{188}Re-sulfur colloid	65%, 1-5 17%, <1	^{188}W-^{188}Re (^{188}W 69d)	0.7	2.12 γ 0.155(15)	11.0	
^{90}Y-citrate colloid	30%, 0.01-1 10%, >1 60%, <0.01		0.7			
^{90}Y-ferric hydroxide colloid	0.08-0.1	^{90}Sr-^{90}Y (^{90}Sr 28.8d)	0.7			

In radionuclide therapy, interstitial, intracavitary, intratumoral, and intraarterial injection through feeding artery to tumor, rely on microspheres distribution to ensure local confinement of the injected radiation dose. In all these and other diagnostic,

therapeutic, and related research applications, the size (or size range) of the particles must be chosen on the basis of the desired biodistribution and localization.

In medical research, radiolabeled microspheres of various sizes are used for studying physiological function (e.g. phagocytosis), circulatory physiology such as blood flow to various organs and tissues, presence of arteriovenous shunts and anastomotic flow. Radiolabeled microspheres are also indispensable research tools in development of biomedical methods based on nonradioactive microparticles. For example, radiolabeled nano- and microspheres are used widely for tracing biodistribution and in vivo fate of microparticulate drug delivery systems.

Radiolabeled microspheres are also currently the focus of extensive research for a number of other potential applications. A particularly interesting idea aims at a triple anticancer treatment - arterial occlusion, targeted chemotherapy and internal radiation. The idea is based on biodegradable microcapsules carrying both radiotherapeutic and chemotherapeutic agents for combination therapy of hepatic tumors.

Pr-142 beta emitting source

This study focuses on consideration of microspheres with uniformly distributed beta emitting Pr-142 beta source.

Praseodymium-142 emits about 96.3% beta rays with the endpoint energy 2.16 MeV, 3.7% of gamma rays with the energy 1.575 MeV, and very small portion X-rays

and electron capture energies per disintegration. The half-life of the isotope is about 19.12 hours and it significantly effects time management for clinical applications.

The calculation of average beta energy can be performed by eqn (2.30):

$$E_{\beta} = \frac{\int_{0}^{E_{max}} ES(E)\,dE}{\int_{0}^{E_{max}} S(E)\,dE}, \tag{2.30}$$

where S(E) is the relative number of beta particles in the spectrum with the energy between E and E+dE.

SADDE MOD 2 code developed by Reece in 1989 was used to generate beta spectrum for MCNP input. The SADDE MOD2 uses the subroutine BETA, originally developed at the Kansas State University by Richard Faw and Gale Simons. The beta spectrum calculation is made through several major steps described below.

First, using atomic number and atomic mass of the radionuclide, end point energy of beta particles, the yield and the degree of forbiddance for particular decay the BETA subroutine determines a normalized beta spectrum n(E) such that:

$$\int_{0}^{E_{max}} n(E)\,dE = 1 \tag{2.31}$$

The calculated spectrum is divided into 150 energy bins and then interpolated into 1500 values using a spline interpolation approach which is a form of interpolation where the interpolant is a special type of piecewise polynomial called a spline. Spline interpolation is preferred over polynomial interpolation because the interpolation error can be made small even when using low degree polynomials for the spline. Thus, spline interpolation avoids the problem of Runge's phenomenon which occurs when using high degree polynomials.The average energy of composite spectrum is calculated using the following equation:

$$E_{avg} = \int_{0}^{E_{max}} COMP(E)\,dE, \tag{2.32}$$

where COMP is an array storage with 1500 interpolated values and E_{max} is the maximum endpoint energy for the composite spectrum.

Next, the subroutine SADD calculates the scaled absorbed dose function $\varphi_{\beta}(x)$. The generated spectrum data (Fig. 2.2) is then used in MCNP input file for source description (Lee 2004).

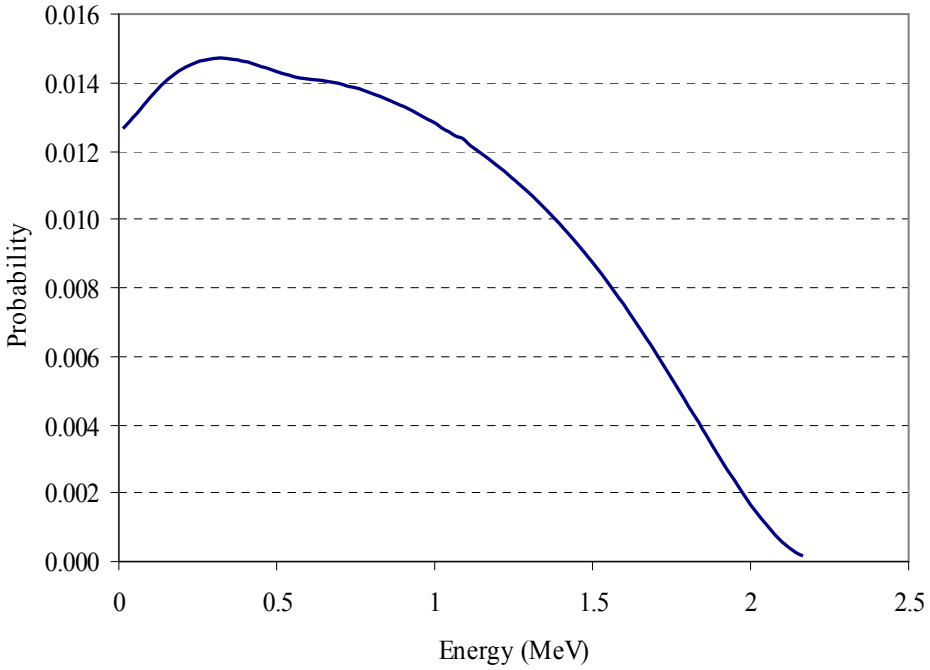

Fig. 2.2 Normalized beta spectrum for Pr-142

CHAPTER III

MICROSPHERES IN HUMAN ARTERIES

Spherical volume source

The dose rates presented here are based on Berger kernels published in 1971. Beta sources emit electrons in a spectrum of energies, however the average beta energy is used in the Berger kernel and the effect of the energy spectrum is folded into the dose distribution function:

$$\varsigma(\rho) = \frac{kE_{\beta}Y}{4\pi\delta\rho^{2}X_{90}} F_{\beta}\left(\frac{path}{X_{90}}\right), \tag{3.1}$$

where ρ is distance between source point and dose point (cm), k is unit conversion constant, Y is the beta yield per disintegration, E_{β} is the average beta energy, $F_{\beta}(path/X_{90})$ is the dimensionless scaled absorbed dose distribution as a function of the modified path length and the X_{90} distance, path is the modified path length between the source point and dose point (g/cm^2), δ is the density of the irradiated medium (g/cm^3) and X_{90} is the radius of the sphere with which 90% of the beta energy is deposited (Berger 1971). One may notice that $\varsigma(\rho)$ is in units of MeV/g.s when the unit conversion constant k is not used, and is converted into rad/hr when multiplied by k.

With respect to defined terms, dose can be determined as multiplication of point kernel described in eqn (3.1) and the source strength (SS). So for a given radiation and medium, the dose is given by multiplication of two factors. One factor depends only on the source terms of eqn (3.2) where all components are known and tabulated:

$$K = \frac{SSkE_{\beta}Y}{4\pi\delta X_{90}} \tag{3.2}$$

The other factor depends only on geometry terms and is a function of the source-to-point distance ρ and the modified "path".

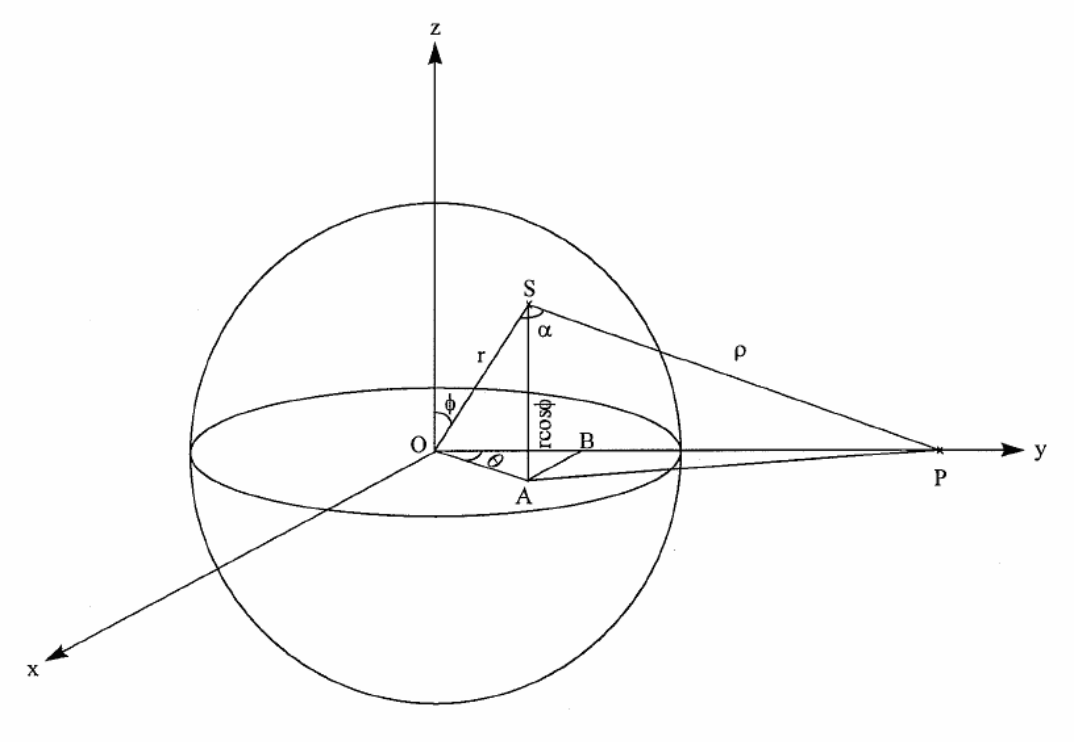

Fig. 3.1 Three-dimensional presentation of sphere

The three-dimensional geometry of a sphere is shown in Fig. 3.1 (Dauffy 1998). O is the center of the spherical source, S is the source point, P is the dose point situated on the y axis, A is the projection of S onto the xy plane, B is the projection of A onto the y axis, and r is the distance between the center of the sphere O and the point source S. The two angles necessary to situate a point in spherical coordinates are φ and θ. For purpose of calculation, another angle α between r and ρ has been added.

To simplify determining the value of variable "path", and therefore the dose, we divide the distance traveled by the beta particle into two parts: the distance traveled inside the spherical source ρ_s and the distance traveled outside, through tissue, ρ_t. The equation for ρ_s is:

$$\rho_s = r\cos\alpha + \sqrt{r^2\left(\cos\alpha^2 - 1\right) + R_{max}^2} \tag{3.3}$$

The modified path length between the source point and the dose point is given by eqn (3.4) where density of the source material is labeled "density" and the density of tissue is unity:

$$\text{path} = \rho_s \times \text{density} + \rho_t \tag{3.4}$$

For a single sphere dose calculation, symmetry allows the distances ρ, ρ_s and ρ_t to be calculated using two-dimensional geometry.

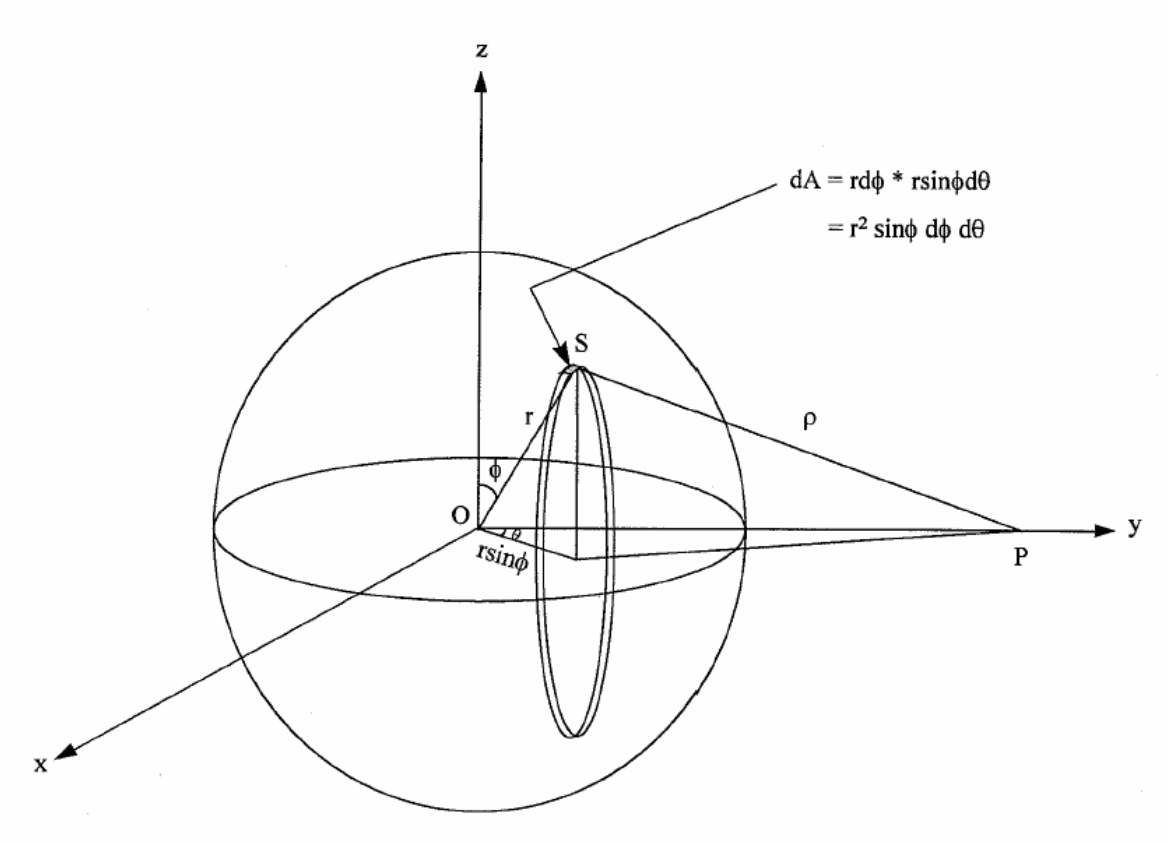

Fig. 3.2 Two-dimensional integration of a sphere

The integration of the volume of the sphere over θ is trivial, as shown in Fig. 3.2 above (Dauffy 1998) and eqn (3.5).

$$V = \int_0^r \int_0^{2\pi} \int_0^{\pi} r^2 \sin\varphi \, d\varphi d\theta dr = \int_0^{2\pi} d\theta \int_0^r \int_0^{\varphi} r^2 \sin\varphi \, d\varphi dr = 2\pi \int_0^r \int_0^{\varphi} r^2 \sin\varphi \, d\varphi dr \quad (3.5)$$

In this case, the expression for ρ is given by:

$$\rho^2 = r^2 + OP^2 - 2 \times OP \times r\cos\varphi\,, \tag{3.6}$$

where OP is the distance between the center of the sphere and the dose point.

The distance within the source ρ_s and the modified path have the same expression and are described by eqns (3.3) and (3.4) respectively.

Line of spherical volume sources

For a line of spheres we use a central sphere and an equal number of spheres below and above it. Dose rate for the central sphere is calculated using the two-dimensional model, and for other spheres the three-dimensional model. Fig. 3.3 (Dauffy 1998) illustrates this approach showing central sphere (#0) and one sphere (#1) below it. By symmetry, the dose resulting from the spheres lying below central one is the same as that from spheres above it.

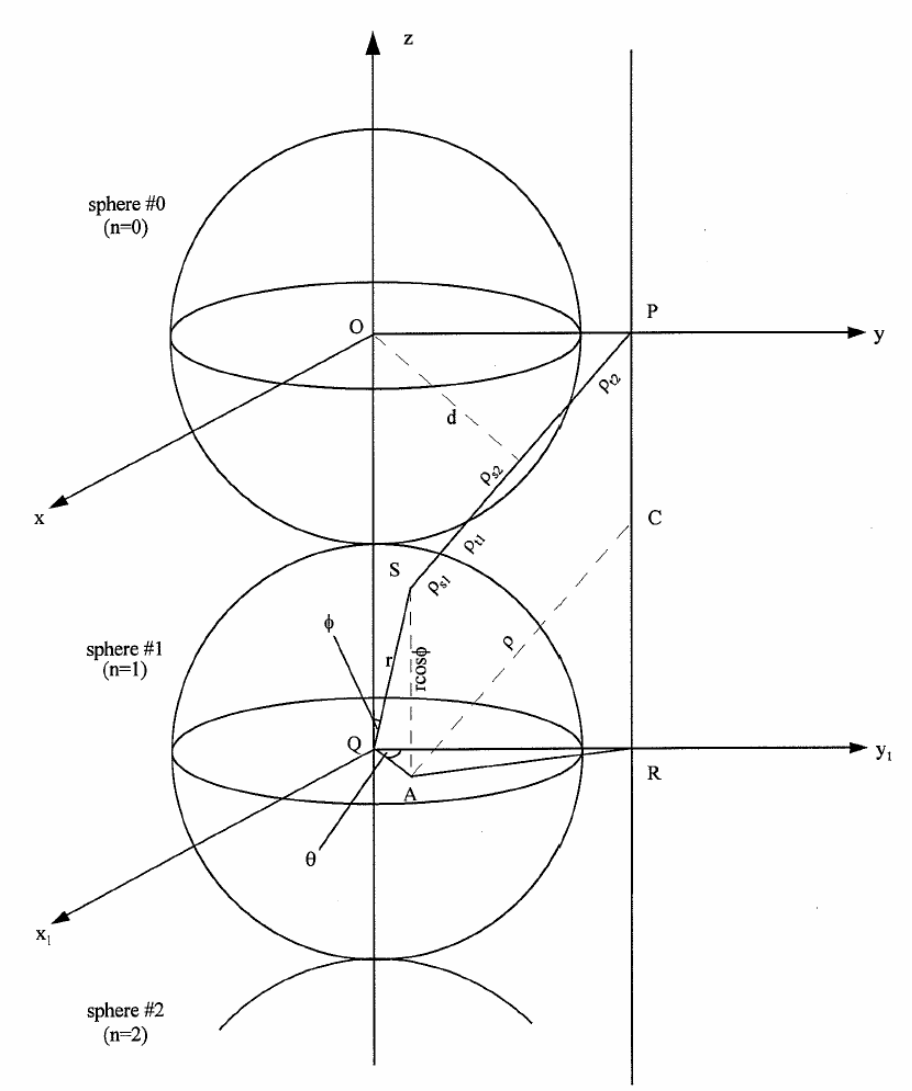

Fig. 3.3 Three-dimensional presentation of a line of spheres

Let ρ_{S1} be the distance traveled through the source sphere and ρ_{S2} be the sum of the distances traveled through all the other spheres. From the figure above the ρ_{S1} can be determined as:

$$\rho_{S1} = r\cos\alpha + \sqrt{r^2\left(\cos\alpha^2 - 1\right) + Rmax^2}\,, \tag{3.7}$$

The value of ρ_{S2} is calculated using a different approach. The shortest distance d between the center of a sphere and the source-to-dose point line SP is derived as (Selby 1967):

$$d = \sqrt{\frac{\left(cy_p + bz_0\right)^2 + a^2\left(y_p^2 + z_0^2\right)}{a^2 + b^2 + c^2}}\,, \tag{3.8}$$

where y_p is a y coordinate of point P

z_0 is a z coordinate of point O

$c = r\cos\varphi - 2nR_{max}$

n is number of sphere considered in line above

$b = r\sin\varphi\sin\varphi - OP$

$a = r\sin\varphi\sin\varphi$

The final relation between ρ_{S2} and d is determined from the Fig. 3.4 (Dauffy 1998).

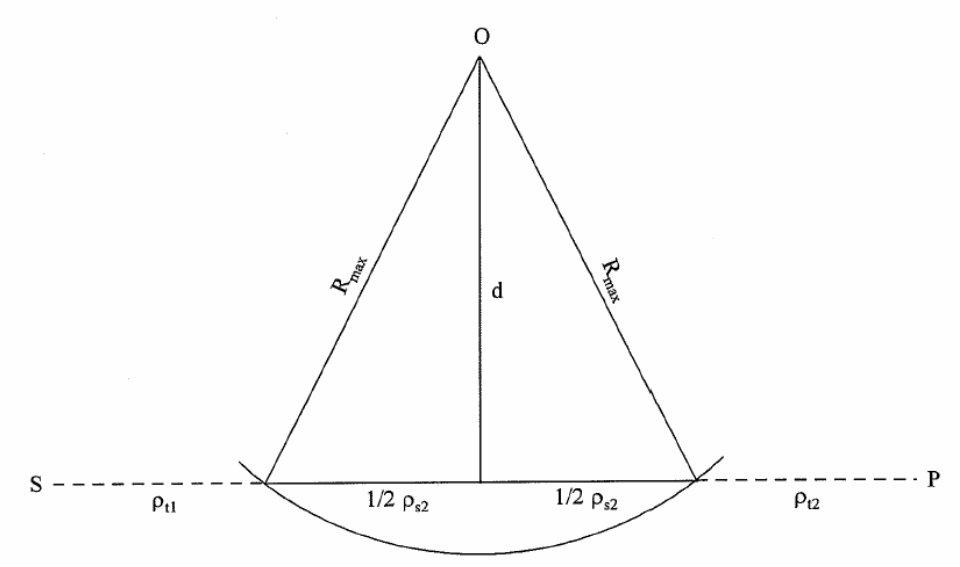

Fig. 3.4 Triangle inside a sphere

$$\rho_{S2} = 2\sqrt{R_{max}^2 - d^2} \tag{3.9}$$

Once the total distance traveled through the source media is found, the total distance traveled through the tissue is calculated using equation below:

$$\rho_t = \rho - (\rho_{S1} + \rho_{S2}) \tag{3.10}$$

Random packing of spheres in a cylinder

The dose to the arterial wall by microspheres is strongly affected by the packing ratio of the microspheres. Kepler's well known theory shows that hexagonal close packing is the densest method of filling. This study focuses on random packing which yields considerably smaller packing ratios of spheres in a cylinder. Several cases of sphere and cylinder sizes are considered and dose distribution is obtained at different distances around the cylinder.

The codes developed in FORTRAN and Visual Basic are used to simulate random packing and generate data for MCNP input files. Visual Basic provides visualization tools but consumes much more time to execute the code. On the other hand, FORTRAN saves calculation time for the actual simulations. Due to large number of calculations, the code developed in FORTRAN is used to generate the required set of sphere coordinates used in this study. The code developed in Visual Basic is used to provide visualization and to obtain data in the format suitable for incorporation into MCNP input file such as cell, surface and tally cards specification. The algorithm placed spheres randomly in the cylinder by specifying parameters of the model such as radius of the cylinder and spheres; and the number of attempts to be made to place spheres in the cylinder.

For this study the height of the cylinder is permanently set at 3.018 cm. One exception is made when the cylinder radius is 0.3 cm and the sphere's radius is 0.03 cm. This exception is made because of the restriction of the number of surfaces allowed in

MCNP input files. The number of spheres for this case exceeds the maximum allowable number of surfaces. For this case the cylinder height is reduced to 1.059 cm and equals the maximum electron path in tissue. The cylinder height of 1.059 cm works as well as 3.018 cm for this study; the difference is that the height of 3.018 cm gives an opportunity to collect 56 measurements for each distance after one MCNP run versus eight measurements in case with the height of 1.059 cm. The more data gathered in each run, the less total runs and time required to collect sufficient statistics. That is crucial for considering a wide variety of cases and collecting meaningful statistics for each of them.

The height of the cylinders is chosen based on the maximum range of emitted electrons by Pr-142 in water and the location of points of interest where the measurements of dose are taken. The maximum range of electrons in water is determined as 1.059 cm. The seven points of dose measurements were chosen along the cylinder axis with the steps of 0.15 cm starting from the middle. Thus required height is determined as:

$$\text{Cylinder height} = (3 \times 0.15 \text{ cm} + 1.059 \text{ cm}) \times 2 = 3.018 \text{ cm} \qquad (3.11)$$

Random numbers were generated by the imbedded FORTRAN random generator function. First, cylinder and sphere sizes are specified. The format of data is chosen to match that used in MCNP input files, so parameter units are centimeters or they are unitless. Next, x, y and z coordinates of spheres are generated based on uniform distribution within specified intervals. Let R and H be the cylinder radius and height

respectively; and r be the sphere radius. The x, y and z coordinate intervals can be determined through equations illustrated below:

$$\begin{aligned} -(R - r) \le x \le R - r, \\ -(R - r) \le y \le R - r, \\ r \le z \le H - r \end{aligned} \tag{3.12}$$

After choosing an x and y coordinates, the sphere coordinates are checked for fitting into the cylinder using sample rejection. The x and y coordinates are substituted into the circle equation below and the coordinates are accepted if they satisfy the condition:

$$x^2 + y^2 \le (R - r)^2 \tag{3.13}$$

Next, the sphere is checked for intersection with previously positioned spheres if any. If there is no intersection then the new sphere is positioned in the cylinder and the coordinates of this sphere are stored. This method of filling the cylinder with spheres doesn't consider sphere movement such as fall or rolling over the adjacent sphere after it is positioned at the specific location. Attempts to further fill the cylinder with spheres stop after a specified number of attempts to place randomly generated spheres in the cylinder.

Due to the nature of algorithm there is a spread of possible number of spheres placed in the cylinder. Results obtained in this study are based on the mode of the number of spheres placed in the cylinder. The mode for each case is determined through embedding necessary number of loops in the code. Table 3.1 presents the mode of the number of spheres observed for each case as well as corresponding packing ratio.

Table 3.1 Most probable number of spheres and packing ratios

Case (cylinder radius, cm / sphere radius, cm)	Number of spheres	Packing ratio
0.1/0.03	257	0.31
0.1/0.05	52	0.29
0.1/0.07	16	0.24
0.15/0.03	610	0.32
0.15/0.05	120	0.3
0.15/0.07	35	0.24
0.3/0.03 (H=1.059 cm)	910	0.34
0.3/0.05	538	0.33
0.3/0.07	184	0.31

This study covers several cases of cylinder and sphere radii. The selected cylinder radii are 0.1, 0.15 and 0.3 cm and sphere radii studied for each cylinder size are 0.03, 0.05 and 0.07 cm. This choice of cases is made based on dimensions of human arteries, sphere manufacturing specification and consistence with Lee's dissertation data (Lee 2004).

The MCNP limit of the maximum number of surfaces is set to 1000 and it restricts variety of cases that can be considered. For an example, for the case with cylinder radius of 0.15 cm and sphere radius of 0.01 cm even with modification of the cylinder height from 3.018 cm to 1.059 cm the number of spheres generated is about

5500. Obviously further decrement of cylinder height results in dose underestimation due to exclusion from consideration sources distant from the dose point beyond cylinder height but less than 1.059 cm.

Geometry used for multiple microspheres

The model used in this study matches the one used by Sung-Woo Lee (2004). The human artery is modeled as a cylinder of specific radius and sufficient height to establish the highest dose from beta-rays. Microspheres are modeled as spheres filled with Pr-142 beta emitting source. Specifically, the weight fraction of each sphere is praseodymium, 10.5%, oxygen, 63.2%, aluminum, 10.5%, and silicon, 15.8%. The Pr-142 is assumed to be uniformly distributed throughout the sphere and the sphere density is assumed to be 3 g/cm^3. Water is considered as tissue media in and around the cylinder.

Dose is calculated utilizing MCNP *F8 tallies for energy deposition in the cell and point detectors are approximated as spheres with the radius equal to 0.01 cm. Three different distances for placing detectors around the cylinder are considered. They are chosen as 0, 0.075 and 0.15 cm from the surface of the cylinder and correspond to a dose in drop of approximately 0, 50 and 75% respectively. Points beyond 0.3 cm from the surface were not studied because the dose at these distances is usually a factor of 10 lower than the surface doses. A graph of dose versus distance is presented in Fig. 3.5. The data graphed is for a cylinder radius of 0.15 cm and a sphere radius of 0.05 cm.

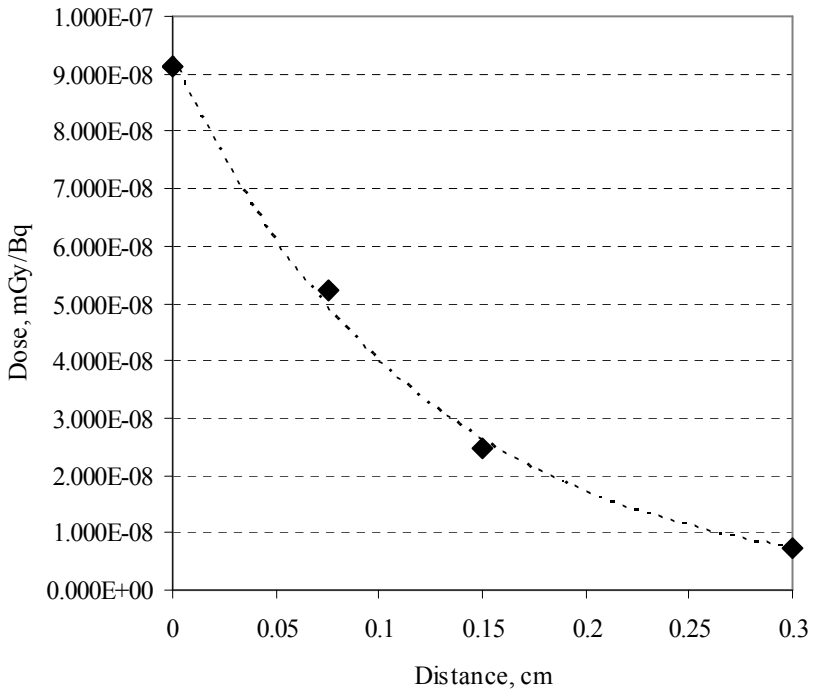

Fig. 3.5 Dose versus distance from the cylinder for a cylinder radius of 0.15 cm packed with 0.05 cm radius spheres

To obtain better data at each distance, 56 different detector locations are specified for each particular distance. The detectors are positioned around the cylinder and along its axis. Eight radial positions and seven axial locations are specified for each distance. The distance between detectors along the axis is 0.15 cm. As discussed earlier, the maximum range of electrons in water for Pr-142 betas is 1.059 cm and the height of the cylinder in the model is set to 3.018 cm. The schematic view of the model used in this study is presented on Fig. 3.6.

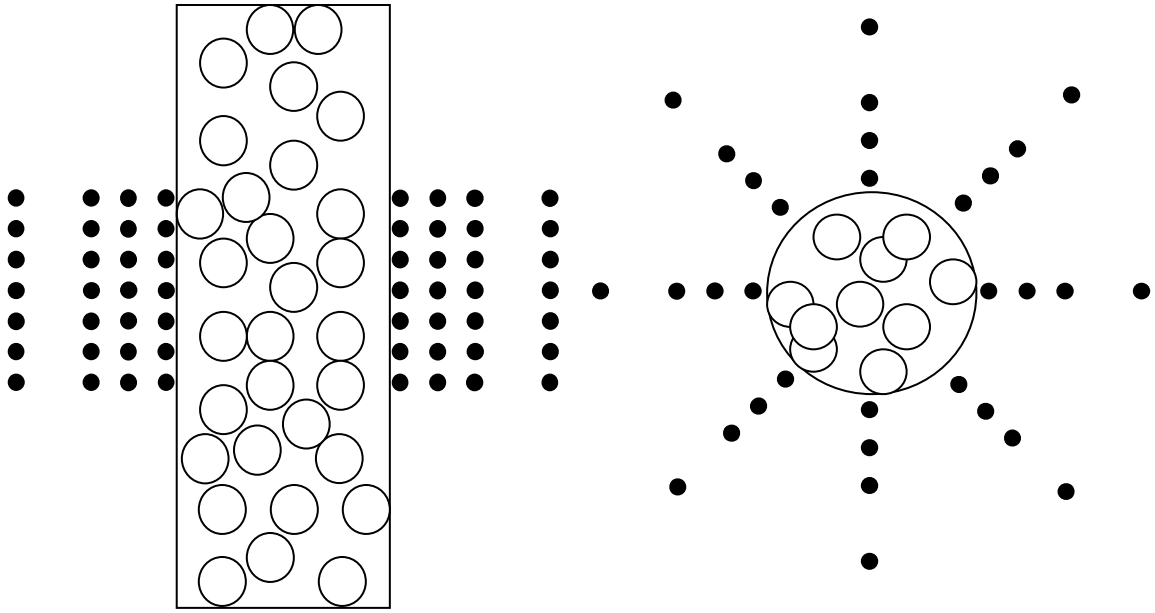

Fig. 3.6 Schematic view of model used in calculations (● - position of point detectors, ○ - microsphere)

This scheme determines dose distribution around the cylinder with acceptable error. The results are considered more detail in the next section. The same data points are used for limiting cases of uniformly distributed source and a line of spheres.

CHAPTER IV

RESULTS

Number of histories (simulations)

Important in MCNP simulations is a number of histories (simulations) generated - more histories yield more precise results and less random. However, a reasonable balance between the number of simulations and the cost of calculations should be struck for a particular application. The relative random error in the results as a function of simulation histories for a uniformly distributed cylindrical source with radius of 0.15 cm is shown on Fig. 4.1.

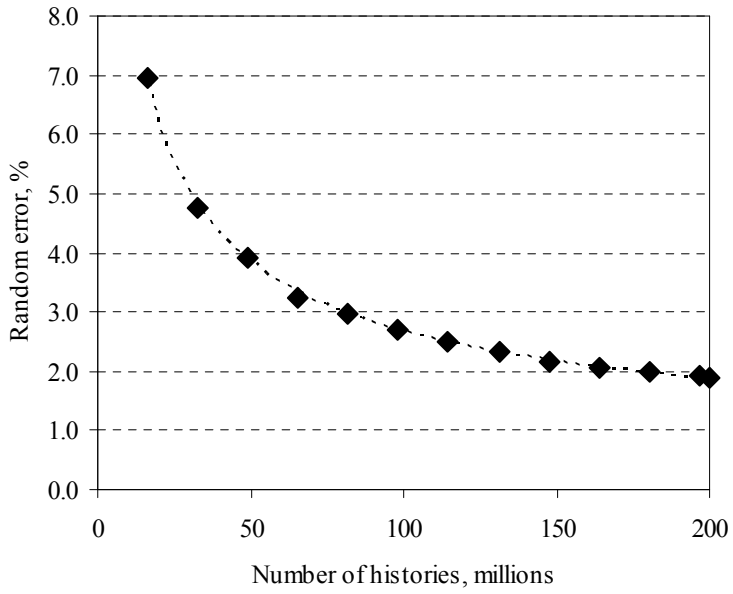

Fig. 4.1 Random error versus number of histories

The random error is correlated with the number of hits in the detector. When the total number of hits is small, one additional event in the detector causes sufficient change to the average dose. As number of histories increases the average dose to the detector becomes closer to the true value. The detectors distant from the cylinder have the lowest number of hits and therefore establish the upper boundary of calculation error. As expected from the properties of random error statistics, Fig. 4.1 indicates that the error decreases approximately as:

$$\text{error} \cong \frac{1}{\sqrt{\#\text{ of histories}}} \tag{4.1}$$

Two percent relative random error was deemed adequate for this study which sets the acceptable number of histories to 200 million.

Dose distribution

The dose distribution for each study case (a particular combination of cylinder and sphere radii) is determined based on unit source activity is presented as histograms in Figs. 4.2 - 4.10. The sphere case results for each cylinder size are plotted on the same figure. Eight intervals are chosen for plotting histograms and an average dose and its standard deviation are determined for each case. The intervals are chosen based on the

data spread throughout the sphere cases within a given cylinder size. The relative standard deviation is determined using eqn (4.2).

$$\text{Relative standard deviation} = \frac{\text{Standard deviation}}{\text{Average dose value}} * 100\% \qquad (4.2)$$

Figs. 4.2–4.4 illustrate the calculated distributions for a cylinder radius of 0.1 cm at three distances of interest.

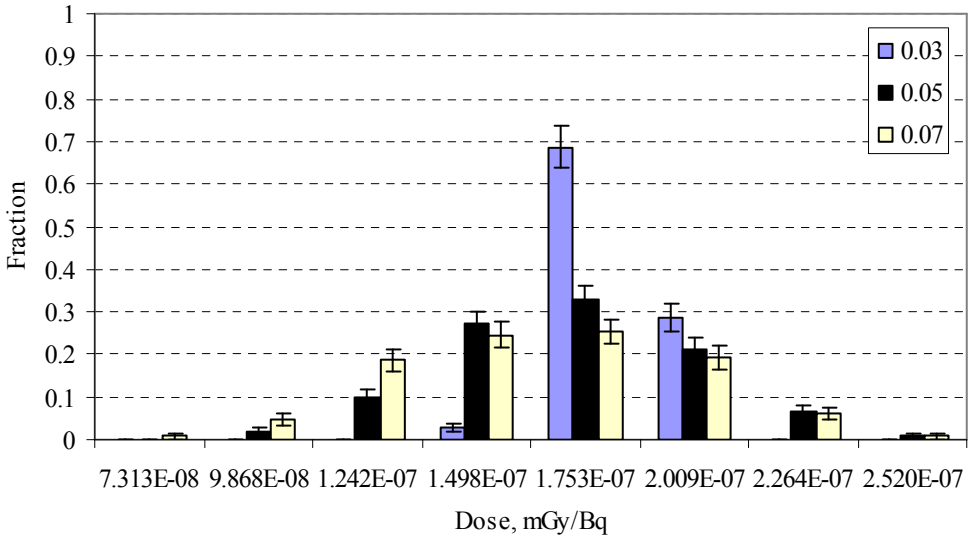

Fig. 4.2 Dose distribution for the cylinder radius of 0.1 cm at the distance of 0 cm (Note: As shown in the caption box 0.03 represents sphere radius of 0.03 cm)

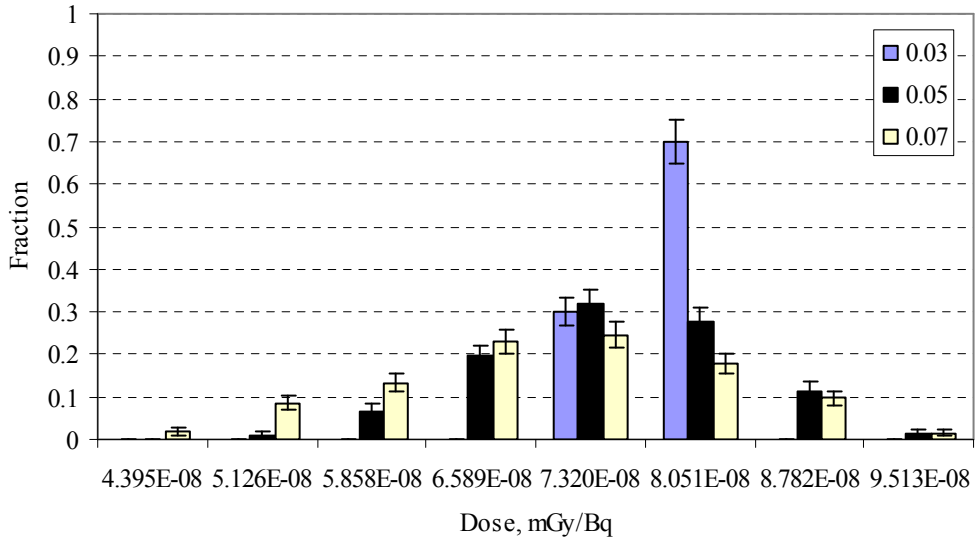

Fig. 4.3 Dose distribution for the cylinder radius of 0.1 cm at the distance of 0.075 cm

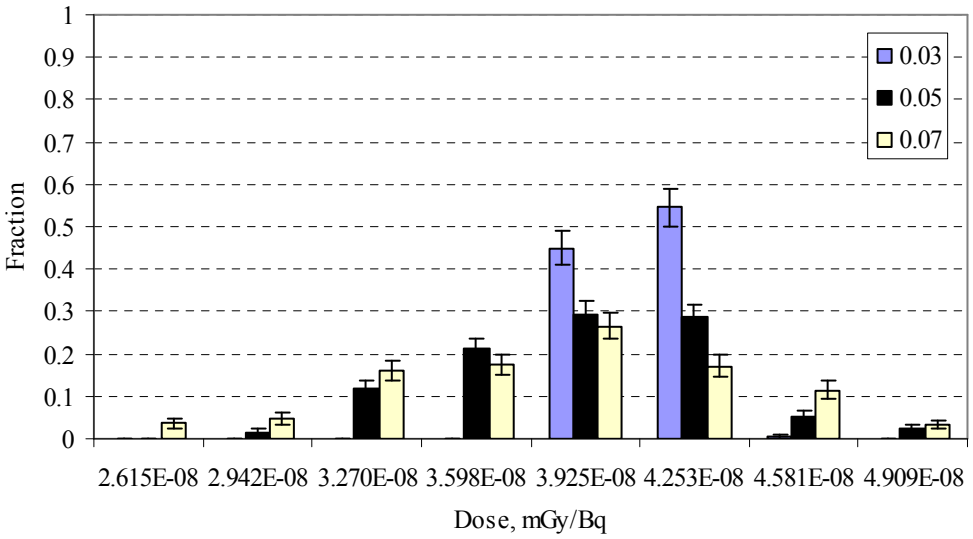

Fig. 4.4 Dose distribution for the cylinder radius of 0.1 cm at the distance of 0.15 cm

Figs. 4.5–4.7 present the calculated distributions for a cylinder radius of 0.15 cm at three distances of interest.

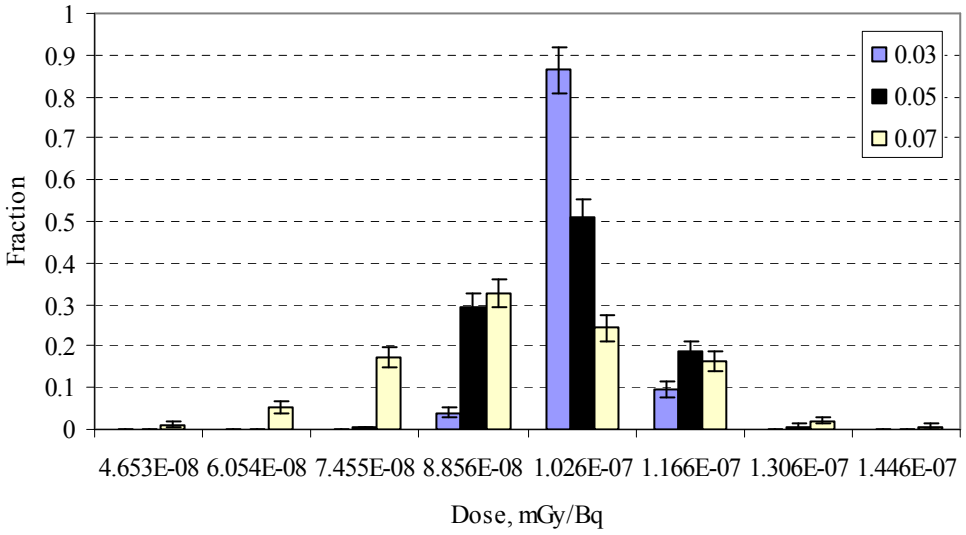

Fig. 4.5 Dose distribution for the cylinder radius of 0.15 cm at the distance of 0 cm

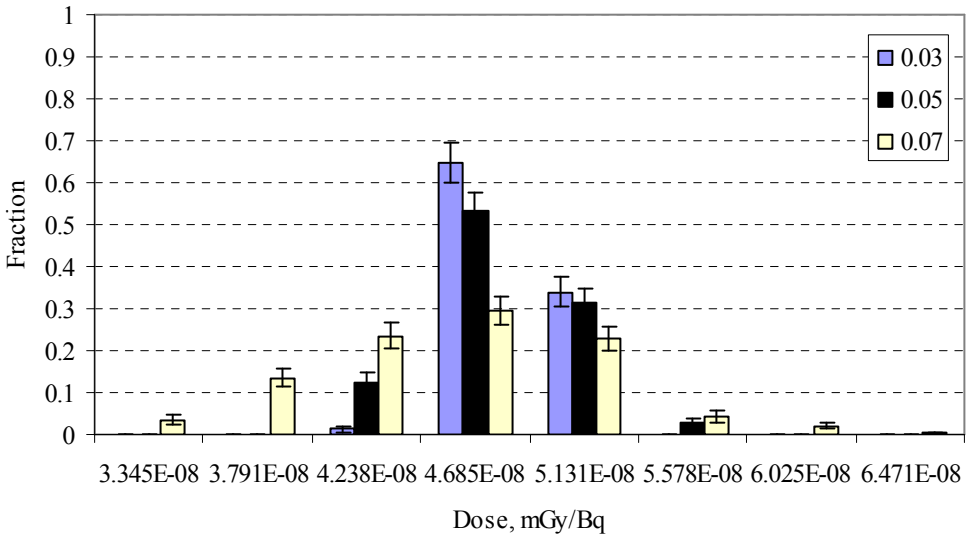

Fig. 4.6 Dose distribution for the cylinder radius of 0.15 cm at the distance of 0.075 cm

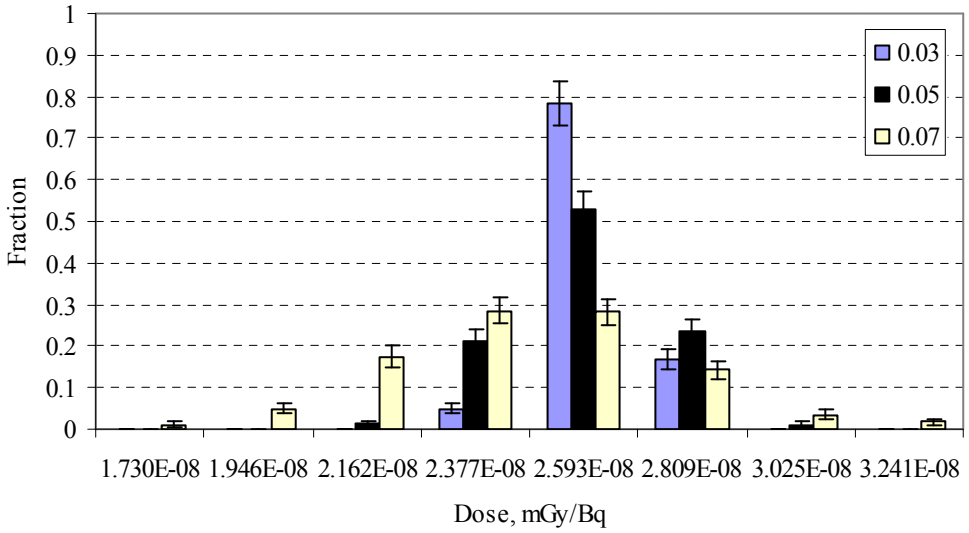

Fig. 4.7 Dose distribution for the cylinder radius of 0.15 cm at the distance of 0.15 cm

Figs. 4.8–4.10 illustrate the calculated distributions for a cylinder radius of 0.3 cm at three distances of interest.

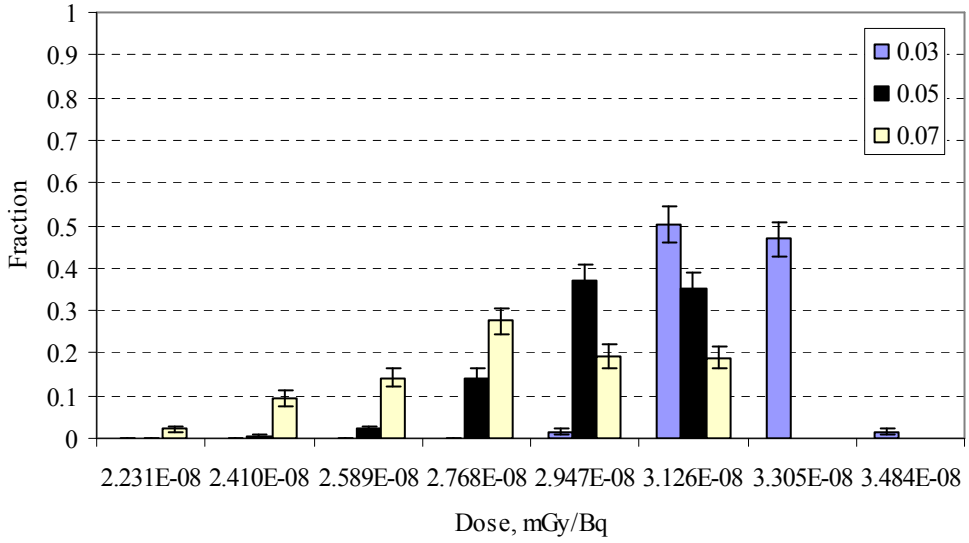

Fig. 4.8 Dose distribution for the cylinder radius of 0.3 cm at the distance of 0 cm

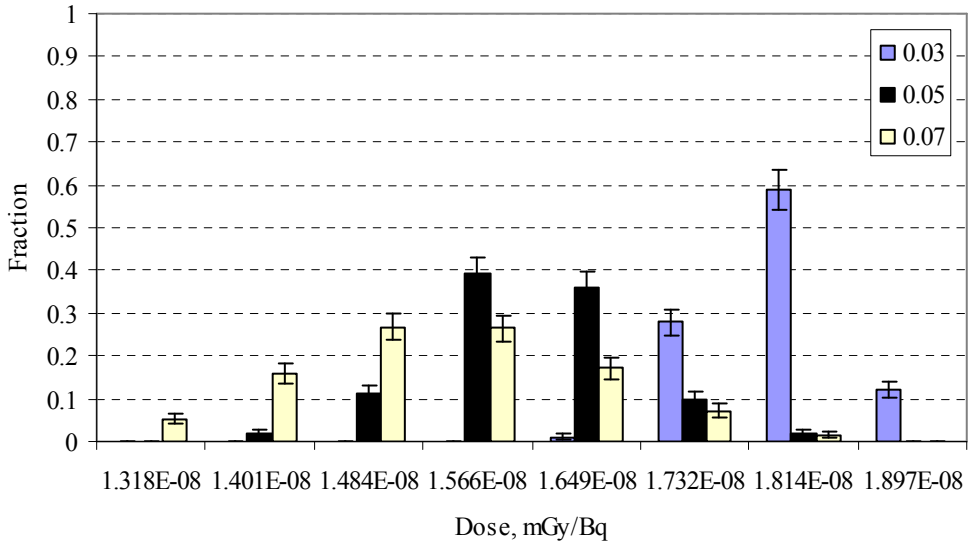

Fig. 4.9 Dose distribution for the cylinder radius of 0.3 cm at the distance of 0.075 cm

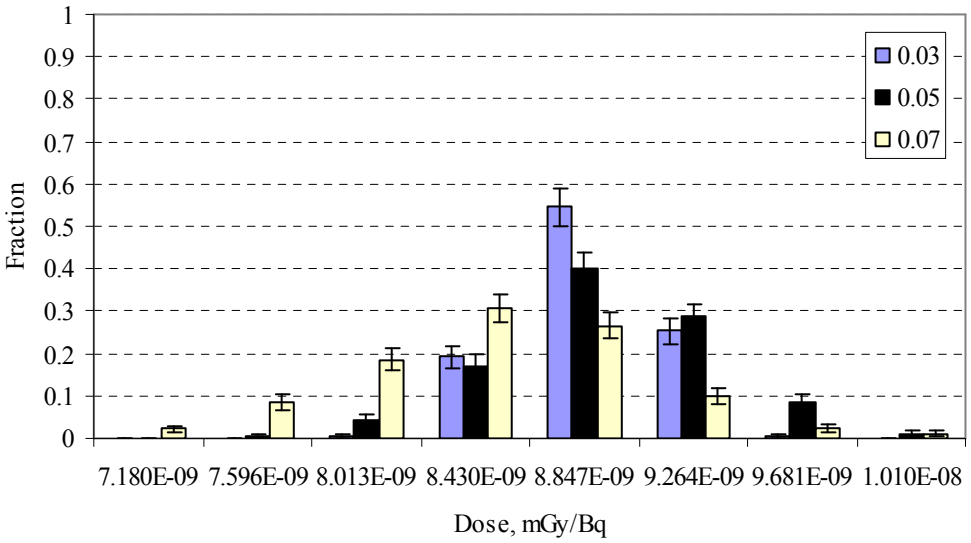

Fig. 4.10 Dose distribution for the cylinder radius of 0.3 cm at the distance of 0.15 cm

The figures above give a general idea about distribution shape and provide information regarding the average dose for each case and the relative standard deviations. The distributions plotted separately for each case are presented in Appendixes E-G. From Figs. 4.2–4.10 note that the smaller the sphere radius, the smaller the dose variance observed in each cylinder case. Also note that for the same sphere radius in different cylinder cases, the larger the cylinder size, the smaller the dose variances for a given sphere size.

Dose distribution shapes

Based on the shape of the dose distribution histograms as illustrated in the Appendixes E-G, a normal distribution can be fit within calculated error bars. This simplifies the dose calculations and gives an opportunity to specify target doses with known confidence intervals. As the average dose and relative standard deviation are determined for the chosen case, the target dose at the desired distance can be estimated within specific confidence intervals. Well-known confidence levels of 68, 90, 95 and 99 percent correspond to the 1, 1.64, 1.96 and 2.58 standard deviations respectively. Clinical use of microspheres requires consideration of affects on the target and surrounding tissues from dose variance at the distance of interest. The choice of the sphere radii should be made with an understanding of the spread in the dose values based on the data in this study.

Data collected

Tables 4.1–4.3 present calculated values of average doses and relative standard deviations (RSTD) at the distances of interest with respect to sphere and cylinder sizes as well as the sphere radius to the cylinder radius ratios (r/R).

Table 4.1 The average dose values and related variance at the distance of 0 cm

	Cylinder radius (R), cm								
	0.1			0.15			0.3		
Sphere radius (r), cm	r/R	Average dose, mGy/Bq	RSTD, %	r/R	Average dose, mGy/Bq	RSTD, %	r/R	Average dose, mGy/Bq	RSTD, %
0.03	0.30	1.696e-7	6.247	0.20	9.635e-8	4.759	0.10	3.123e-8	2.650
0.05	0.50	1.577e-7	17.698	0.33	9.418e-8	9.791	0.17	2.931e-8	5.776
0.07	0.70	1.517e-7	22.634	0.47	8.625e-8	20.368	0.23	2.761e-8	9.910

Table 4.2 The average dose values and related variance at the distance of 0.075 cm

	Cylinder radius (R), cm								
	0.1			0.15			0.3		
Sphere radius (r), cm	r/R	Average dose, mGy/Bq	RSTD, %	r/R	Average dose, mGy/Bq	RSTD, %	r/R	Average dose, mGy/Bq	RSTD, %
0.03	0.30	7.436e-8	3.413	0.20	4.609e-8	3.394	0.10	1.760e-8	2.787
0.05	0.50	7.072e-8	11.812	0.33	4.572e-8	6.346	0.17	1.563e-8	4.748
0.07	0.70	6.653e-8	16.269	0.47	4.371e-8	13.267	0.23	1.492e-8	7.411

Table 4.3 The average doses and related variance at the distance of 0.15 cm

	Cylinder radius (R), cm								
	0.1			0.15			0.3		
Sphere radius (r), cm	r/R	Average dose, mGy/Bq	RSTD, %	r/R	Average dose, mGy/Bq	RSTD, %	r/R	Average dose, mGy/Bq	RSTD, %
0.03	0.30	3.946e-8	2.876	0.20	2.512e-8	3.236	0.10	8.669e-9	3.010
0.05	0.50	3.756e-8	10.654	0.33	2.489e-8	5.950	0.17	8.729e-9	4.644
0.07	0.70	3.666e-8	14.559	0.47	2.362e-8	11.767	0.23	8.280e-9	6.663

The data above suggest that there is a correlation between r/R ratios and the average dose and the relative standard deviations. Picking two cases with the same r/R ratio from the Table 4.1, for example, the cylinder radius of 0.1 cm with the sphere radii of 0.03 cm and the cylinder radius of 0.15 cm and the sphere radii of 0.05 cm, note a correlation between an average dose and its relative variance. In the case with the cylinder radius of 0.15 cm and the sphere radii of 0.05 cm, there is about 50% decrease in the average dose value and about 50% increase in the relative standard deviation value with respect to the values for a cylinder radius of 0.1 cm. The difference of about 50% in values follows the difference in the cylinder sizes, which is also 50%. A linear correlation between the average dose values, the relative standard deviation values and the cylinder size within specified r/R ratio can be postulated. This correlation is true for the surface values but is not true for dose points off the surface.

Results verification

Doses from a uniformly distributed source and a line of spheres are calculated to verify results obtained in this study. The cylinder radii considered for the limiting cases are 0.1, 0.15 and 0.3 cm. The density of the media for uniformly distributed source case was set as the average density throughout the cylinder for the sphere cases in a given cylinder case. The cylinder size is the same as that for sphere cases and the radii of spheres in a line match the radius of the cylinder. The number of spheres is determined as 15, 10 and 5 for the cylinder radius of 0.1, 0.15 and 0.3 cm respectively.

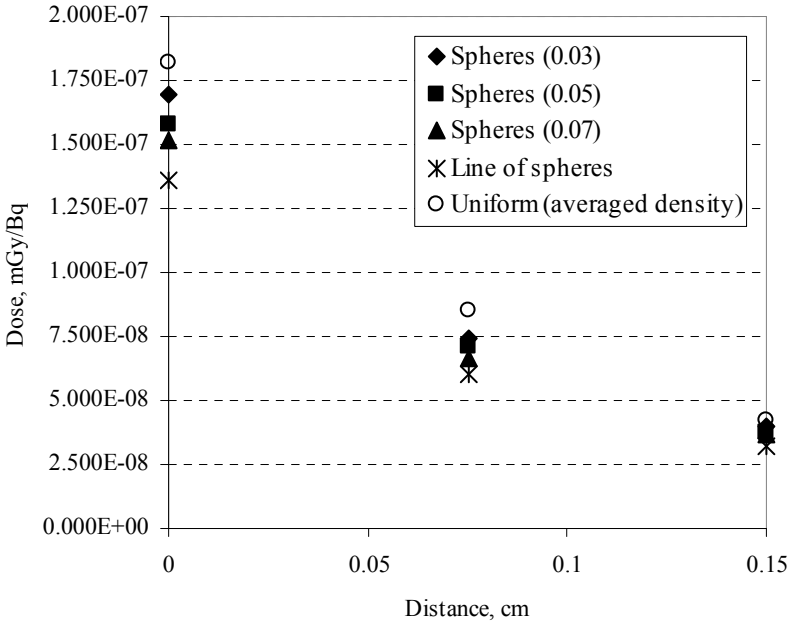

Fig. 4.11 Dose versus distance: cylinder radius of 0.1 cm
(Note: As shown in the caption box Spheres (0.03) represents sphere radii of 0.03 cm)

Fig. 4.11 illustrates the average dose for a cylinder with a radius of 0.1 cm. The locations of detectors for limiting cases are the same as those for the sphere cases. All simulations set the source activity to one becquerel over the volume of the source material. The dose decreases monotonically from the uniformly distributed source case to the sphere cases and then to the line of spheres case. These results can be explained if the attenuation property of media is taken into account. For the sphere cases with the same cylinder size, the difference in doses lies in source volume and the attenuation within the cylinder. All electrons originate in random locations within the spheres and the energy of each electron that exits the source sphere depends on the initial energy and the length of its path through the sphere. An electron loses more energy on average going through the sphere with the radius of 0.07 than through the ones with the radii of 0.05 and 0.03 cm. Beyond the source sphere the attenuation of the electron is effected by the volume of the material throughout the cylinder and its density.

The same explanation applies to the line of spheres and the uniformly distributed source for a given cylinder size. The uniformly distributed source case has the highest source volume but the density of intervening material is about two times lower than that of sphere material, so more electrons escape the cylinder. The density of the sphere material in the line of spheres case is the same as that in the sphere cases, but the volume of the dense material is larger in the line of spheres case and as a result the dose values are lower. Fig. 4.12 illustrates doses corresponding to the sphere, line and uniformly distributed source cases with the cylinder radius of 0.15 cm.

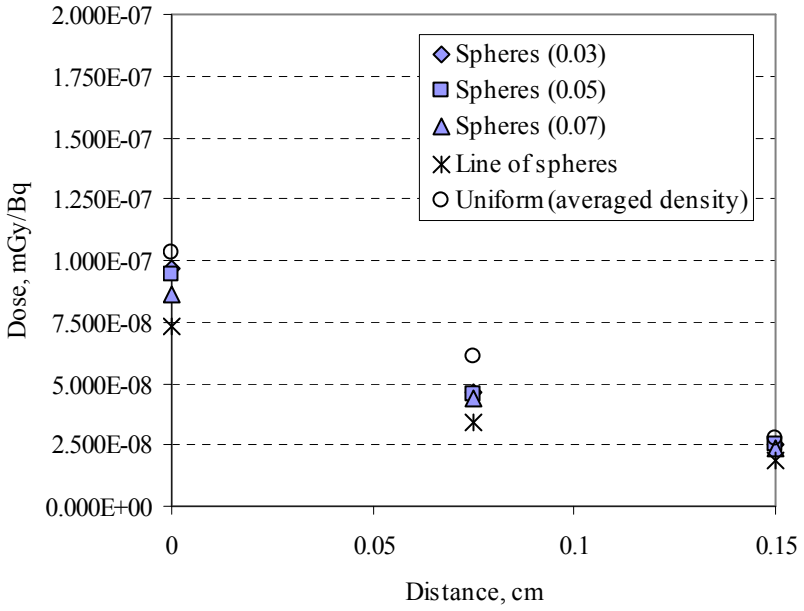

Fig. 4.12 Dose versus distance: cylinder radius of 0.15 cm

In Fig. 4.12 note that the microsphere results are bounded by a uniform cylinder source and a line of spheres. The absolute doses are smaller for the 0.15 cm cylinder compared to the 0.1 cm cylinder. The decline in the dose is caused by the increase in the volume of the dense source material. In the sphere cases, with increase of cylinder size, there is the increase in the number of spheres distributed in the cylinder. Thus we have more high density material throughout the cylinder. Fig. 4.13 presents results for the cases with the cylinder radius of 0.3 cm.

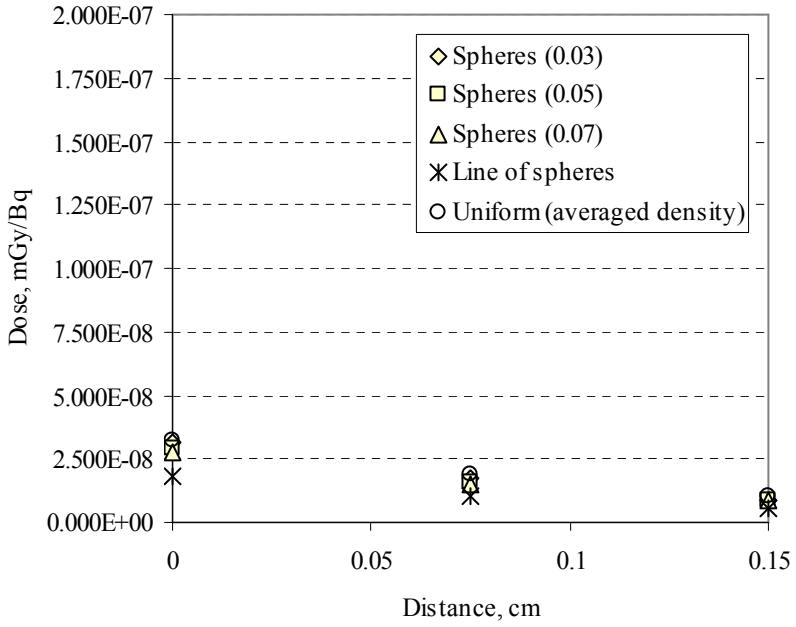

Fig. 4.13 Dose versus distance: cylinder radius of 0.3 cm

Fig. 4.13 follows the same pattern determined for the two previous cases. Based on these results some general conclusions can be made. Increasing the cylinder radius decreases the dose in all cases. Also in a given cylinder case, the dose is correlated to the sphere to cylinder radius (r/R) ratio. As the ratio increases the dose decreases.

An additional consistency check can be based on the difference of doses in each case versus the distance from the cylinder. The figures above show that the further the detectors are from the cylinder, the stronger the convergence among the results for the spheres, the uniformly distributed source, and the line of spheres cases.

Average dose estimation

For clinical applications the dose must be assessed accurately at any distance of interest. From Figs. 4.11-4.13 the correlation between average dose values and distance can be seen. Fig. 4.14 is a plot of average dose versus distance as a fraction of the surface doses.

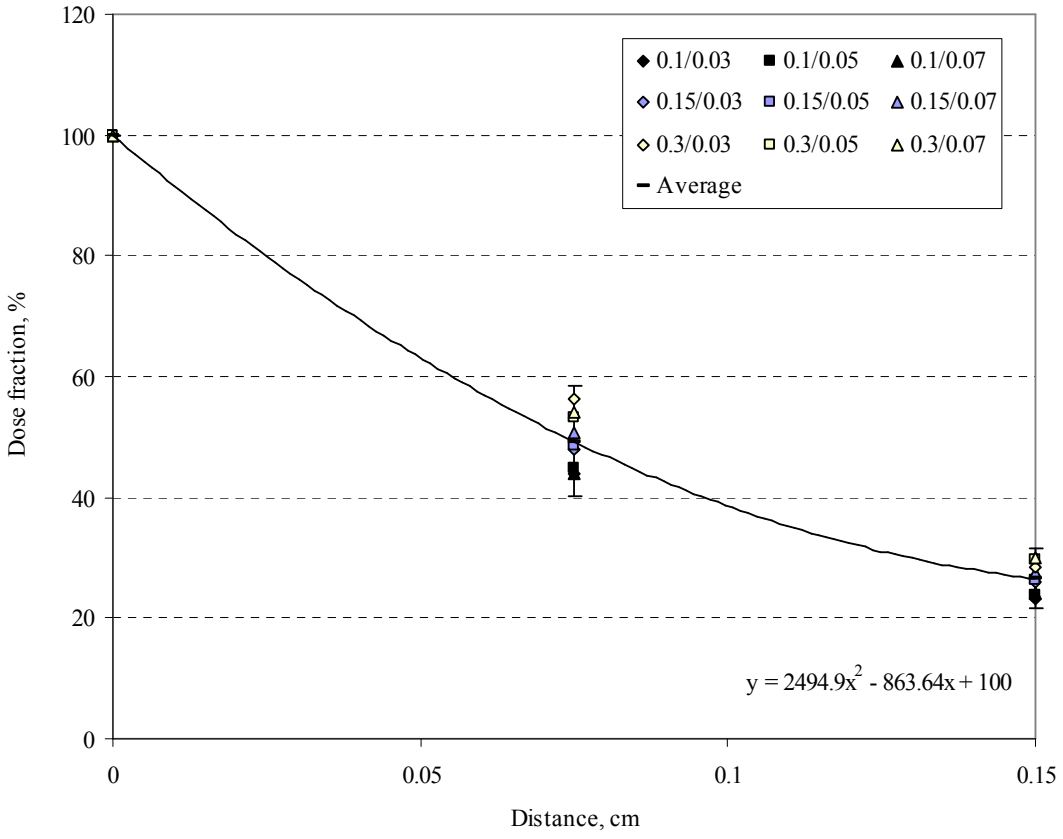

Fig. 4.14 Average dose fractions versus distance

The equation shown in Fig. 4.14 is based on the average dose fractions and provides an estimate of the average dose at distances out to 0.15 cm as a fraction of the surface dose. The error bars correspond to the 95% confidence level. For clinical application a simple and fast method is needed to calculate target dose values and the variance in dose. Uniformly distributed sources are very well studied and there are methods to determine the dose quickly and accurately. Ideally a correlation exists between sphere and uniformly distributed source cases. Tables 4.4–4.6 present correction factors between the uniformly distributed source and the sphere cases. The density of the media for uniformly distributed source case was set to the average density in the cylinder volume for the particular case. For the cylinder radii of 0.1, 0.15 and 0.3 cm this density corresponded to the most probable number of spheres is 1.5, 1.57 and 1.66 g/cm^3 respectively.

Table 4.4 Correction factors for the cylinder radius of 0.1 cm

	Distance from the cylinder surface, cm		
	0	0.075	0.15
	Uniformly distributed source (averaged density) Average dose, mGy/Bq		
	1.81789e-7	8.47771e-8	4.22929e-8
Sphere radius, cm	Average dose correction factors from uniform to sphere case		
0.03	0.933	0.877	0.933
0.05	0.867	0.834	0.888
0.07	0.835	0.785	0.867

Table 4.5 Correction factors for the cylinder radius of 0.15 cm

	Distance from the cylinder surface, cm		
	0	0.075	0.15
	Uniformly distributed source (averaged density) Average dose, mGy/Bq		
	1.03477e-7	6.12674e-8	2.74309e-8
Sphere radius, cm	Average dose correction factors from uniform to sphere case		
0.03	0.931	0.752	0.916
0.05	0.910	0.746	0.907
0.07	0.834	0.713	0.861

Table 4.6 Correction factors for the cylinder radius of 0.3 cm

	Distance from the cylinder surface, cm		
	0	0.075	0.15
	Uniformly distributed source (averaged density) Average dose, mGy/Bq		
	3.25155e-8	1.90368e-8	1.00897e-8
Sphere radius, cm	Average dose correction factors from uniform to sphere case		
0.03	0.960	0.924	0.859
0.05	0.901	0.821	0.865
0.07	0.849	0.784	0.821

Once surface doses are known we can predict doses throughout the volume studied. Fig. 4.15 presents the surface dose correction factors as a fraction of the surface dose for uniformly distributed source with respect to r/R ratio.

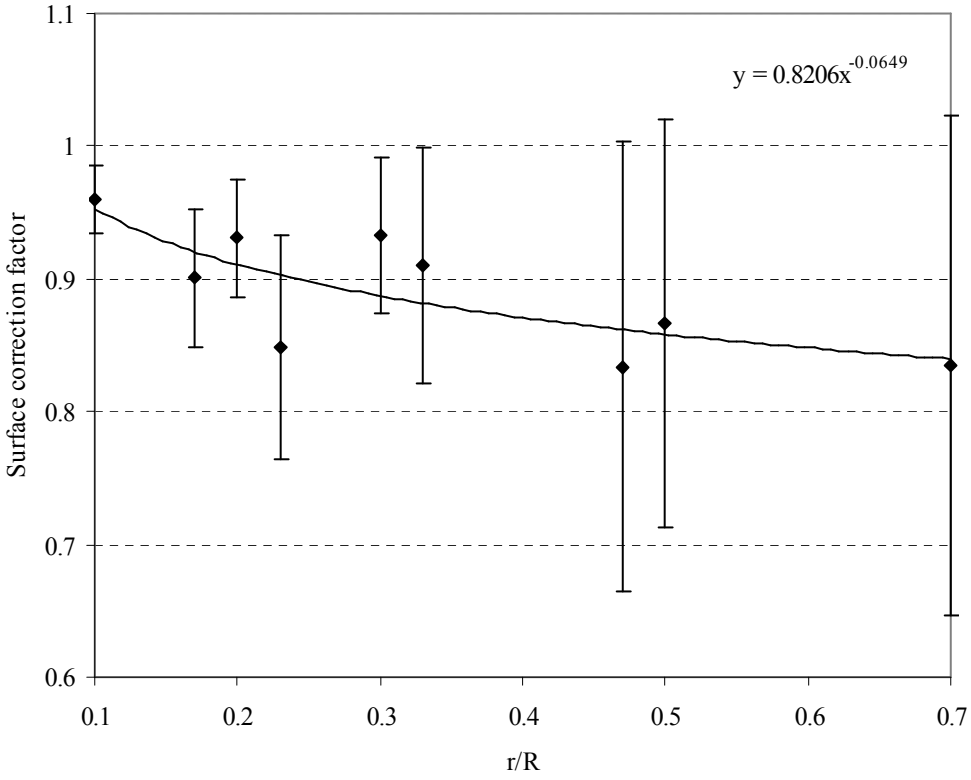

Fig. 4.15 Surface dose correction factors versus r/R ratio

Dose variance estimation

The dose variance can have an effect on the application of microsphere therapy. The next step is to determine how to assess dose variance. Fig. 4.16 illustrates the relative standard deviation values for each case at the distances of interest.

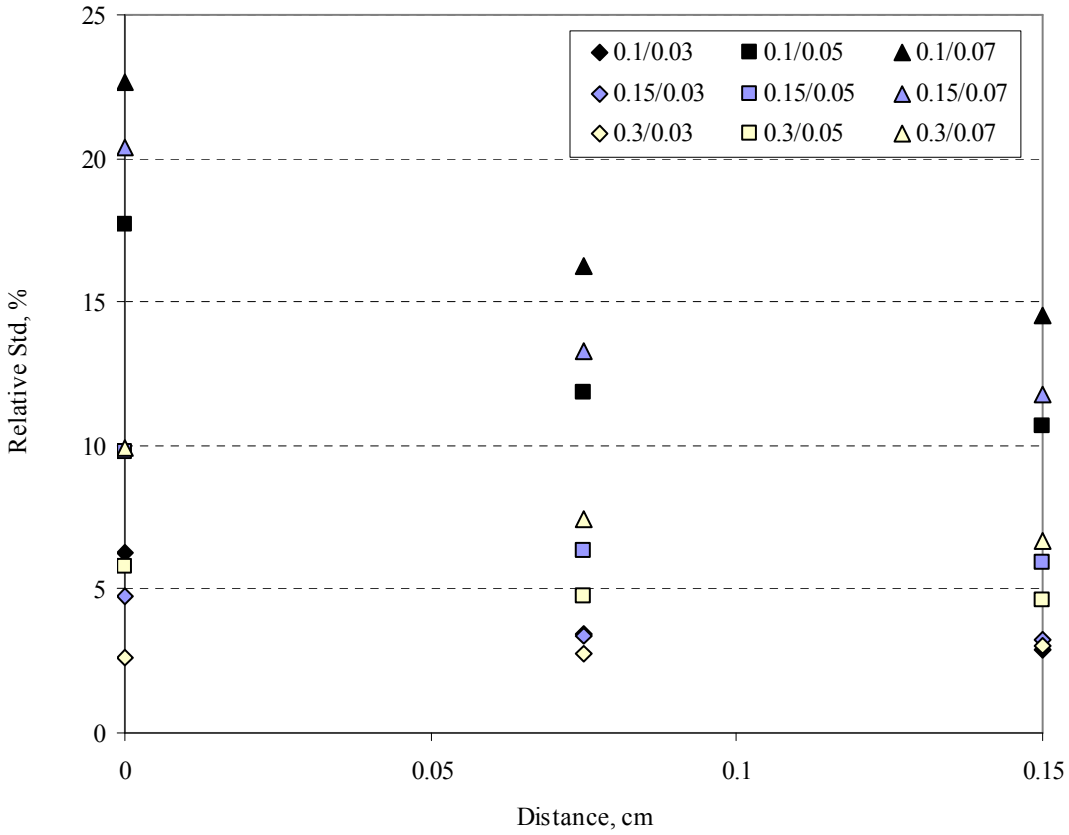

Fig. 4.16 Dose variance for each case at the distances of interest
(Note: As shown in the caption box 0.1/0.03 represents cylinder radius of 0.1 cm and sphere radius of 0.03 cm)

From Fig. 4.16 note that the relative standard deviations for each case are maximum on the surface of the cylinder, demonstrating that the sphere's distribution in a cylinder has a large effect on the dose variance. The further away the dose point, the lower the relative standard deviation. If we go far enough away, the variation is dominated by random error inherent in the Monte Carlo method. The MCNP statistical error increases with increasing distance from the source and plays the major role in dose variance at 0.3 cm. The variance for the cylinder radius of 0.3 cm and spheres radii of

0.03 cm actually increases instead of decreasing as expected, confirming the effect of the MCNP random calculation error.

Also note that the error decreases with the decreasing sphere radius to cylinder radius ratio. As the sphere size decreases within specified cylinder case, the uniformly distributed source case is approached. This correlation can be identified clearly for sphere cases in a given cylinder case as well as among the cylinder cases.

The correlation between the dose variances and distance from the cylinder is studied by determining the fractions of the dose variances with respect to the surface variance. Fig. 4.17 presents the dose variance fractions versus distance.

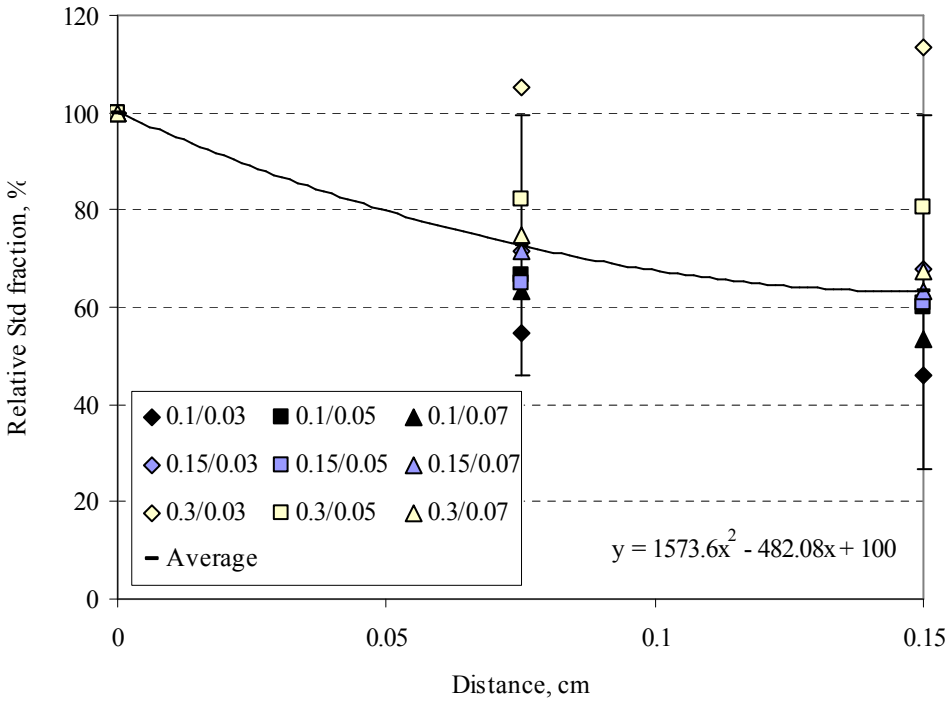

Fig. 4.17 Relative standard deviation versus distance
(Note: As shown in the caption box 0.1/0.03 represents cylinder radius of 0.1 cm and sphere radius of 0.03 cm)

The approximation equation is determined based on the average value of fractions. The related error corresponds to the 95% confidence level. The correlation allows estimation of the dose variance at any distance of interest as a fraction of the surface dose variances. The final step in the dose variance estimation technique is to find out a way to predict the surface dose variance.

Based on the data collected it is reasonable to find a correlation between the dose variances on the surface and the r/R ratios. Theoretically, we can expect the correlation curve to be a sigmoid. Fig. 4.18 presents the expected correlation curve between the surface dose variance and the r/R ratio.

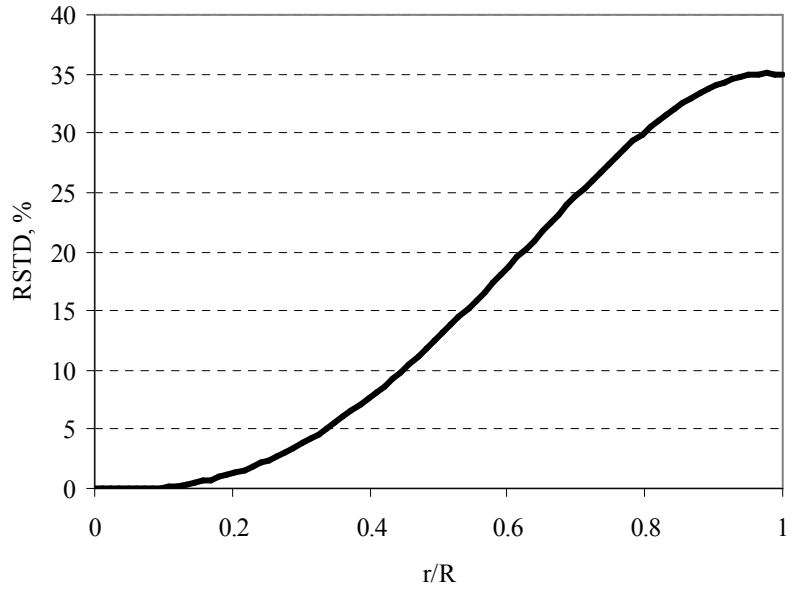

Fig. 4.18 Expected relative standard deviation versus r/R ratio

The minimum value on the curve, as r/R approaches zero, corresponds to the uniformly distributed source case. For this case we expect the variance to approach zero. The maximum value corresponds to the line of spheres case. For this case we expect to see the maximum variance of dose values due to geometrical distribution of spheres. Fig. 4.19 presents the relative standard deviation versus r/R ratio for each cylinder size.

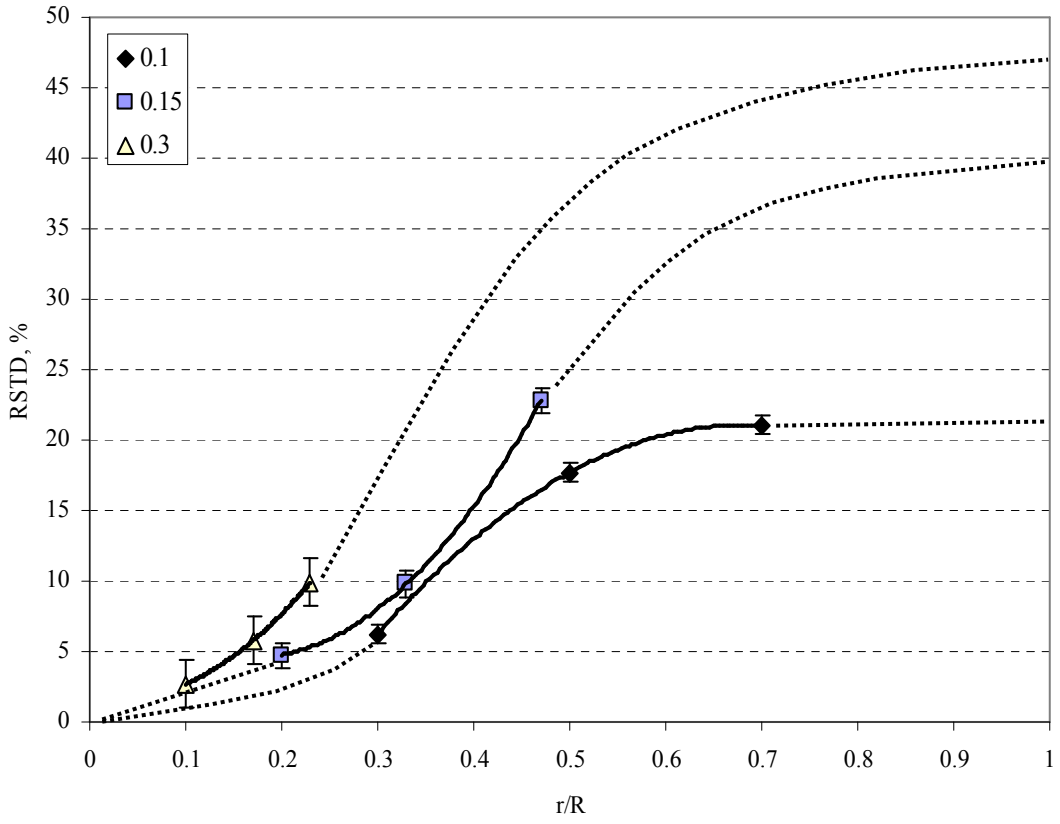

Fig. 4.19 Observed relative standard deviation versus r/R ratio (Note: As shown in the caption box 0.1 represents the cylinder radius of 0.1 cm)

The shape of the curve for the cylinder radius of 0.1 cm confirms the expected shape of the curve when the maximum of r/R ratio is approached. On the other hand the other two cases confirm the shape when the minimum of r/R ratio is approached. The dotted line represents the expected curves. Nevertheless for a clear validation additional data points are required. If the shape of the curves is confirmed then each of the curves representing different cylinder sizes can be approximated with the sigmoid equation. One of the possible sigmoid approximations is the cumulative Gaussian distribution (cdf). If this equation is utilized then the equation for each curve will have two parameters. When the equations are determined the correlation between the equation parameters and the sizes of spheres and cylinders can be found.

CHAPTER V

CONCLUSIONS

The purpose of this study was to determine the dose distribution for randomly packed microspheres and to develop a technique for estimating dose and its variance. A model consisting of a cylinder filled with microspheres was utilized. The cylinder height was set as 3.018 cm for all cases. Sphere radii of 0.03, 0.05 and 0.07 cm; and cylinder radii of 0.1, 0.15 and 0.3 cm were considered. The packing ratio of the spheres in the cylinder was about 0.3. Exception was made for two cases with the sphere radius to the cylinder radius ratio of about 0.2. For those cases the packing ratio of microspheres was about 0.2. Dose calculations were performed on the cylinder surface, and at distances where the dose is approximately 50% and 75% of the surface dose. Doses were calculated at 56 locations around the cylinder for each distance. The average dose and its relative standard deviation were determined based on five different random distributions of spheres for each case.

The random filling of the cylinder with microspheres was simulated by an algorithm developed in FORTRAN 95. The simulations of dose were performed using Monte Carlo Neutron Particle Code developed at the Los Alamos National Laboratory (X-5 Monte Carlo Team 2003). The dose values were determined through the MCNP *F8 tally for energy deposition in a cell. All calculations were performed for the source activity of one becquerel in the cylinder volume using Pr-142 as the beta source. The point detectors at the locations of interest were cast as spherical cells with a radius of

0.01 cm. The material uniformly distributed throughout the microspheres consisted of Pr-142, Al-27, O-16 and Si-28 and its density was assumed to be 3 g/cm^3. The tissue media density was equal to water.

The results obtained in the study included the average doses and the relative standard deviations for each case at the distances of interest. The dose distribution shape for each case was determined and shown as histograms.

The results were verified by comparing with two limiting cases: the line of spheres and the uniformly distributed source. The results obtained for the spheres cases lay between these two limiting cases. The dose values converged with the results obtained for the limiting cases with increasing distance.

Based on the data obtained, the following conclusions regarding correlations between the dose values, the relative standard deviations, and the radii of spheres and cylinders were made. Comparing average doses and dose variances for the same sphere radius in different cylinder cases led to the conclusion that the larger the cylinder size, the smaller the average dose and dose variance for a given sphere size.

A correlation between the sphere to cylinder radius ratios (r/R) and the average dose and its variance was found. Within a specified r/R ratio, a linear correlation exists between the average dose values, the related variances, and the cylinder size. The data suggest that with an increase in cylinder size there is a linear decrease of the average dose and an increase of the dose variance. For example, for the r/R ratio equal to 0.2, when the cylinder radius was increased from 0.15 cm to 0.3 cm there is about 100%

decrease of the average dose and about 100% increase of the dose variance. However this conclusion was true only for the dose values on the surface of the cylinder.

The distribution of the spheres within a cylinder had a major effect on the dose variance on the surface of the cylinder. The further away from the surface the dose points were, the lower the dose variance. MCNP calculation error increased with the distance from the source and was comparable to the geometric dose variance at 0.3 cm. If the dose variance approached the MCNP calculation error for a particular case, the error followed the MCNP error pattern and increased with distance from the cylinder.

Based on the data collected, the correlations between the average dose, its related variance, and distance from the cylinder were determined. An approach for estimating the surface average dose was developed and suggestions regarding an approach to assess surface variance estimation were presented. The dose distribution shapes could be approximated with the Gaussian distribution. This known distribution combined with the approaches developed for average dose and its variance prediction give an opportunity to determine the target dose and related variance within determined confidence intervals.

Although the microsphere applications in brachytherapy seem to be very promising, there is still a sufficient lack of knowledge in the application techniques and methods. The theoretical research of microsphere applications is the first essential step. The data available today covers a limited number of the microsphere sizes and filling techniques.

Future studies should extend the number of cases to provide theoretical basis for practical applications and confirm the conclusions made herein. A study of other

possible filling techniques should be performed. The advanced transport codes utilized today provide a high degree of accuracy for any geometry complexity, although some calculations consume large amounts of computer time. On the other hand, the point kernel methods require much less computational time and provide relatively high accuracy for simple geometries. For practical application the time to calculate target dose estimation can be very crucial. Future studies should examine applicability and advantages of different transport codes.

REFERENCES

American Brachytherapy Society. Brachytherapy description. www.americanbrachytherapy.org; Web site accessed on April 2006.

Archady, R. Microspheres, Microcapsules and Liposomes. Volume 3: Radiolabeled and Magnetic Particulates in Medicine and Biology. London: Citus Books; 2001.

Attix, F. H. Introduction to Radiological Physics and Radiation Dosimetry. New York: John Wiley and Sons, Inc; 1986.

Berger, M. J. Monte Carlo Calculation of the Penetration and Diffusion of Fast Charged Particles. Methods in Computational Physics. Volume 1. New York: Academic Press; 1963.

Bethe, H. A.; Ashkin, J. Experimental Nuclear Physics. Volume 1; New York: Wiley; 1953.

Blunck, O.; Leisegang, S. Zum Energieverlust schneller Elektronen in dünnen Schichten, Z. Physik. 128: 13-25; 1950.

Carlson, T. A. Photoelectron and Auger Spectroscopy. New York: Plenum Press; 1975.

Dauffy, L. Calculation of Dose to Soft Tissue from Implanted Beta Sources. Manchester: Heckman Bindery Inc; 1998, Thesis.

Heitler, W. Quantum Theory of Radiation. 3d ed. London: Oxford University Press; 1954.

Goudsmit, S.; Saunderson, J. L. Multiple Scattering of Electrons. Physics Review Journal. 57: 21-37; 1940.

Landau, L. On the Energy Loss of Fast Particles by Ionization. Journal of Physics. 8: 24-37; 1944.

Lee, Sung-Woo Beta Dose Calculation in Human Arteries for Various Brachytherapy Seed Types. College Station, TX: Texas A&M University; 2004, Dissertation.

Mayfield Clinic. Brain tumors. www.mayfieldclinic.com; Web site accessed on April 2006.

Riley, M. E.; MacCallum, C. J.; Biggs, F. Theoretical Electron-Atom Elastic Scattering Cross Sections. Selected Elements, 1 keV to 256 keV. Atomic and Nuclear Data Tables. 15: 37-45; 1975.

Rutherford, E. The Scattering of α and β Particles by Matter and the Structure of the Atom. Philosophy Magazine. 21: 10-23; 1911.

Seltzer, S. M. An Overview of ETRAN Monte Carlo Methods. Monte Carlo Transport of Electrons and Photons. New York: Plenum Press; 1988.

Sternheimer, R. M.; Berger, M. J.; Seltzer, S. M. Density Effect for the Ionization Loss of Charged Particles in Various Substances. Physics Review Journal. B26: 27-32; 1982.

Sternheimer, R. M.; Peierls, R. F. General Expression for the Density Effect for the Ionization Loss of Charged Particles. Physics Review Journal. B3: 11-20; 1982.

X-5 Monte Carlo Team. MCNP – A General Monte Carlo N-Particle Transport Code, Version 5. Los Alamos, NM: Los Alamos National Laboratory; 2003.

APPENDIX A

FLOW CHART OF RANDOM FILLING ALGORITHM

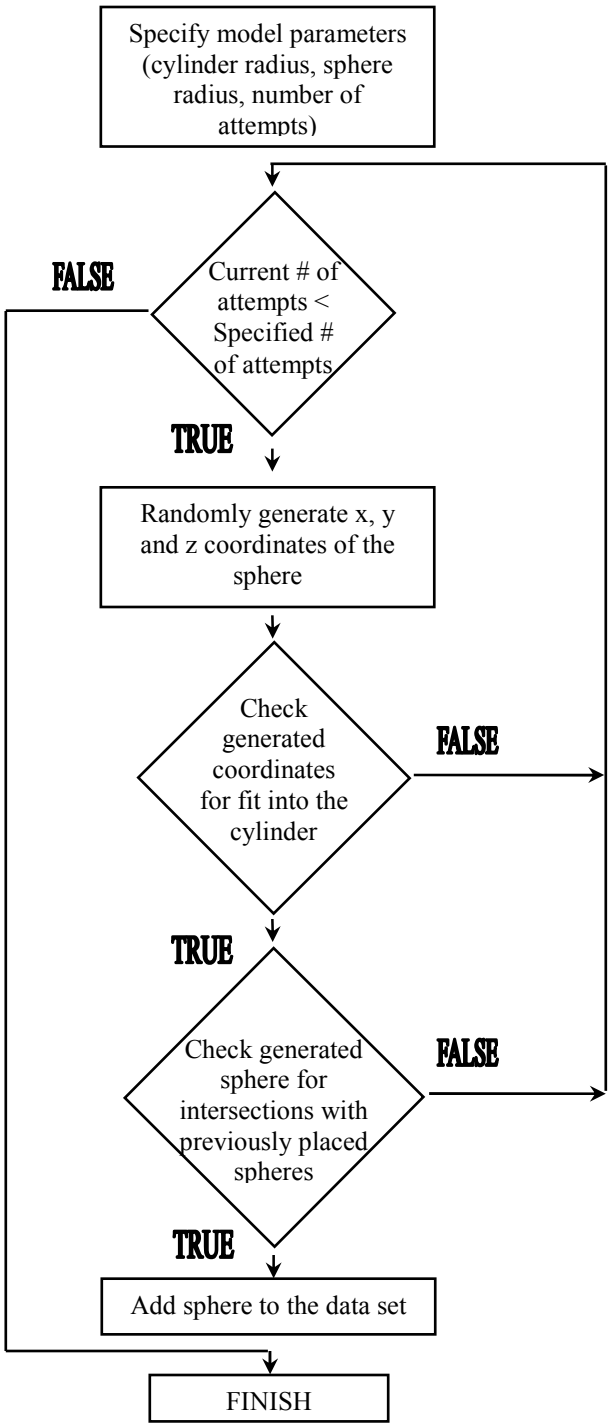

Fig. A.1 Flowchart of filling algorithm developed in FORTRAN

APPENDIX B

MCNP INPUT FILE

```
c Case: cylinder radius = 0.15 cm (middle case in the sizes set)
c       cylinder height = 3.018 cm (2*1.059+2*0.45)
c       sphere radius   = 0.05 cm
c       # of spheres    = 120 (most probable)
c Coordinates of spheres generated using code written in FORTRAN
c Packing ration = 0.31 (volume of spheres / cylinder volume)
c Detector locations: along the axe: Z = 1.059 cm
c                                       1.209 cm
c                                       1.359 cm
c                                       1.509 cm
c                                       1.659 cm
c                                       1.809 cm
c                                       1.959 cm
c Distance from the cylinder: 0 cm, 0.15cm, 0.3cm, 0.45cm
c
c*************************************
c***************CELL CARD***************
c*************************************
c
c 1-st # - cell #
c 2-nd # - material #
c 3-d #  - density
c 4-th # - surfaces #'s defining cell
c
c Spheres cells
c
1 1 -3 -1
2 1 -3 -2
3 1 -3 -3
4 1 -3 -4
5 1 -3 -5
6 1 -3 -6
7 1 -3 -7
8 1 -3 -8
9 1 -3 -9
10 1 -3 -10
11 1 -3 -11
12 1 -3 -12
13 1 -3 -13
14 1 -3 -14
15 1 -3 -15
16 1 -3 -16
17 1 -3 -17
18 1 -3 -18
19 1 -3 -19
20 1 -3 -20
21 1 -3 -21
22 1 -3 -22
23 1 -3 -23
24 1 -3 -24
25 1 -3 -25
26 1 -3 -26
27 1 -3 -27
28 1 -3 -28
```

```
29 1 -3 -29
30 1 -3 -30
31 1 -3 -31
32 1 -3 -32
33 1 -3 -33
34 1 -3 -34
35 1 -3 -35
36 1 -3 -36
37 1 -3 -37
38 1 -3 -38
39 1 -3 -39
40 1 -3 -40
41 1 -3 -41
42 1 -3 -42
43 1 -3 -43
44 1 -3 -44
45 1 -3 -45
46 1 -3 -46
47 1 -3 -47
48 1 -3 -48
49 1 -3 -49
50 1 -3 -50
51 1 -3 -51
52 1 -3 -52
53 1 -3 -53
54 1 -3 -54
55 1 -3 -55
56 1 -3 -56
57 1 -3 -57
58 1 -3 -58
59 1 -3 -59
60 1 -3 -60
61 1 -3 -61
62 1 -3 -62
63 1 -3 -63
64 1 -3 -64
65 1 -3 -65
66 1 -3 -66
67 1 -3 -67
68 1 -3 -68
69 1 -3 -69
70 1 -3 -70
71 1 -3 -71
72 1 -3 -72
73 1 -3 -73
74 1 -3 -74
75 1 -3 -75
76 1 -3 -76
77 1 -3 -77
78 1 -3 -78
79 1 -3 -79
80 1 -3 -80
81 1 -3 -81
82 1 -3 -82
```

```
83 1 -3 -83
84 1 -3 -84
85 1 -3 -85
86 1 -3 -86
87 1 -3 -87
88 1 -3 -88
89 1 -3 -89
90 1 -3 -90
91 1 -3 -91
92 1 -3 -92
93 1 -3 -93
94 1 -3 -94
95 1 -3 -95
96 1 -3 -96
97 1 -3 -97
98 1 -3 -98
99 1 -3 -99
100 1 -3 -100
101 1 -3 -101
102 1 -3 -102
103 1 -3 -103
104 1 -3 -104
105 1 -3 -105
106 1 -3 -106
107 1 -3 -107
108 1 -3 -108
109 1 -3 -109
110 1 -3 -110
111 1 -3 -111
112 1 -3 -112
113 1 -3 -113
114 1 -3 -114
115 1 -3 -115
116 1 -3 -116
117 1 -3 -117
118 1 -3 -118
119 1 -3 -119
120 1 -3 -120
c
c Tally cells
c
9011 2 -1 -9011
9012 2 -1 -9012
9013 2 -1 -9013
9014 2 -1 -9014
9015 2 -1 -9015
9016 2 -1 -9016
9017 2 -1 -9017
c
9021 2 -1 -9021
9022 2 -1 -9022
9023 2 -1 -9023
9024 2 -1 -9024
9025 2 -1 -9025
```

```
9026 2 -1 -9026
9027 2 -1 -9027
c
9031 2 -1 -9031
9032 2 -1 -9032
9033 2 -1 -9033
9034 2 -1 -9034
9035 2 -1 -9035
9036 2 -1 -9036
9037 2 -1 -9037
c
9041 2 -1 -9041
9042 2 -1 -9042
9043 2 -1 -9043
9044 2 -1 -9044
9045 2 -1 -9045
9046 2 -1 -9046
9047 2 -1 -9047
c
c
*************************************************************************
c
9111 2 -1 -9111
9112 2 -1 -9112
9113 2 -1 -9113
9114 2 -1 -9114
9115 2 -1 -9115
9116 2 -1 -9116
9117 2 -1 -9117
c
9121 2 -1 -9121
9122 2 -1 -9122
9123 2 -1 -9123
9124 2 -1 -9124
9125 2 -1 -9125
9126 2 -1 -9126
9127 2 -1 -9127
c
9131 2 -1 -9131
9132 2 -1 -9132
9133 2 -1 -9133
9134 2 -1 -9134
9135 2 -1 -9135
9136 2 -1 -9136
9137 2 -1 -9137
c
9141 2 -1 -9141
9142 2 -1 -9142
9143 2 -1 -9143
9144 2 -1 -9144
9145 2 -1 -9145
9146 2 -1 -9146
9147 2 -1 -9147
c
```

```
c
*********************************************************************
c
9211 2 -1 -9211
9212 2 -1 -9212
9213 2 -1 -9213
9214 2 -1 -9214
9215 2 -1 -9215
9216 2 -1 -9216
9217 2 -1 -9217
c
9221 2 -1 -9221
9222 2 -1 -9222
9223 2 -1 -9223
9224 2 -1 -9224
9225 2 -1 -9225
9226 2 -1 -9226
9227 2 -1 -9227
c
9231 2 -1 -9231
9232 2 -1 -9232
9233 2 -1 -9233
9234 2 -1 -9234
9235 2 -1 -9235
9236 2 -1 -9236
9237 2 -1 -9237
c
9241 2 -1 -9241
9242 2 -1 -9242
9243 2 -1 -9243
9244 2 -1 -9244
9245 2 -1 -9245
9246 2 -1 -9246
9247 2 -1 -9247
c
c
*********************************************************************
c
9311 2 -1 -9311
9312 2 -1 -9312
9313 2 -1 -9313
9314 2 -1 -9314
9315 2 -1 -9315
9316 2 -1 -9316
9317 2 -1 -9317
c
9321 2 -1 -9321
9322 2 -1 -9322
9323 2 -1 -9323
9324 2 -1 -9324
9325 2 -1 -9325
9326 2 -1 -9326
9327 2 -1 -9327
c
```

```
9331 2 -1 -9331
9332 2 -1 -9332
9333 2 -1 -9333
9334 2 -1 -9334
9335 2 -1 -9335
9336 2 -1 -9336
9337 2 -1 -9337
C
9341 2 -1 -9341
9342 2 -1 -9342
9343 2 -1 -9343
9344 2 -1 -9344
9345 2 -1 -9345
9346 2 -1 -9346
9347 2 -1 -9347
C
C
*********************************************************************
C
9411 2 -1 -9411
9412 2 -1 -9412
9413 2 -1 -9413
9414 2 -1 -9414
9415 2 -1 -9415
9416 2 -1 -9416
9417 2 -1 -9417
C
9421 2 -1 -9421
9422 2 -1 -9422
9423 2 -1 -9423
9424 2 -1 -9424
9425 2 -1 -9425
9426 2 -1 -9426
9427 2 -1 -9427
C
9431 2 -1 -9431
9432 2 -1 -9432
9433 2 -1 -9433
9434 2 -1 -9434
9435 2 -1 -9435
9436 2 -1 -9436
9437 2 -1 -9437
C
9441 2 -1 -9441
9442 2 -1 -9442
9443 2 -1 -9443
9444 2 -1 -9444
9445 2 -1 -9445
9446 2 -1 -9446
9447 2 -1 -9447
C
C
*********************************************************************
C
```

```
9511 2 -1 -9511
9512 2 -1 -9512
9513 2 -1 -9513
9514 2 -1 -9514
9515 2 -1 -9515
9516 2 -1 -9516
9517 2 -1 -9517
C
9521 2 -1 -9521
9522 2 -1 -9522
9523 2 -1 -9523
9524 2 -1 -9524
9525 2 -1 -9525
9526 2 -1 -9526
9527 2 -1 -9527
C
9531 2 -1 -9531
9532 2 -1 -9532
9533 2 -1 -9533
9534 2 -1 -9534
9535 2 -1 -9535
9536 2 -1 -9536
9537 2 -1 -9537
C
9541 2 -1 -9541
9542 2 -1 -9542
9543 2 -1 -9543
9544 2 -1 -9544
9545 2 -1 -9545
9546 2 -1 -9546
9547 2 -1 -9547
C
C
*********************************************************************************
C
9611 2 -1 -9611
9612 2 -1 -9612
9613 2 -1 -9613
9614 2 -1 -9614
9615 2 -1 -9615
9616 2 -1 -9616
9617 2 -1 -9617
C
9621 2 -1 -9621
9622 2 -1 -9622
9623 2 -1 -9623
9624 2 -1 -9624
9625 2 -1 -9625
9626 2 -1 -9626
9627 2 -1 -9627
C
9631 2 -1 -9631
9632 2 -1 -9632
9633 2 -1 -9633
```

```
9634 2 -1 -9634
9635 2 -1 -9635
9636 2 -1 -9636
9637 2 -1 -9637
c
9641 2 -1 -9641
9642 2 -1 -9642
9643 2 -1 -9643
9644 2 -1 -9644
9645 2 -1 -9645
9646 2 -1 -9646
9647 2 -1 -9647
c
c
*************************************************************************
c
9711 2 -1 -9711
9712 2 -1 -9712
9713 2 -1 -9713
9714 2 -1 -9714
9715 2 -1 -9715
9716 2 -1 -9716
9717 2 -1 -9717
c
9721 2 -1 -9721
9722 2 -1 -9722
9723 2 -1 -9723
9724 2 -1 -9724
9725 2 -1 -9725
9726 2 -1 -9726
9727 2 -1 -9727
c
9731 2 -1 -9731
9732 2 -1 -9732
9733 2 -1 -9733
9734 2 -1 -9734
9735 2 -1 -9735
9736 2 -1 -9736
9737 2 -1 -9737
c
9741 2 -1 -9741
9742 2 -1 -9742
9743 2 -1 -9743
9744 2 -1 -9744
9745 2 -1 -9745
9746 2 -1 -9746
9747 2 -1 -9747
c
c
*************************************************************************
c
c Cell defining media inside the cylinder excluding spheres
c
5025 2 -1 1 2 3 4
```

```
          5 6 7 8
          9 10 11 12
          13 14 15 16
          17 18 19 20
          21 22 23 24
          25 26 27 28
          29 30 31 32
          33 34 35 36
          37 38 39 40
          41 42 43 44
          45 46 47 48
          49 50 51 52
          53 54 55 56
          57 58 59 60
          61 62 63 64
          65 66 67 68
          69 70 71 72
          73 74 75 76
          77 78 79 80
          81 82 83 84
          85 86 87 88
          89 90 91 92
          93 94 95 96
          97 98 99 100
          101 102 103 104
          105 106 107 108
          109 110 111 112
          113 114 115 116
          117 118 119 120
          -5000 6001 -6002
c
c
c Cell defining media outside the cylinder excluding point detectors
c
5027 2 -1 (5000:-6001:6002)
          9011 9012 9013 9014 9015 9016
          9017 9021 9022 9023 9024 9025
          9026 9027 9031 9032 9033 9034
          9035 9036 9037 9041 9042 9043
          9044 9045 9046 9047
          9111 9112 9113 9114 9115 9116
          9117 9121 9122 9123 9124 9125
          9126 9127 9131 9132 9133 9134
          9135 9136 9137 9141 9142 9143
          9144 9145 9146 9147
          9211 9212 9213 9214 9215 9216
          9217 9221 9222 9223 9224 9225
          9226 9227 9231 9232 9233 9234
          9235 9236 9237 9241 9242 9243
          9244 9245 9246 9247
          9311 9312 9313 9314 9315 9316
          9317 9321 9322 9323 9324 9325
          9326 9327 9331 9332 9333 9334
          9335 9336 9337 9341 9342 9343
```

```
          9344 9345 9346 9347
          9411 9412 9413 9414 9415 9416
          9417 9421 9422 9423 9424 9425
          9426 9427 9431 9432 9433 9434
          9435 9436 9437 9441 9442 9443
          9444 9445 9446 9447
          9511 9512 9513 9514 9515 9516
          9517 9521 9522 9523 9524 9525
          9526 9527 9531 9532 9533 9534
          9535 9536 9537 9541 9542 9543
          9544 9545 9546 9547
          9611 9612 9613 9614 9615 9616
          9617 9621 9622 9623 9624 9625
          9626 9627 9631 9632 9633 9634
          9635 9636 9637 9641 9642 9643
          9644 9645 9646 9647
          9711 9712 9713 9714 9715 9716
          9717 9721 9722 9723 9724 9725
          9726 9727 9731 9732 9733 9734
          9735 9736 9737 9741 9742 9743
          9744 9745 9746 9747
          -6033
c
c Cell defining media outside the sphere bounding region of interest
c
5028 0 6033

c*************************************************
c******************SURFACE CARDS*****************
c*************************************************
c
c Spheres surfaces
c
c 1st - surface #
c 2nd - surface shape - sphere
c 3d  - X coordinate of sphere center
c 4th - Y coordinate of sphere center
c 5th - Z coordinate of sphere center
c 6th - sphere radius
c
1 s -0.06943209 0.04952054 2.45016 0.05
2 s 0.006137062 0.09251309 1.3437 0.05
3 s 0.07265486 -0.06019988 2.15453 0.05
4 s 0.004529143 -0.04561754 2.80863 0.05
5 s 0.0582785 -0.06650276 2.90364 0.05
6 s 0.06715922 0.07092969 1.9851 0.05
7 s 0.006797791 -0.01603772 2.49853 0.05
8 s -0.04890448 -0.05988089 0.657491 0.05
9 s 0.06566408 -0.04242642 0.48779 0.05
10 s -0.08984856 -0.003787208 0.759925 0.05
11 s 0.01901815 0.0123173 1.23347 0.05
12 s 0.04094297 0.03912198 1.66542 0.05
13 s -0.0008341194 0.06729923 2.73071 0.05
14 s 0.0419714 0.05086623 0.635782 0.05
```

```
15 s -0.00757686 -0.09498082 0.217774 0.05
16 s -0.03487194 -0.0486874 0.841346 0.05
17 s 0.04381086 0.000006973744 1.83228 0.05
18 s -0.07306654 0.02209053 1.14484 0.05
19 s 0.02860135 0.05702123 0.147623 0.05
20 s -0.03331468 -0.02107269 2.61906 0.05
21 s 0.02906324 -0.07949834 0.972246 0.05
22 s -0.03054918 0.06615762 2.25255 0.05
23 s 0.02705407 0.06456738 2.92492 0.05
24 s -0.01417142 -0.03845304 0.308302 0.05
25 s -0.02183313 -0.06872264 2.19461 0.05
26 s 0.03837024 0.01842359 0.738257 0.05
27 s 0.03757897 0.08687847 0.95864 0.05
28 s 0.06769033 -0.02941422 2.3945 0.05
29 s 0.07711057 -0.04560962 1.74909 0.05
30 s -0.07519045 -0.02652518 2.38019 0.05
31 s -0.05873689 0.009412969 1.77309 0.05
32 s -0.02590153 -0.06853619 1.58266 0.05
33 s 0.005174363 0.07837018 0.502414 0.05
34 s -0.04027569 -0.007633681 2.04066 0.05
35 s 0.04500078 0.07102653 2.40809 0.05
36 s -0.04307901 -0.08587005 1.10679 0.05
37 s -0.08303663 -0.03717687 2.86579 0.05
38 s -0.08109479 0.0003535867 0.949366 0.05
39 s -0.04267385 0.002144945 1.34532 0.05
40 s -0.03590823 0.09144885 1.6017 0.05
41 s -0.04668728 -0.08812577 2.95733 0.05
42 s -0.0571081 0.05259209 0.30852 0.05
43 s 0.06766216 -0.01903888 9.454181E-02 0.05
44 s 0.0704975 0.05303289 2.26244 0.05
45 s 0.04047348 0.03752872 1.44268 0.05
46 s 0.07857619 -0.02388079 2.68267 0.05
47 s -0.04644197 0.05007543 1.04546 0.05
48 s 0.08744837 -0.02098995 1.94291 0.05
49 s 0.08322556 -0.03845421 1.51745 0.05
50 s -0.09549339 -0.01887971 0.157715 0.05
51 s 0.008600665 0.09151096 2.57341 0.05
52 s 0.08943903 -0.04449756 1.12271 0.05
53 s -0.07323179 -0.03650168 2.73117 0.05
54 s 0.02136612 0.08803764 1.75931 0.05
55 s -0.05666911 -0.04812456 0.429109 0.05
56 s -0.07760111 0.0422696 1.25683 0.05
57 s 0.09905258 0.01291337 0.274759 0.05
58 s -0.06368552 -0.02570772 1.44262 0.05
59 s -0.02042916 -0.06329797 1.68467 0.05
60 s 0.002000582 0.05593222 0.824568 0.05
61 s 0.09888351 0.006552196 2.83482 0.05
62 s -0.09714055 -0.001177365 2.17062 0.05
63 s 0.08932291 0.01014861 0.896651 0.05
64 s 0.05607704 0.08163683 1.53942 0.05
65 s 0.06565942 -0.03955466 0.373725 0.05
66 s -0.05514205 0.07500592 0.600818 0.05
67 s 0.04449522 0.04398603 1.09027 0.05
68 s -0.005665541 -0.05711836 1.92975 0.05
```

```
69 s -0.006247819 -0.07748359 1.28643 0.05
70 s 0.06974207 0.01512785 1.3251 0.05
71 s 0.07777245 -0.06043384 2.29541 0.05
72 s -0.04373397 -0.0413812 0.529277 0.05
73 s -0.02630199 0.09006533 2.08632 0.05
74 s 0.06972654 -0.06843822 1.39189 0.05
75 s 0.07208763 0.04927351 0.430967 0.05
76 s 0.06122299 -0.05791228 0.669108 0.05
77 s -0.09736665 0.01248386 1.5484 0.05
78 s -0.06093648 0.04951079 1.94102 0.05
79 s 0.06572878 -0.05766905 1.62625 0.05
80 s -0.06650361 -0.06720753 5.849405E-02 0.05
81 s 0.03388283 -0.08951484 2.57841 0.05
82 s 0.007880784 0.09897115 1.18096 0.05
83 s 0.08418778 0.05374629 2.10878 0.05
84 s -0.08535353 0.02053665 1.65449 0.05
85 s 0.005083979 0.09232782 1.85978 0.05
86 s -0.08027054 0.03994407 2.95633 0.05
87 s 0.059063 -0.0632815 0.808795 0.05
88 s -0.06629801 0.05176665 0.434609 0.05
89 s 0.06060521 -0.05874259 2.042 0.05
90 s -0.03349173 -0.08039261 1.82063 0.05
91 s -0.07702442 0.06305566 2.65437 0.05
92 s 0.002765239 0.02592089 2.16097 0.05
93 s -0.03147404 0.03631896 6.221468E-02 0.05
94 s 0.03815915 0.08574624 0.310807 0.05
95 s -0.04706943 0.07007542 1.47908 0.05
96 s -0.06863881 -0.06090488 2.28322 0.05
97 s -0.01395468 0.06745355 2.83197 0.05
98 s -0.001946485 -0.09247373 2.35925 0.05
99 s -0.04298285 0.07951164 0.710236 0.05
100 s -0.0610994 0.07438905 0.203216 0.05
101 s 0.08685357 0.01599062 2.59084 0.05
102 s -0.006841577 -0.09950866 2.67825 0.05
103 s -0.09334248 -0.03161656 2.53499 0.05
104 s 0.06804304 0.07111225 5.059448E-02 0.05
105 s 0.09789094 0.003281951 1.01402 0.05
106 s -0.07086199 -0.05627158 1.20902 0.05
107 s 0.007002426 -0.0883961 1.47546 0.05
108 s -0.09620803 -0.01258868 1.8669 0.05
109 s 0.03959784 -0.08898778 0.573052 0.05
110 s -0.05212522 0.07352208 2.35401 0.05
111 s 0.02366206 -0.09090683 1.1856 0.05
112 s 0.08823099 0.0386522 0.547756 0.05
113 s -0.01475566 -0.09669336 2.09681 0.05
114 s -0.02085165 -0.09306177 0.749237 0.05
115 s 0.09918984 0.006199909 2.96256 0.05
116 s 0.08716521 -0.04852748 0.191567 0.05
117 s -0.04874689 0.08684234 0.906404 0.05
118 s 0.09435114 0.03183831 2.48729 0.05
119 s 0.009720231 -0.09797353 0.116559 0.05
120 s -0.04234893 -0.09003263 2.45182 0.05
c
c Cylinder surface
```

```
c
5000 cz 0.15
c
c Planes defining cylinder height
c
6001 pz 0
6002 pz 3.018
c
c Tally surfaces
c
c cases - X = 0.16 cm - 0.61 cm
c         Y = 0 cm
c         Z = 1.059 cm - 1.959 cm
c
9011 s 0.16 0 1.059 0.01
9012 s 0.16 0 1.209 0.01
9013 s 0.16 0 1.359 0.01
9014 s 0.16 0 1.509 0.01
9015 s 0.16 0 1.659 0.01
9016 s 0.16 0 1.809 0.01
9017 s 0.16 0 1.959 0.01
c
9021 s 0.31 0 1.059 0.01
9022 s 0.31 0 1.209 0.01
9023 s 0.31 0 1.359 0.01
9024 s 0.31 0 1.509 0.01
9025 s 0.31 0 1.659 0.01
9026 s 0.31 0 1.809 0.01
9027 s 0.31 0 1.959 0.01
c
9031 s 0.46 0 1.059 0.01
9032 s 0.46 0 1.209 0.01
9033 s 0.46 0 1.359 0.01
9034 s 0.46 0 1.509 0.01
9035 s 0.46 0 1.659 0.01
9036 s 0.46 0 1.809 0.01
9037 s 0.46 0 1.959 0.01
c
9041 s 0.61 0 1.059 0.01
9042 s 0.61 0 1.209 0.01
9043 s 0.61 0 1.359 0.01
9044 s 0.61 0 1.509 0.01
9045 s 0.61 0 1.659 0.01
9046 s 0.61 0 1.809 0.01
9047 s 0.61 0 1.959 0.01
c
c cases - X = 0 cm
c         Y = 0.16 cm - 0.61 cm
c         Z = 1.059 cm - 1.959 cm
c
9111 s 0 0.16 1.059 0.01
9112 s 0 0.16 1.209 0.01
9113 s 0 0.16 1.359 0.01
9114 s 0 0.16 1.509 0.01
```

```
9115 s 0 0.16 1.659 0.01
9116 s 0 0.16 1.809 0.01
9117 s 0 0.16 1.959 0.01
c
9121 s 0 0.31 1.059 0.01
9122 s 0 0.31 1.209 0.01
9123 s 0 0.31 1.359 0.01
9124 s 0 0.31 1.509 0.01
9125 s 0 0.31 1.659 0.01
9126 s 0 0.31 1.809 0.01
9127 s 0 0.31 1.959 0.01
c
9131 s 0 0.46 1.059 0.01
9132 s 0 0.46 1.209 0.01
9133 s 0 0.46 1.359 0.01
9134 s 0 0.46 1.509 0.01
9135 s 0 0.46 1.659 0.01
9136 s 0 0.46 1.809 0.01
9137 s 0 0.46 1.959 0.01
c
9141 s 0 0.61 1.059 0.01
9142 s 0 0.61 1.209 0.01
9143 s 0 0.61 1.359 0.01
9144 s 0 0.61 1.509 0.01
9145 s 0 0.61 1.659 0.01
9146 s 0 0.61 1.809 0.01
9147 s 0 0.61 1.959 0.01
c
c cases - X = -0.16 cm - -0.61 cm
c         Y = 0 cm
c         Z = 1.059 cm - 1.959 cm
c
9211 s -0.16 0 1.059 0.01
9212 s -0.16 0 1.209 0.01
9213 s -0.16 0 1.359 0.01
9214 s -0.16 0 1.509 0.01
9215 s -0.16 0 1.659 0.01
9216 s -0.16 0 1.809 0.01
9217 s -0.16 0 1.959 0.01
c
9221 s -0.31 0 1.059 0.01
9222 s -0.31 0 1.209 0.01
9223 s -0.31 0 1.359 0.01
9224 s -0.31 0 1.509 0.01
9225 s -0.31 0 1.659 0.01
9226 s -0.31 0 1.809 0.01
9227 s -0.31 0 1.959 0.01
c
9231 s -0.46 0 1.059 0.01
9232 s -0.46 0 1.209 0.01
9233 s -0.46 0 1.359 0.01
9234 s -0.46 0 1.509 0.01
9235 s -0.46 0 1.659 0.01
9236 s -0.46 0 1.809 0.01
```

```
9237 s -0.46 0 1.959 0.01
c
9241 s -0.61 0 1.059 0.01
9242 s -0.61 0 1.209 0.01
9243 s -0.61 0 1.359 0.01
9244 s -0.61 0 1.509 0.01
9245 s -0.61 0 1.659 0.01
9246 s -0.61 0 1.809 0.01
9247 s -0.61 0 1.959 0.01
c
c cases - X = 0 cm
c         Y = -0.16 cm - -0.61 cm
c         Z = 1.059 cm - 1.959 cm
c
9311 s 0 -0.16 1.059 0.01
9312 s 0 -0.16 1.209 0.01
9313 s 0 -0.16 1.359 0.01
9314 s 0 -0.16 1.509 0.01
9315 s 0 -0.16 1.659 0.01
9316 s 0 -0.16 1.809 0.01
9317 s 0 -0.16 1.959 0.01
c
9321 s 0 -0.31 1.059 0.01
9322 s 0 -0.31 1.209 0.01
9323 s 0 -0.31 1.359 0.01
9324 s 0 -0.31 1.509 0.01
9325 s 0 -0.31 1.659 0.01
9326 s 0 -0.31 1.809 0.01
9327 s 0 -0.31 1.959 0.01
c
9331 s 0 -0.46 1.059 0.01
9332 s 0 -0.46 1.209 0.01
9333 s 0 -0.46 1.359 0.01
9334 s 0 -0.46 1.509 0.01
9335 s 0 -0.46 1.659 0.01
9336 s 0 -0.46 1.809 0.01
9337 s 0 -0.46 1.959 0.01
c
9341 s 0 -0.61 1.059 0.01
9342 s 0 -0.61 1.209 0.01
9343 s 0 -0.61 1.359 0.01
9344 s 0 -0.61 1.509 0.01
9345 s 0 -0.61 1.659 0.01
9346 s 0 -0.61 1.809 0.01
9347 s 0 -0.61 1.959 0.01
c
c cases - X = 0.113139705598762 cm - 0.431345127595279 cm
c         Y = 0.113139705598762 cm - 0.431345127595279 cm
c         Z = 1.059 cm - 1.959 cm
c
9411 s 0.113139705598762 0.113134464320231 1.059 0.01
9412 s 0.113139705598762 0.113134464320231 1.209 0.01
9413 s 0.113139705598762 0.113134464320231 1.359 0.01
9414 s 0.113139705598762 0.113134464320231 1.509 0.01
```

```
9415 s 0.113139705598762 0.113134464320231 1.659 0.01
9416 s 0.113139705598762 0.113134464320231 1.809 0.01
9417 s 0.113139705598762 0.113134464320231 1.959 0.01
c
9421 s 0.219208179597601 0.219198024620447 1.059 0.01
9422 s 0.219208179597601 0.219198024620447 1.209 0.01
9423 s 0.219208179597601 0.219198024620447 1.359 0.01
9424 s 0.219208179597601 0.219198024620447 1.509 0.01
9425 s 0.219208179597601 0.219198024620447 1.659 0.01
9426 s 0.219208179597601 0.219198024620447 1.809 0.01
9427 s 0.219208179597601 0.219198024620447 1.959 0.01
c
9431 s 0.32527665359644 0.325261584920663 1.059 0.01
9432 s 0.32527665359644 0.325261584920663 1.209 0.01
9433 s 0.32527665359644 0.325261584920663 1.359 0.01
9434 s 0.32527665359644 0.325261584920663 1.509 0.01
9435 s 0.32527665359644 0.325261584920663 1.659 0.01
9436 s 0.32527665359644 0.325261584920663 1.809 0.01
9437 s 0.32527665359644 0.325261584920663 1.959 0.01
c
9441 s 0.431345127595279 0.431325145220879 1.059 0.01
9442 s 0.431345127595279 0.431325145220879 1.209 0.01
9443 s 0.431345127595279 0.431325145220879 1.359 0.01
9444 s 0.431345127595279 0.431325145220879 1.509 0.01
9445 s 0.431345127595279 0.431325145220879 1.659 0.01
9446 s 0.431345127595279 0.431325145220879 1.809 0.01
9447 s 0.431345127595279 0.431325145220879 1.959 0.01
c
c cases - X = -0.113139705598762 cm - -0.431345127595279 cm
c         Y = 0.113139705598762 cm - 0.431345127595279 cm
c         Z = 1.059 cm - 1.959 cm
c
9511 s -0.113129222798894 0.113144946634475 1.059 0.01
9512 s -0.113129222798894 0.113144946634475 1.209 0.01
9513 s -0.113129222798894 0.113144946634475 1.359 0.01
9514 s -0.113129222798894 0.113144946634475 1.509 0.01
9515 s -0.113129222798894 0.113144946634475 1.659 0.01
9516 s -0.113129222798894 0.113144946634475 1.809 0.01
9517 s -0.113129222798894 0.113144946634475 1.959 0.01
c
9521 s -0.219187869172856 0.219218334104296 1.059 0.01
9522 s -0.219187869172856 0.219218334104296 1.209 0.01
9523 s -0.219187869172856 0.219218334104296 1.359 0.01
9524 s -0.219187869172856 0.219218334104296 1.509 0.01
9525 s -0.219187869172856 0.219218334104296 1.659 0.01
9526 s -0.219187869172856 0.219218334104296 1.809 0.01
9527 s -0.219187869172856 0.219218334104296 1.959 0.01
c
9531 s -0.325246515546819 0.325291721574117 1.059 0.01
9532 s -0.325246515546819 0.325291721574117 1.209 0.01
9533 s -0.325246515546819 0.325291721574117 1.359 0.01
9534 s -0.325246515546819 0.325291721574117 1.509 0.01
9535 s -0.325246515546819 0.325291721574117 1.659 0.01
9536 s -0.325246515546819 0.325291721574117 1.809 0.01
```

```
9537 s -0.325246515546819 0.325291721574117 1.959 0.01
c
9541 s -0.431305161920782 0.431365109043938 1.059 0.01
9542 s -0.431305161920782 0.431365109043938 1.209 0.01
9543 s -0.431305161920782 0.431365109043938 1.359 0.01
9544 s -0.431305161920782 0.431365109043938 1.509 0.01
9545 s -0.431305161920782 0.431365109043938 1.659 0.01
9546 s -0.431305161920782 0.431365109043938 1.809 0.01
9547 s -0.431305161920782 0.431365109043938 1.959 0.01
c
c cases - X = -0.113139705598762 cm - -0.431345127595279 cm
c         Y = -0.113139705598762 cm - -0.431345127595279 cm
c         Z = 1.059 cm - 1.959 cm
c
9611 s -0.113150187427361 -0.113123981034762 1.059 0.01
9612 s -0.113150187427361 -0.113123981034762 1.209 0.01
9613 s -0.113150187427361 -0.113123981034762 1.359 0.01
9614 s -0.113150187427361 -0.113123981034762 1.509 0.01
9615 s -0.113150187427361 -0.113123981034762 1.659 0.01
9616 s -0.113150187427361 -0.113123981034762 1.809 0.01
9617 s -0.113150187427361 -0.113123981034762 1.959 0.01
c
9621 s -0.219228488140511 -0.219177713254851 1.059 0.01
9622 s -0.219228488140511 -0.219177713254851 1.209 0.01
9623 s -0.219228488140511 -0.219177713254851 1.359 0.01
9624 s -0.219228488140511 -0.219177713254851 1.509 0.01
9625 s -0.219228488140511 -0.219177713254851 1.659 0.01
9626 s -0.219228488140511 -0.219177713254851 1.809 0.01
9627 s -0.219228488140511 -0.219177713254851 1.959 0.01
c
9631 s -0.325306788853662 -0.32523144547494 1.059 0.01
9632 s -0.325306788853662 -0.32523144547494 1.209 0.01
9633 s -0.325306788853662 -0.32523144547494 1.359 0.01
9634 s -0.325306788853662 -0.32523144547494 1.509 0.01
9635 s -0.325306788853662 -0.32523144547494 1.659 0.01
9636 s -0.325306788853662 -0.32523144547494 1.809 0.01
9637 s -0.325306788853662 -0.32523144547494 1.959 0.01
c
9641 s -0.431385089566813 -0.431285177695029 1.059 0.01
9642 s -0.431385089566813 -0.431285177695029 1.209 0.01
9643 s -0.431385089566813 -0.431285177695029 1.359 0.01
9644 s -0.431385089566813 -0.431285177695029 1.509 0.01
9645 s -0.431385089566813 -0.431285177695029 1.659 0.01
9646 s -0.431385089566813 -0.431285177695029 1.809 0.01
9647 s -0.431385089566813 -0.431285177695029 1.959 0.01
c
c cases - X = 0.113139705598762 cm - 0.431345127595279 cm
c         Y = -0.113139705598762 cm - -0.431345127595279 cm
c         Z = 1.059 cm - 1.959 cm
c
9711 s 0.113139705598762 -0.113134464320231 1.059 0.01
9712 s 0.113139705598762 -0.113134464320231 1.209 0.01
9713 s 0.113139705598762 -0.113134464320231 1.359 0.01
9714 s 0.113139705598762 -0.113134464320231 1.509 0.01
```

```
9715 s 0.113139705598762 -0.113134464320231 1.659 0.01
9716 s 0.113139705598762 -0.113134464320231 1.809 0.01
9717 s 0.113139705598762 -0.113134464320231 1.959 0.01
c
9721 s 0.219208179597601 -0.219198024620447 1.059 0.01
9722 s 0.219208179597601 -0.219198024620447 1.209 0.01
9723 s 0.219208179597601 -0.219198024620447 1.359 0.01
9724 s 0.219208179597601 -0.219198024620447 1.509 0.01
9725 s 0.219208179597601 -0.219198024620447 1.659 0.01
9726 s 0.219208179597601 -0.219198024620447 1.809 0.01
9727 s 0.219208179597601 -0.219198024620447 1.959 0.01
c
9731 s 0.32527665359644 -0.325261584920663 1.059 0.01
9732 s 0.32527665359644 -0.325261584920663 1.209 0.01
9733 s 0.32527665359644 -0.325261584920663 1.359 0.01
9734 s 0.32527665359644 -0.325261584920663 1.509 0.01
9735 s 0.32527665359644 -0.325261584920663 1.659 0.01
9736 s 0.32527665359644 -0.325261584920663 1.809 0.01
9737 s 0.32527665359644 -0.325261584920663 1.959 0.01
c
9741 s 0.431345127595279 -0.431325145220879 1.059 0.01
9742 s 0.431345127595279 -0.431325145220879 1.209 0.01
9743 s 0.431345127595279 -0.431325145220879 1.359 0.01
9744 s 0.431345127595279 -0.431325145220879 1.509 0.01
9745 s 0.431345127595279 -0.431325145220879 1.659 0.01
9746 s 0.431345127595279 -0.431325145220879 1.809 0.01
9747 s 0.431345127595279 -0.431325145220879 1.959 0.01
c
c Surface - sphere defining region of interest
c
6033 so 30

c*****************************************************
c********************DATA SECTIONS********************
c*****************************************************
c
c Defining particles to be considered in simulations
c p - photons
c e - electrons
c
mode p e
c
c Defining cell importance
c
c 225 (point detectors+1) + # of spheres
c
imp:p,e 1 345R 0
c
c Source description
c par=3 - ELECTRON MODE
c erg   - ENERGY DESTRIBUTION
c pos   - POSITION DESTRIBUTION
c rad   - RADIAL POSITION
c
```

```
sdef par=3 erg=D1 pos=D2 rad=D3
c
c Energy values distribution
c
c L - discrete distribution
c
si1 L 0.0108015 0.0324045 0.0540075 0.0756105 0.097216
      0.11882   0.14042   0.16202   0.183625  0.20523
      0.22683   0.248435  0.27004   0.29164   0.313245
      0.33485   0.35645   0.37805   0.399655  0.42126
      0.44286   0.464465  0.48607   0.50767   0.529275
      0.55088   0.57248   0.59408   0.615685  0.63729
      0.65889   0.680495  0.7021    0.72370   0.745305
      0.76691   0.78851   0.81011   0.831715  0.85332
      0.87492   0.896525  0.91813   0.93973   0.96133
      0.982935  1.00452   1.0261    1.0477    1.06935
      1.091     1.1126    1.1342    1.1558    1.1774
      1.199     1.2206    1.2422    1.2638    1.2854
      1.307     1.3286    1.3502    1.3718    1.3934
      1.415     1.4366    1.4582    1.4798    1.5014
      1.523     1.5446    1.5662    1.5878    1.6094
      1.631     1.6526    1.6742    1.695     1.7174
      1.739     1.7606    1.7822    1.80385   1.8255
      1.8471    1.8687    1.8903    1.9119    1.9335
      1.9551    1.9767    1.9983    2.0199    2.0415
      2.0631    2.0847    2.1063    2.1279    2.1495
c
c Probability of energy values - each energy has its determined
c probability
c
c D - bin probability
c
sp1 D 0.012613344 0.012833694 0.013060094 0.013297727 0.01354346
      0.013767192 0.01396742  0.014138712 0.014291125 0.014406552
      0.01450418  0.014583941 0.01462708  0.014655384 0.014670813
      0.014654952 0.014629896 0.014591448 0.014548284 0.014483232
      0.01441908  0.014358332 0.014283648 0.014217336 0.01416319
      0.014107176 0.014072616 0.01404756  0.014031373 0.013999392
      0.0139676   0.01393391  0.01387929  0.013824864 0.013770972
      0.013698504 0.013626576 0.013549248 0.013473187 0.013379472
      0.013287456 0.013196795n0.013089384 0.012983544 0.012873168
      0.012764379 0.012615618 0.012515256 0.012386736 0.012310193
      0.0121154   0.011972448 0.011824488 0.011670912 0.011511936
      0.011347344 0.011176704 0.011000232 0.01081728  0.010627632
      0.010431504 0.010228248 0.01001808  0.009800352 0.009575496
      0.009342864 0.009102672 0.008854704 0.00859896  0.008335656
      0.008064576 0.00778572  0.00749952  0.007206192 0.006905952
      0.006599016 0.006286032 0.005967432 0.005643864 0.005315976
      0.004984416 0.00465048  0.004314816 0.00399714  0.003643272
      0.0033102   0.002980584 0.002656584 0.002339712 0.002031977
      0.001735517 0.001452492 0.001185883 0.000938736 0.000713297
      0.000510991 0.00033467  0.000193095 9.58046E-05 3.78994E-05
c
c LOCATION OF THE SOURCE AND ELECTRON EMITTING PROBABILTY
```

```
c
c Position distribution  - defines position of emitting electron
c Basically defines in which sphere emition occurs
c
c L - discrete distribution
c
si2 L -0.06943209 0.04952054 2.45016
      0.006137062 0.09251309 1.3437
      0.07265486 -0.06019988 2.15453
      0.004529143 -0.04561754 2.80863
      0.0582785 -0.06650276 2.90364
      0.06715922 0.07092969 1.9851
      0.006797791 -0.01603772 2.49853
      -0.04890448 -0.05988089 0.657491
      0.06566408 -0.04242642 0.48779
      -0.08984856 -0.003787208 0.759925
      0.01901815 0.0123173 1.23347
      0.04094297 0.03912198 1.66542
      -0.0008341194 0.06729923 2.73071
      0.0419714 0.05086623 0.635782
      -0.00757686 -0.09498082 0.217774
      -0.03487194 -0.0486874 0.841346
      0.04381086 0.000006973744 1.83228
      -0.07306654 0.02209053 1.14484
      0.02860135 0.05702123 0.147623
      -0.03331468 -0.02107269 2.61906
      0.02906324 -0.07949834 0.972246
      -0.03054918 0.06615762 2.25255
      0.02705407 0.06456738 2.92492
      -0.01417142 -0.03845304 0.308302
      -0.02183313 -0.06872264 2.19461
      0.03837024 0.01842359 0.738257
      0.03757897 0.08687847 0.95864
      0.06769033 -0.02941422 2.3945
      0.07711057 -0.04560962 1.74909
      -0.07519045 -0.02652518 2.38019
      -0.05873689 0.009412969 1.77309
      -0.02590153 -0.06853619 1.58266
      0.005174363 0.07837018 0.502414
      -0.04027569 -0.007633681 2.04066
      0.04500078 0.07102653 2.40809
      -0.04307901 -0.08587005 1.10679
      -0.08303663 -0.03717687 2.86579
      -0.08109479 0.0003535867 0.949366
      -0.04267385 0.002144945 1.34532
      -0.03590823 0.09144885 1.6017
      -0.04668728 -0.08812577 2.95733
      -0.0571081 0.05259209 0.30852
      0.06766216 -0.01903888 9.454181E-02
      0.0704975 0.05303289 2.26244
      0.04047348 0.03752872 1.44268
      0.07857619 -0.02388079 2.68267
      -0.04644197 0.05007543 1.04546
      0.08744837 -0.02098995 1.94291
```

```
0.08322556 -0.03845421 1.51745
-0.09549339 -0.01887971 0.157715
0.008600665 0.09151096 2.57341
0.08943903 -0.04449756 1.12271
-0.07323179 -0.03650168 2.73117
0.02136612 0.08803764 1.75931
-0.05666911 -0.04812456 0.429109
-0.07760111 0.0422696 1.25683
0.09905258 0.01291337 0.274759
-0.06368552 -0.02570772 1.44262
-0.02042916 -0.06329797 1.68467
0.002000582 0.05593222 0.824568
0.09888351 0.006552196 2.83482
-0.09714055 -0.001177365 2.17062
0.08932291 0.01014861 0.896651
0.05607704 0.08163683 1.53942
0.06565942 -0.03955466 0.373725
-0.05514205 0.07500592 0.600818
0.04449522 0.04398603 1.09027
-0.005665541 -0.05711836 1.92975
-0.006247819 -0.07748359 1.28643
0.06974207 0.01512785 1.3251
0.07777245 -0.06043384 2.29541
-0.04373397 -0.0413812 0.529277
-0.02630199 0.09006533 2.08632
0.06972654 -0.06843822 1.39189
0.07208763 0.04927351 0.430967
0.06122299 -0.05791228 0.669108
-0.09736665 0.01248386 1.5484
-0.06093648 0.04951079 1.94102
0.06572878 -0.05766905 1.62625
-0.06650361 -0.06720753 5.849405E-02
0.03388283 -0.08951484 2.57841
0.007880784 0.09897115 1.18096
0.08418778 0.05374629 2.10878
-0.08535353 0.02053665 1.65449
0.005083979 0.09232782 1.85978
-0.08027054 0.03994407 2.95633
0.059063 -0.0632815 0.808795
-0.06629801 0.05176665 0.434609
0.06060521 -0.05874259 2.042
-0.03349173 -0.08039261 1.82063
-0.07702442 0.06305566 2.65437
0.002765239 0.02592089 2.16097
-0.03147404 0.03631896 6.221468E-02
0.03815915 0.08574624 0.310807
-0.04706943 0.07007542 1.47908
-0.06863881 -0.06090488 2.28322
-0.01395468 0.06745355 2.83197
-0.001946485 -0.09247373 2.35925
-0.04298285 0.07951164 0.710236
-0.0610994 0.07438905 0.203216
0.08685357 0.01599062 2.59084
-0.006841577 -0.09950866 2.67825
```

```
      -0.09334248 -0.03161656 2.53499
      0.06804304 0.07111225 5.059448E-02
      0.09789094 0.003281951 1.01402
      -0.07086199 -0.05627158 1.20902
      0.007002426 -0.0883961 1.47546
      -0.09620803 -0.01258868 1.8669
      0.03959784 -0.08898778 0.573052
      -0.05212522 0.07352208 2.35401
      0.02366206 -0.09090683 1.1856
      0.08823099 0.0386522 0.547756
      -0.01475566 -0.09669336 2.09681
      -0.02085165 -0.09306177 0.749237
      0.09918984 0.006199909 2.96256
      0.08716521 -0.04852748 0.191567
      -0.04874689 0.08684234 0.906404
      0.09435114 0.03183831 2.48729
      0.009720231 -0.09797353 0.116559
      -0.04234893 -0.09003263 2.45182
c
c Position probability
c
c D - defines uniform distribution
c
c
sp2 D 1 119R
c
c Bin boundaries for histogram distribution
c
si3 h 0 0.05
c
c Probability defined through probability function - P(X) = C*ABS(X)^a
c -21 - defines function type
c 2   - a parameter value
c
sp3 -21 2
c
c Problem cut off card
c
c Electron energy cut off - energy determined by CSDA range of the
c electron
c 1J    - time cut off
c 0.028 - low energy cut off in MeV
c
cut:e 1j 0.028
c
c Upper energy cut off in MeV
c
phys:e 3
phys:p 3
c
c MATERIAL DESCRIPTION
c
c 1st - material card #
c 2nd - 59000 - Pr(Praseodymium)
```

```
c 3d  - fraction - 0.105 (or 10.5%)
c 4th - 8000 - O(Oxygen)
c 5th - fraction - 0.632 (or 63.2%)
c 6th - 13000 - Al(Aluminum)
c 7th - fraction - 0.105 (or 10.5%)
c 8th - 14000 - Si(Silicon)
c 9th - fraction - 0.158(or 15.8%)
c
m1 59000 0.105 8000 0.632 13000 0.105 14000 0.158 $ inside microspheres
c
c 1st - material card #
c 2nd - 1000 - H(Hydrogen)
c 3d  - fraction - 0.666667 (or 66.6667%)
c 4th - 8000 - O(Oxygen)
c 5th - fraction - 0.333333 (or 33.3333%)
c
m2 1000 0.666667 8000 0.333333 $ elsewhere
c
c Tallies descriptions
c
c *f8 - energy distribution in the cell, MeV
c MCNP has restriction regarding number of tallies defined per input
c file allowed
c The maximum allowed number is 100 tallies
c We have 256 tallies thus it is necessary to split them into three
c input files
c Description of 84 tallies is presented below
c
*f18:e 9011
*f28:e 9012
*f38:e 9013
*f48:e 9014
*f58:e 9015
*f68:e 9016
*f78:e 9017
c
*f88:e 9021
*f98:e 9022
*f108:e 9023
*f118:e 9024
*f128:e 9025
*f138:e 9026
*f148:e 9027
c
*f158:e 9031
*f168:e 9032
*f178:e 9033
*f188:e 9034
*f198:e 9035
*f208:e 9036
*f218:e 9037
c
*f228:e 9041
*f238:e 9042
```

```
*f248:e 9043
*f258:e 9044
*f268:e 9045
*f278:e 9046
*f288:e 9047
c
c
*********************************************************************
*f298:e 9111
*f308:e 9112
*f318:e 9113
*f328:e 9114
*f338:e 9115
*f348:e 9116
*f358:e 9117
c
*f368:e 9121
*f378:e 9122
*f388:e 9123
*f398:e 9124
*f408:e 9125
*f418:e 9126
*f428:e 9127
c
*f438:e 9131
*f448:e 9132
*f458:e 9133
*f468:e 9134
*f478:e 9135
*f488:e 9136
*f498:e 9137
c
*f508:e 9141
*f518:e 9142
*f528:e 9143
*f538:e 9144
*f548:e 9145
*f558:e 9146
*f568:e 9147
c
c
*********************************************************************
*f578:e 9211
*f588:e 9212
*f598:e 9213
*f608:e 9214
*f618:e 9215
*f628:e 9216
*f638:e 9217
c
*f648:e 9221
*f658:e 9222
*f668:e 9223
*f678:e 9224
```

```
*f688:e 9225
*f698:e 9226
*f708:e 9227
c
*f718:e 9231
*f728:e 9232
*f738:e 9233
*f748:e 9234
*f758:e 9235
*f768:e 9236
*f778:e 9237
c
*f788:e 9241
*f798:e 9242
*f808:e 9243
*f818:e 9244
*f828:e 9245
*f838:e 9246
*f848:e 9247
c
c # of histories
c
nps 200000000

c end of input file
```

APPENDIX C

FORTRAN CODE

```
!
! loading spheres into a cylinder
!
program sphere packing

implicit none
integer i, j, k, n_spheres, iter, loops
real cyl_radius, sphere_radius, cyl_height
real x, y, z, store(10000,3), freq(10000)
real diff, p1, p2, p3, start, finish
real sphere_volume, cylinder_volume, density
!
! i,j,k - variables used in loops
! n_spheres - number of spheres positioned in the cylinder
! iter - number of spheres generated and attempted to position
! loops - number of loops
! cyl_radius, sphere_radius, cyl_height - self explanatory
! store - contains the x,y,z coordinates for spheres 1 thru 10000
! freq - contains frequency of appearance for different number of
! spheres
! diff, p1, p2, p3 - used in intermediate calculation
! start, finish - contain start and end time of calculation
! sphere_volume, cylinder_volume - self explanatory
! density - packing ration calculated as ration of spheres volume and
! cylinder volume
!
! Opening files for input data
!
open(10,file='c:\X.dat')
open(11,file='c:\Y.dat')
open(12,file='c:\Z.dat')

open(6,file='c:\output.dat')
open(7,file='c:\freq.dat')
!
! Entering model parameters
!
write(*,*)'Enter cylinder radius'
read(*,*)cyl_radius

write(*,*)'Enter sphere radius'
read(*,*)sphere_radius

write(*,*)'Enter cylinder height'
read(*,*)cyl_height

write(*,*)'Enter number of iterations'
read(*,*)iter

write(*,*)'Enter number of loops'
read(*,*)loops
!
! Starting clock
!
```

```
call clock@(start)

n_spheres = 0
!
! data array initialization
!
do i=1,10000
      freq(i)=0.
end do

diff = cyl_radius - sphere_radius

do j=1,loops
      !
      ! reinitializing of seed for random generator
      !
      call date_time_seed@

      do 99 k=1,iter

            x=2.*random@()*diff-diff
            y=2.*random@()*diff-diff
            !
            ! rejection sampling - determining if sphere inside the
            ! cylinder
            !
            if (x*x+y*y.gt.diff*diff)then
                  goto 99
            endif

            z = sphere_radius+random@()*(cyl_height-2*sphere_radius)

            !
            !check to see if sphere fits with other ones
            !
            do i=1,n_spheres

                  p1=(store(j,1)-x)**2
                  p2=(store(j,2)-y)**2
                  p3=(store(j,3)-z)**2

                  if (sqrt(p1+p2+p3).lt.2.0*sphere_radius) then
                        goto 99
                  endif

            end do

            n_spheres = n_spheres + 1
            store(n_spheres,1) = x
            store(n_spheres,2) = y
            store(n_spheres,3) = z

            write(6,*)(store(n_spheres,j), j=1,3)
```

```
            write(10,*)x
            write(11,*)y
            write(12,*)z

      99    continue

      freq(n_spheres)=freq(n_spheres)+1

end do

do i=1,10000
      write(7,*)freq(i)
end do

sphere_volume=(4./3.)*3.1415*(sphere_radius**3)
cylinder_volume=3.1415*(cyl_radius**2)*cyl_height

density=(n_spheres*sphere_volume)/cylinder_volume

write(*,*)'density', density

write(*,*)'number of spheres', n_spheres

write(6,*)n_spheres
!
! Closing files
!
close (6)
close (7)
close(10)
close(11)
close(12)
!
! Stopping clock
!
call clock@(finish)

write(*,*)'time elapsed',finish-start

end
```

APPENDIX D

USER INTERFACE DEVELOPED IN VISUAL BASIC

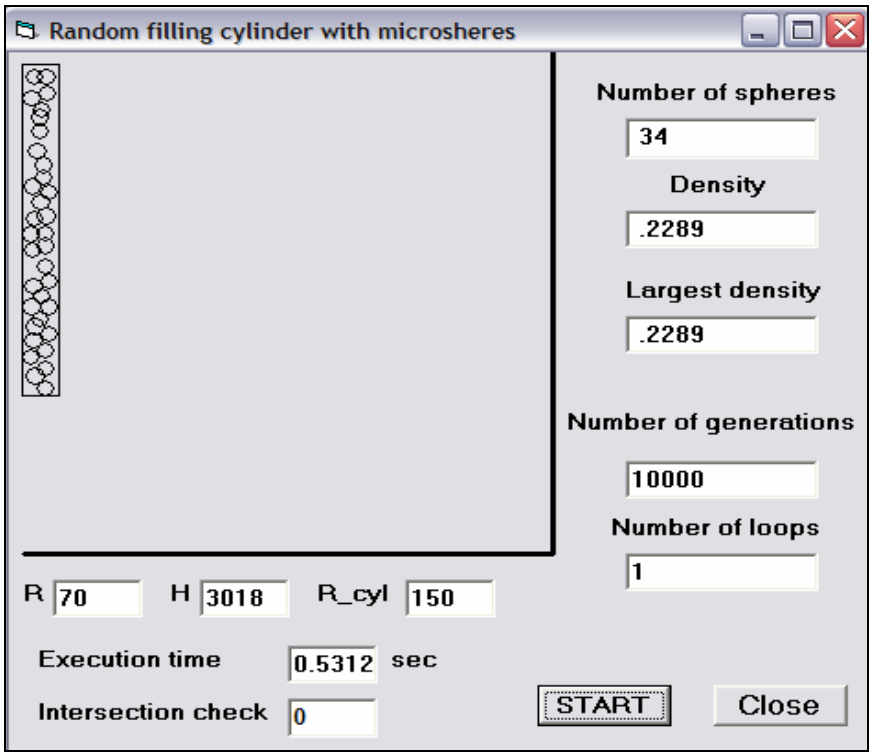

Fig. D.1 User interface in Visual Basic for random filling the cylinder with microspheres and generation data for MCNP input file

APPENDIX E

DOSE DISTRIBUTION HISTOGRAMS (CYLINDER RADIUS: 0.1 CM)

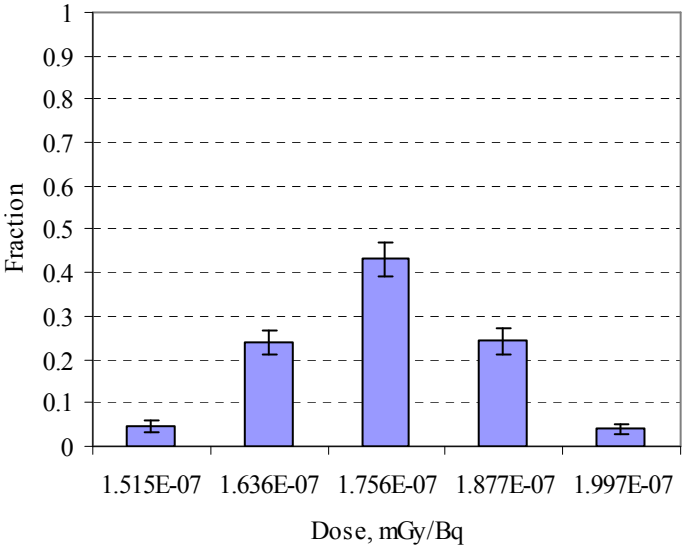

Fig. E.1 Dose distribution (cylinder radius: 0.1 cm, sphere radius: 0.03 cm, distance: 0 cm)

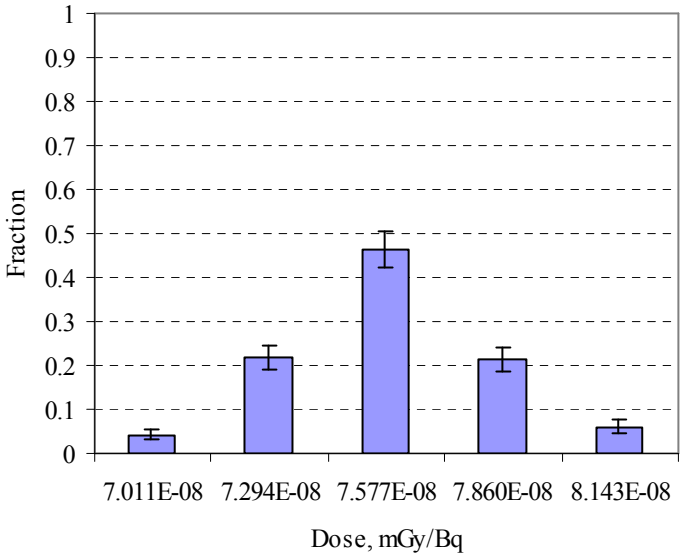

Fig. E.2 Dose distribution (cylinder radius: 0.1 cm, sphere radius: 0.03 cm, distance: 0.075 cm)

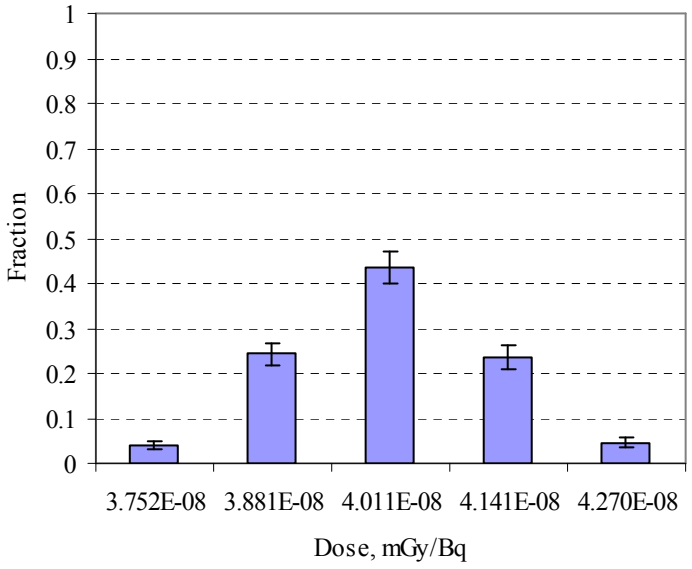

Fig. E.3 Dose distribution (cylinder radius: 0.1 cm, sphere radius: 0.03 cm, distance: 0.15 cm)

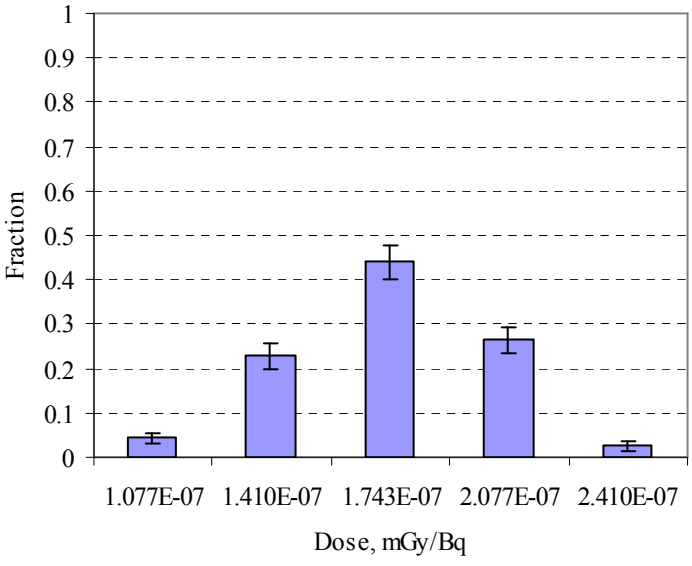

Fig. E.4 Dose distribution (cylinder radius: 0.1 cm, sphere radius: 0.05 cm, distance: 0 cm)

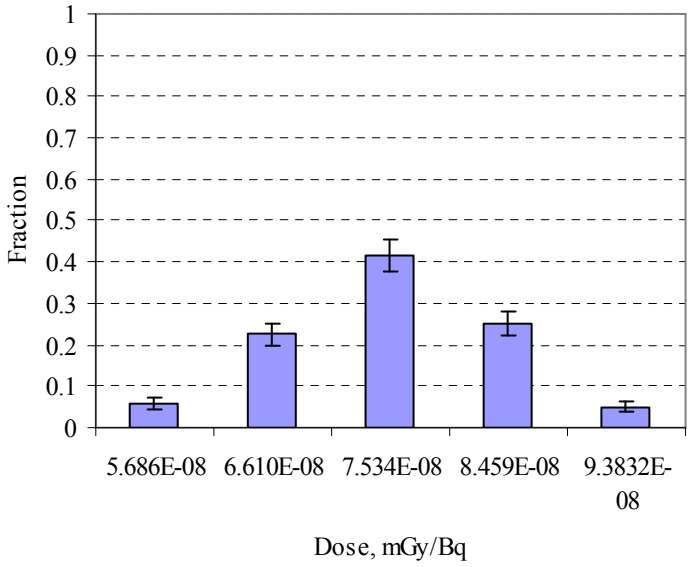

Fig. E.5 Dose distribution (cylinder radius: 0.1 cm, sphere radius: 0.05 cm, distance: 0.075 cm)

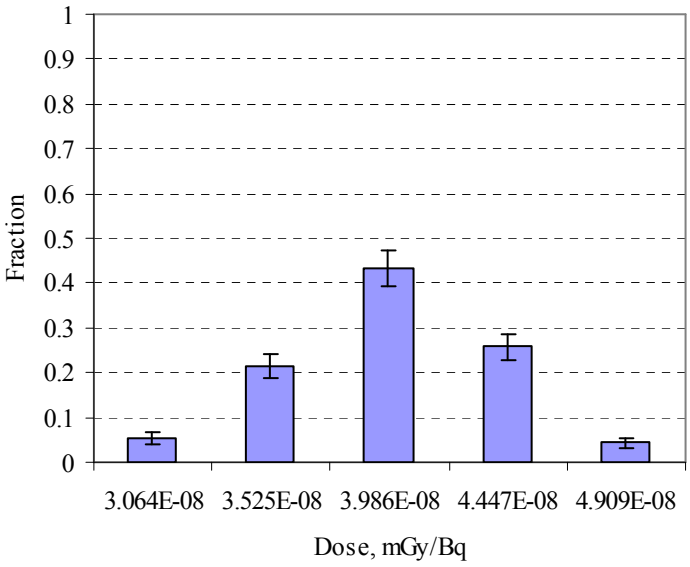

Fig. E.6 Dose distribution (cylinder radius: 0.1 cm, sphere radius: 0.05 cm, distance: 0.15 cm)

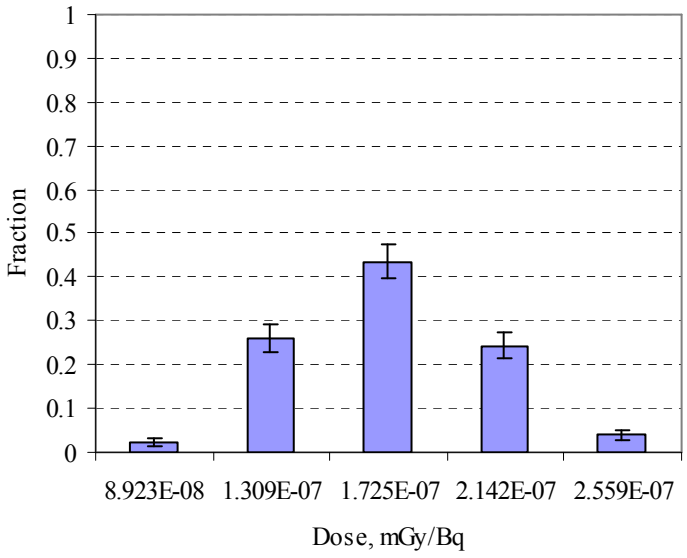

Fig. E.7 Dose distribution (cylinder radius: 0.1 cm, sphere radius: 0.07 cm, distance: 0 cm)

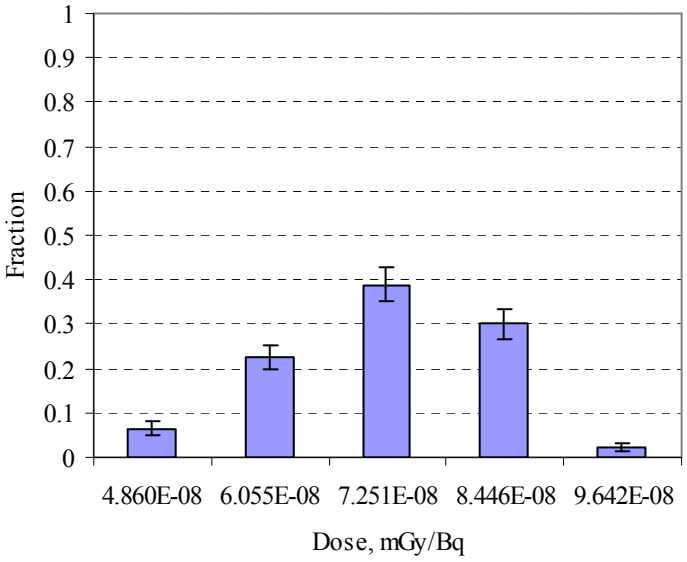

Fig. E.8 Dose distribution (cylinder radius: 0.1 cm, sphere radius: 0.07 cm, distance: 0.075 cm)

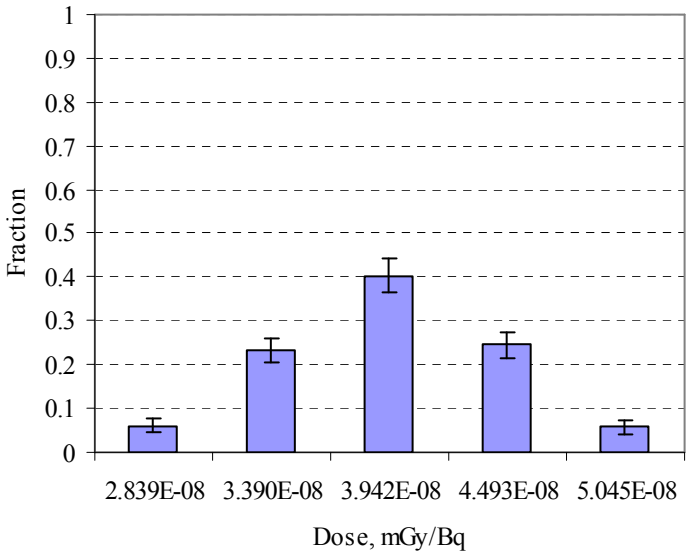

Fig. E.9 Dose distribution (cylinder radius: 0.1 cm, sphere radius: 0.07 cm, distance: 0.15 cm)

APPENDIX F

DOSE DISTRIBUTION HISTOGRAMS (CYLINDER RADIUS: 0.15 CM)

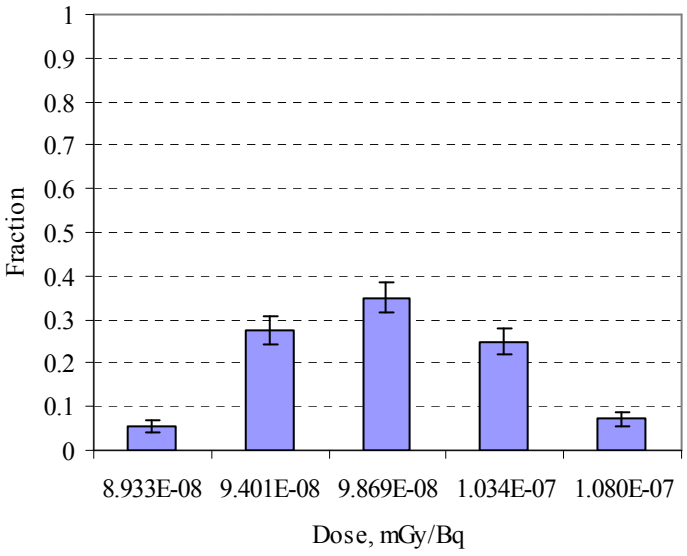

Fig. F.1 Dose distribution (cylinder radius: 0.15 cm, sphere radius: 0.03 cm, distance: 0 cm)

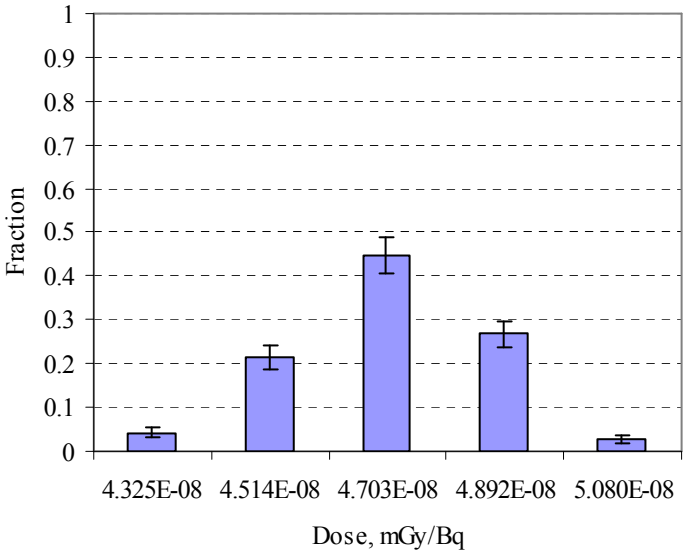

Fig. F.2 Dose distribution (cylinder radius: 0.15 cm, sphere radius: 0.03 cm, distance: 0.075 cm)

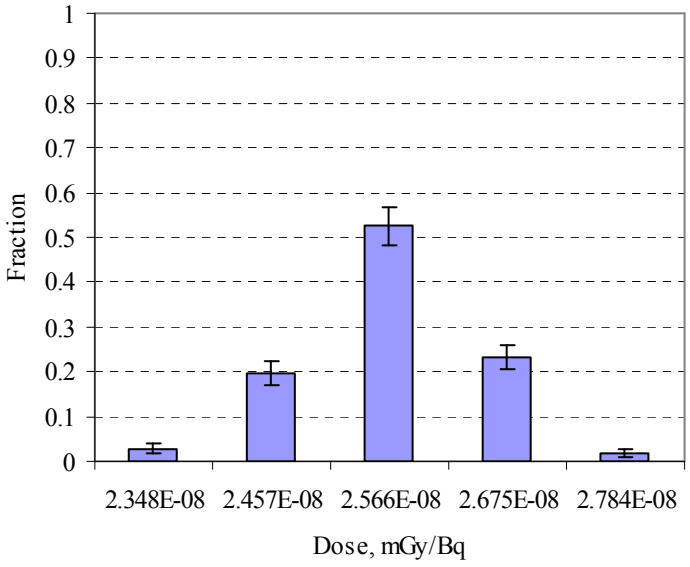

Fig. F.3 Dose distribution (cylinder radius: 0.15 cm, sphere radius: 0.03 cm, distance: 0.15 cm)

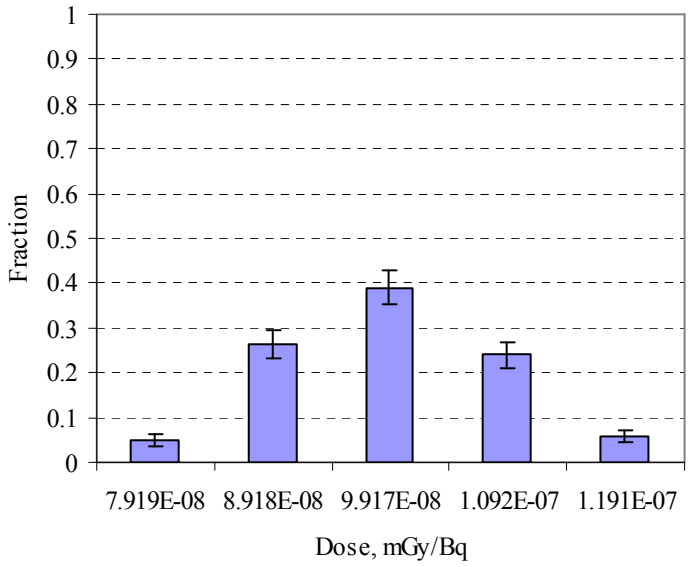

Fig. F.4 Dose distribution (cylinder radius: 0.15 cm, sphere radius: 0.05 cm, distance: 0 cm)

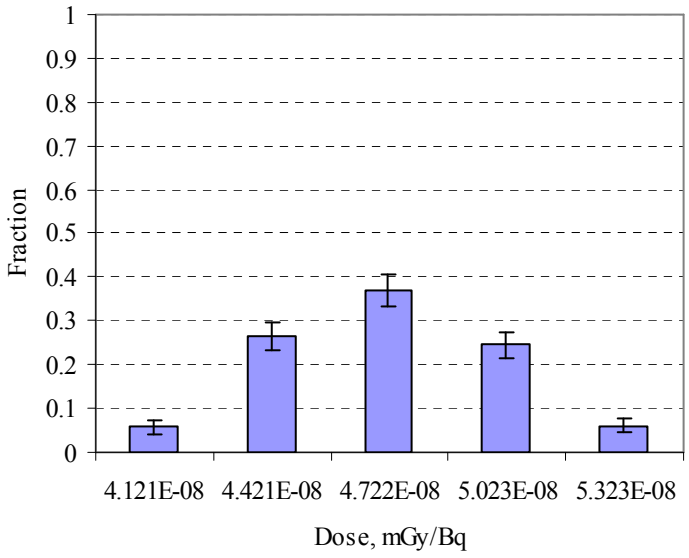

Fig. F.5 Dose distribution (cylinder radius: 0.15 cm, sphere radius: 0.05 cm, distance: 0.075 cm)

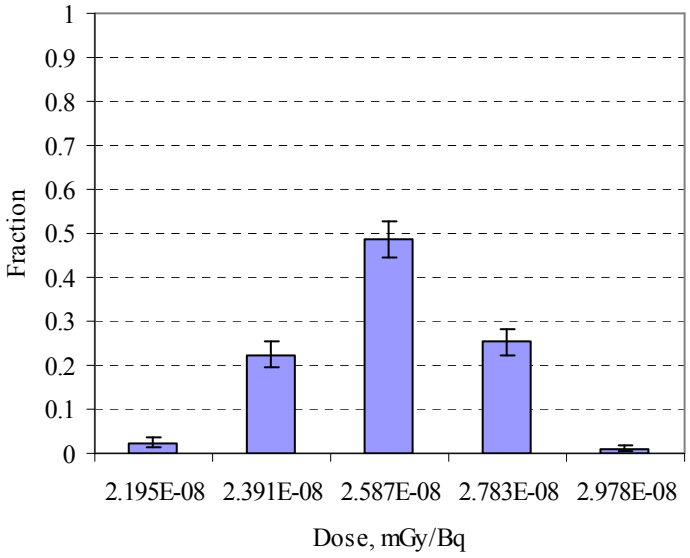

Fig. F.6 Dose distribution (cylinder radius: 0.15 cm, sphere radius: 0.05 cm, distance: 0.15 cm)

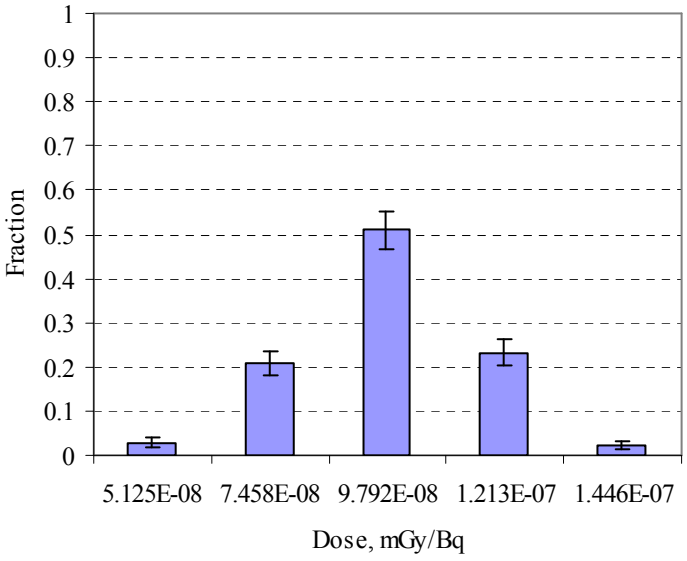

Fig. F.7 Dose distribution (cylinder radius: 0.15 cm, sphere radius: 0.07 cm, distance: 0 cm)

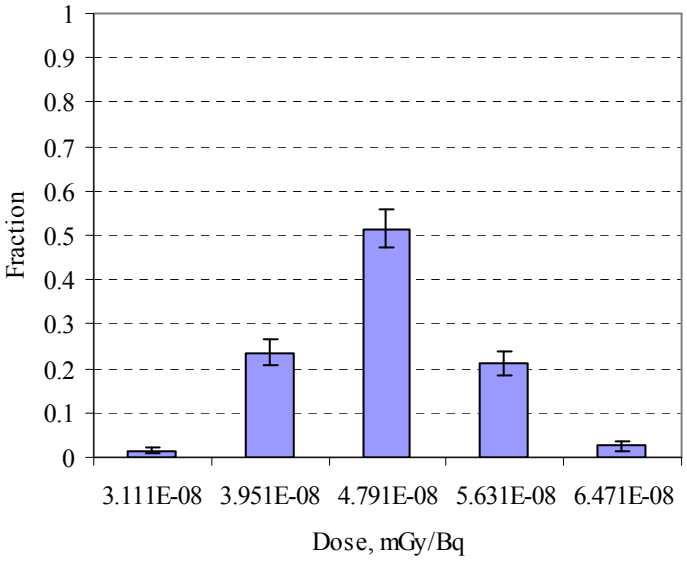

Fig. F.8 Dose distribution (cylinder radius: 0.15 cm, sphere radius: 0.07 cm, distance: 0.075 cm)

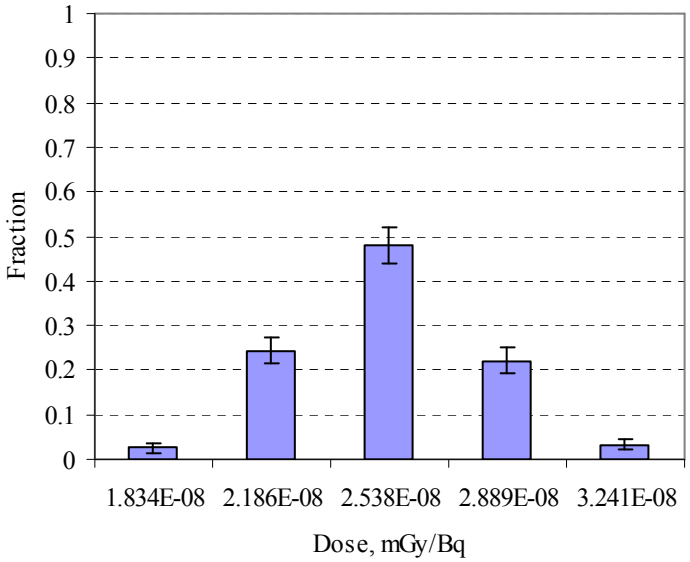

Fig. F.9 Dose distribution (cylinder radius: 0.15 cm, sphere radius: 0.07 cm, distance: 0.15 cm)

APPENDIX G

DOSE DISTRIBUTION HISTOGRAMS (CYLINDER RADIUS: 0.3 CM)

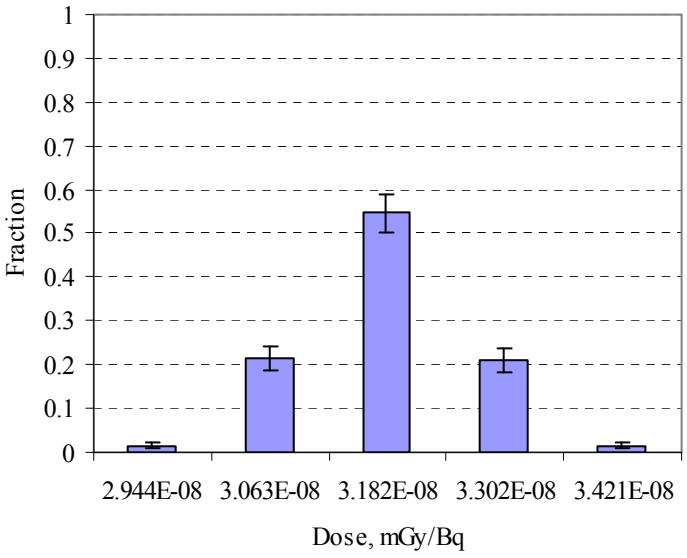

Fig. G.1 Dose distribution (cylinder radius: 0.3 cm, sphere radius: 0.03 cm, distance: 0 cm)

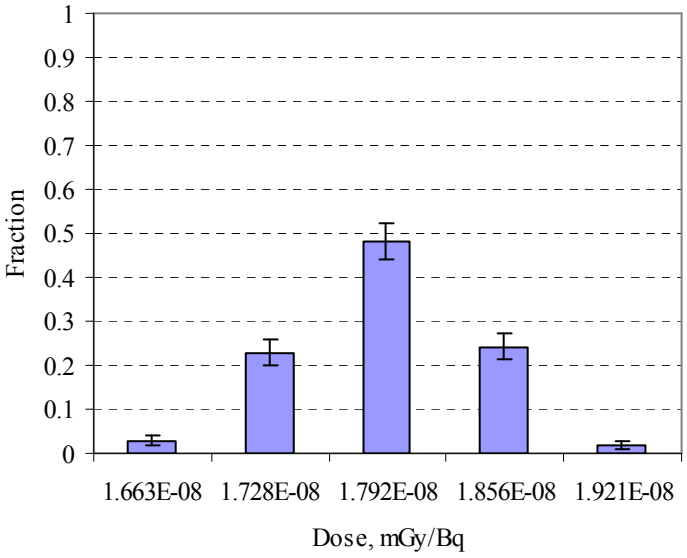

Fig. G.2 Dose distribution (cylinder radius: 0.3 cm, sphere radius: 0.03 cm, distance: 0.075 cm)

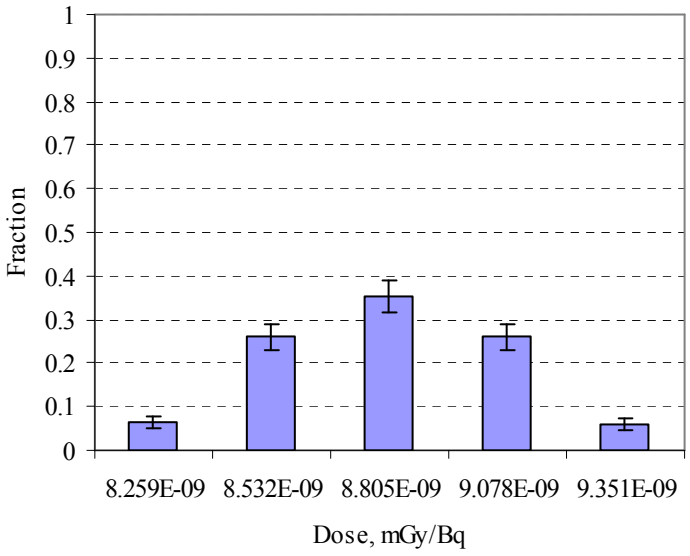

Fig. G.3 Dose distribution (cylinder radius: 0.3 cm, sphere radius: 0.03 cm, distance: 0.15 cm)

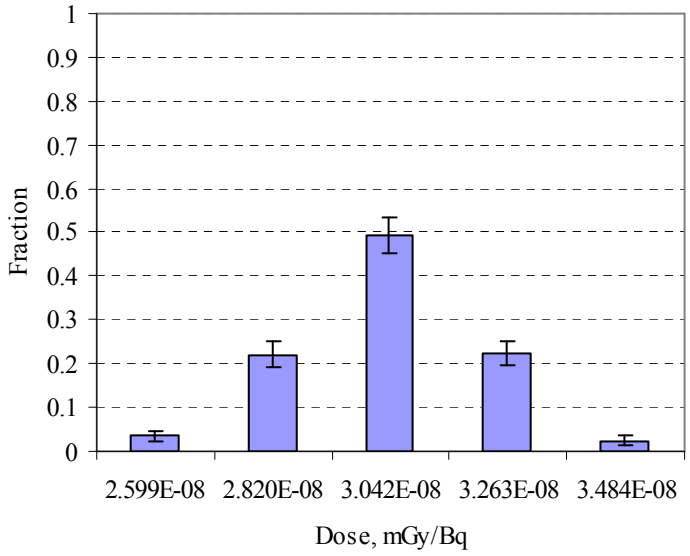

Fig. G.4 Dose distribution (cylinder radius: 0.3 cm, sphere radius: 0.05 cm, distance: 0 cm)

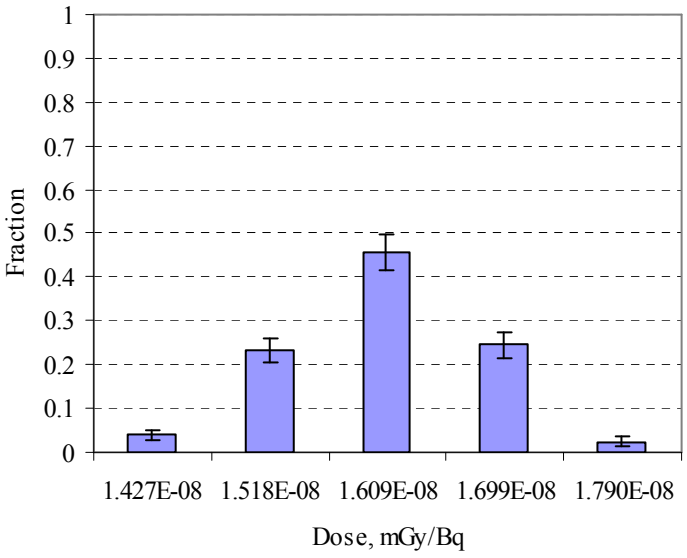

Fig. G.5 Dose distribution (cylinder radius: 0.3 cm, sphere radius: 0.05 cm, distance: 0.075 cm)

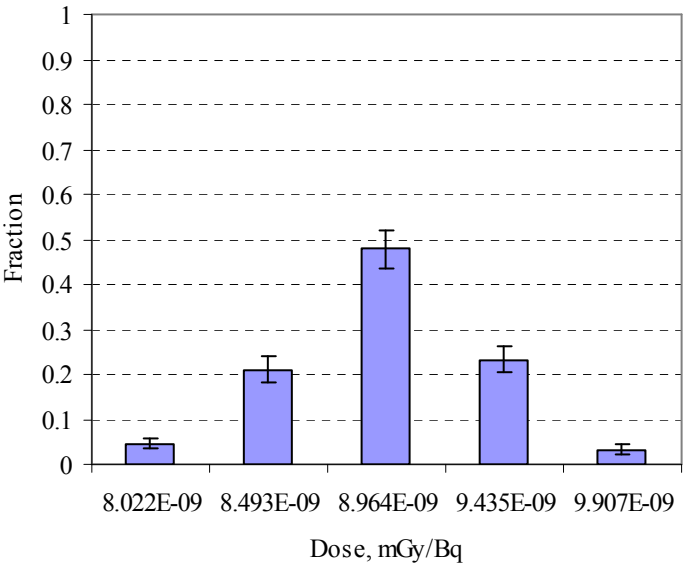

Fig. G.6 Dose distribution (cylinder radius: 0.3 cm, sphere radius: 0.05 cm, distance: 0.15 cm)

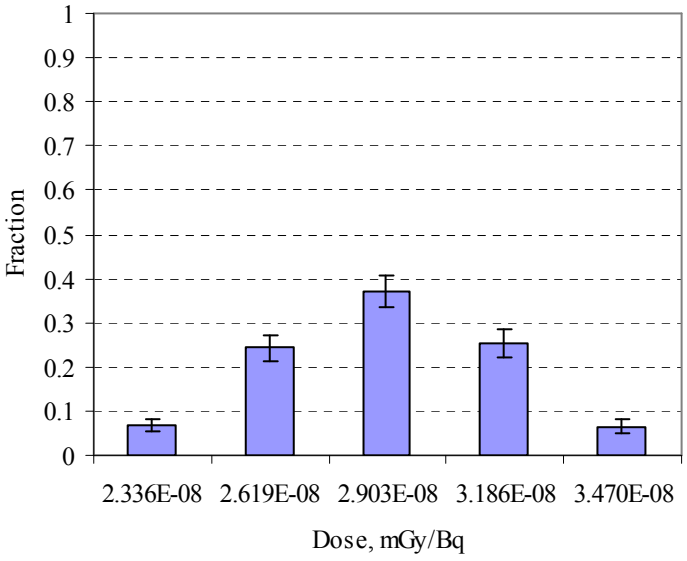

Fig. G.7 Dose distribution (cylinder radius: 0.3 cm, sphere radius: 0.07 cm, distance: 0 cm)

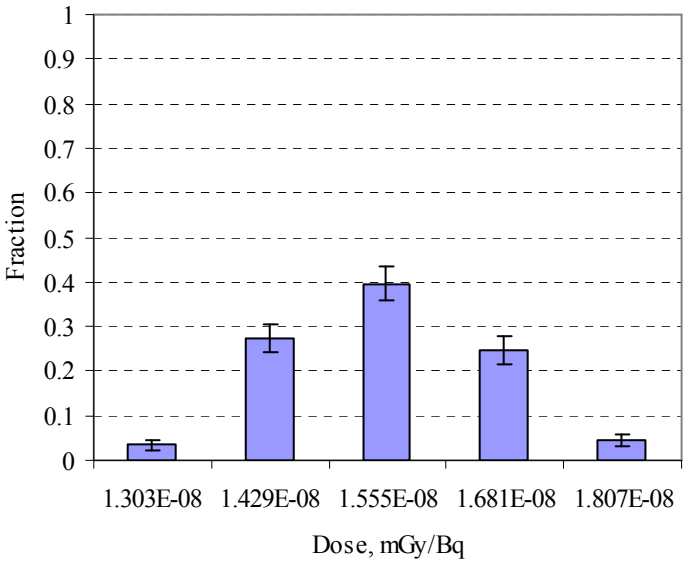

Fig. G.8 Dose distribution (cylinder radius: 0.3 cm, sphere radius: 0.07 cm, distance: 0.075 cm)

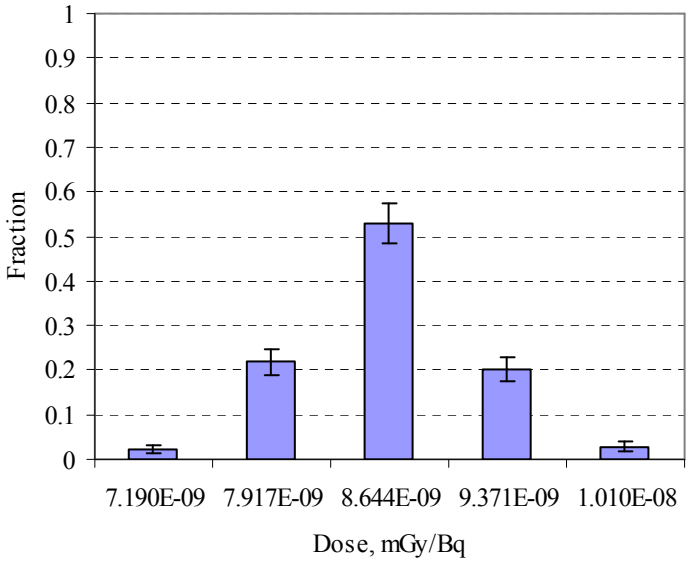

Fig. G.9 Dose distribution (cylinder radius: 0.3 cm, sphere radius: 0.07 cm, distance: 0.15 cm)

VITA

Alexander Urashkin was born in Obninsk, Russia. He received his bachelor's and master's degrees in information technology and computer engineering from Obninsk State Technical University for nuclear power engineering in 2001 and 2003 respectively. He went on to Texas A&M University and entered the Department of Nuclear Engineering in 2004 and received a M.S. in health physics in December 2006. He can be contacted through Dr. Warren D. Reece at: Department of Nuclear Engineering, Texas A&M University, College Station, Texas 77843-3133.